Donostia International Physics Center

Universidad del País Vasco

Euskal Herriko Unibertsitatea

CSIC

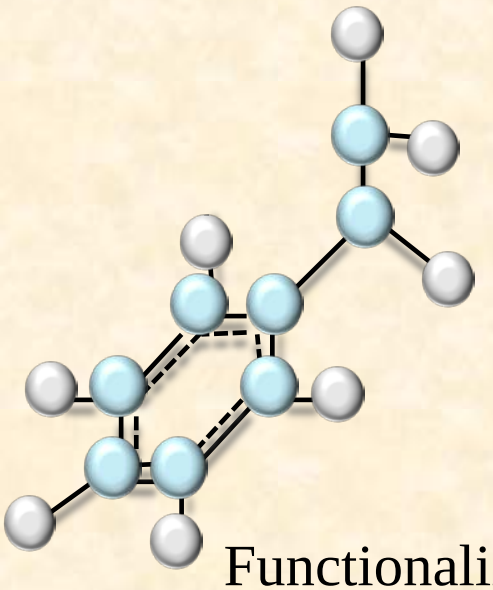

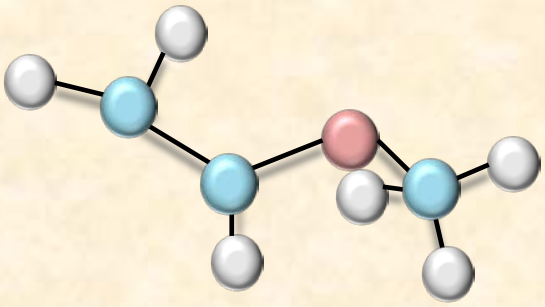

Functionalized Polymers as a Tool for Investigating the Component Dynamics of Polymer Blends

by Sandra Plaza García

Thesis Director: Prof. Angel Alegría Loinaz

Also supervised by Dr. Reidar Lund

Donostia – San Sebastián, October 2011

Acknowledgements

First, I would like to thank Prof. Juan Colmenero de León for giving me the opportunity to work in his research group “Polymers and Soft Matter”, which has been a very enriching experience for my life.

Deep thanks to my thesis director Angel Alegría Loinaz for his constant encouragement and dedication, interest in my thesis work, helpful advices in the proceedings carried out for this research, guidance and support. Also, many thanks to my direct supervisor Dr. Reidar Lund, a post-doctoral researcher of the group, for introducing me to Polymer Dynamics, showing me how to manipulate the obtained results, good advices and attention during these four years. Without their help this work would not have been possible.

Professor Roderic P. Quirk and his research group at the University of Akron are also gratefully acknowledged for their collaboration with regard to the synthesis of the functionalized polymers. This thesis work would not have been carried out without their collaboration.

Many thanks to Prof. Juan Colmenero de León and Prof. Arantxa Arbe Méndez for introducing me to Neutron’s world and in particular to the Small Angle Neutron Scattering (SANS) technique at the Institut Laue-Langevin in Grenoble (France). It was a memorable experience and I will never forget it.

Thanks to Luis Botana, Silvia Arrese and Gustavo Schwartz, who have helped me with the experimental measurements introducing me to the technique and giving me helpful advices in punctual situations.

Finally, I would like to thank my family and my partner for their daily encouragement and support.

Table of Contents

1. Introduction

The dynamics of polymer systems has attracted the interest of numerous investigations in the past becoming a very important topic not only from the scientific point of view but also from the industrial field looking for useful technological applications. Polymers, commonly called plastics, play an important role in our daily life since their simple processability linked to their low density and price make them the ideal material for a variety of applications such as in the alimentary, medical, electronic and car industries.

Most polymers are classified as glass-forming systems due to the fact that their slow global dynamics on the one hand and their 'chemical complexity' on the other hand, often prevent the material crystallization, so they generally present amorphous structures. The glass transition phenomenon, i.e. the transformation between a deeply super-cooled liquid/melt and a glassy material has a kinetic nature, and for polymers it is directly related to the segmental dynamics. The polymer segmental dynamics is the responsible of the so-called α-relaxation. This is the most important relaxation process that takes place in amorphous polymers and although it has been extensively studied over the last decades, it has not been completely understood.
Connectivity is a specific characteristic of polymers that play an important role on the segmental dynamics behavior not only in pure polymers but also in multicomponent polymer systems as polymer blends, block-copolymers, nanocomposites, ...

Due to the complexity that polymer systems present, a combination of different techniques covering a broad time/frequency range is required for the experimental study of the dynamics. Moreover, the direct relation between dynamics, thermodynamics and structure involve the use of other complementary experimental techniques accessing both thermal and structural properties, like Differential Scanning Calorimetry (DSC) and Small Angle Neutron Scattering (SANS), respectively.

From the dynamical point of view, a fundamental experimental problem to understand the dynamics of multicomponent polymer systems is to find the way to separate the component responses contributing to the whole signal experimentally detected. This can be solved using potential selective experimental techniques depending on the component nature. In this way, Nuclear Magnetic Resonance (RMN) allows accessing to each of the components of the system whenever the resonance lines do not overlap. Neutron scattering methods require using selective deuteration. On the other hand, Broadband Dielectric Spectroscopy (BDS) enables resolving one of the contributions of two-component systems when the two components present very different dipole moments, being this methodology the one of the most used in previous investigations. Unfortunately, this limits the access to dynamic information about the other component.

Other possibility to separate the two components contributions to the whole dynamics would be by using functionalized polymers. In fact, in the present work, this novel strategy based on the combination of functionalized polymers with BDS is presented to address such problem. Here, the dynamical behavior of

functionalized polymers “selectively” labeled, either at the end of the chain (chain-end functionalized polymers) or in the middle of the chain (in-chain functionalized polymers), was studied using a combination of experimental techniques such as BDS, DSC and Rheology. The very similar overall properties obtained for the two in-chain functionalized polymers having a largely distinct dipole moment was the key point that allowed us to resolve the contribution of both components to the segmental dynamics in PS/PVME miscible polymer blends.

This thesis work manuscript is organized as follows:

- First we present in detail the general background, which will constitute the framework of the present investigation.
- In the experimental section, we describe in detail the techniques used to produce the functionalized polystyrene polymers and samples preparation. Also the details of the techniques and instruments used for this investigation are presented.
- Concerning the obtained results, we first present the detailed comparison between polystyrene (PS) functionalized either at the end of the chain or in the middle of the chain, which allowed us to evidence that the fluctuations of the functional group are sensitive to their location along the polymer chain. From these results we were able to select the most appropriate functionalization to be used when investigating the component dynamics in the blends with poly(vinyl mehtyl ether) (PVME).
- The following chapter presents the results obtained for the blends using this new methodology also in comparison with those obtained in conventional polymer

PS/PVME blends. Thus, in addition of confirming the results obtained previously for PVME, we present new results on this component in PS rich blends and, for the first time, the resolved contribution of PS to the segmental dynamics on the blends.

- Finally, in the last section we present the most important conclusions of the work.

2. Background

2.1. Polymers

2.1.1. General Concepts

Polymers are structures of high molecular weights, which are composed of monomeric repeating units (between 100 and 10000 approximately) connected by covalent chemical bonds. They may exhibit a variety of architectures, i.e. linear, branched and network, depending on the structure of the monomer or monomers and on the polymerization methodology employed. The simplest form of a polymer molecule is a straight chain or linear polymer, composed of a single main chain formed by the same repeating unit.

Among the different types of polymerization the "living anionic polymerization" (see Scheme 2.1.1.1.) is a type of addition polymerization which mechanism does not involve a termination reaction, being a remarkable feature to be taken into account. The main advantages of this synthesis procedure concern a much more controlled manner in terms of the molecular weight and molecular weight distribution.

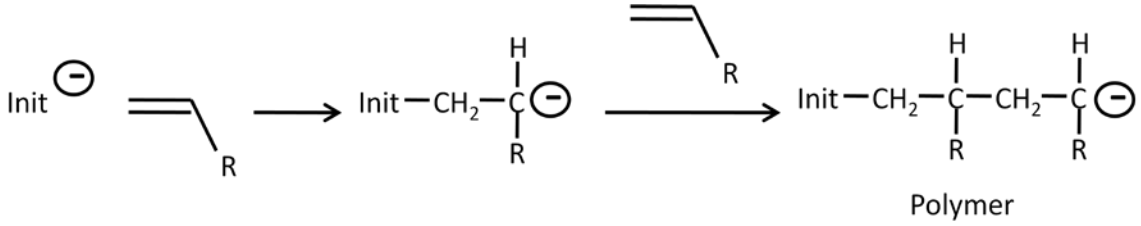

Scheme 2.1.1.1. Mechanism of the anionic polymerization (Michael reaction)

However, even in the most controlled conditions, chains in a given polymer do not grow in the same way giving rise to a distribution of chain lengths and molecular weights [1]. Several quantities are used to characterize this distribution. The number-average molecular weight ($\overline{M}_n$), which is related with the first moment of the distribution, is calculated as:

$$\overline{M}_n = \frac{\Sigma_i \, N_i \, M_i}{\Sigma_i \, N_i} \qquad [2.1.1.1.]$$

being N_i the number of molecules with M_i molecular weight.

The weight-average molecular weight ($\overline{M}_w$), which is related with the second moment of the distribution, is calculated as:

$$\overline{M}_w = \frac{\Sigma_i \, N_i \, M_i^2}{\Sigma_i \, N_i \, M_i} \qquad [2.1.1.2.]$$

From these two characteristic molecular weights the parameter commonly used to characterize the distribution width (see Figure 2.1.1.1.) is the polydispersity index (*PDI*). It is determined by dividing the weight-average molecular weight by the number-average molecular weight, i.e.

$$PDI = \frac{\overline{M}_w}{\overline{M}_n} \qquad [2.1.1.3.]$$

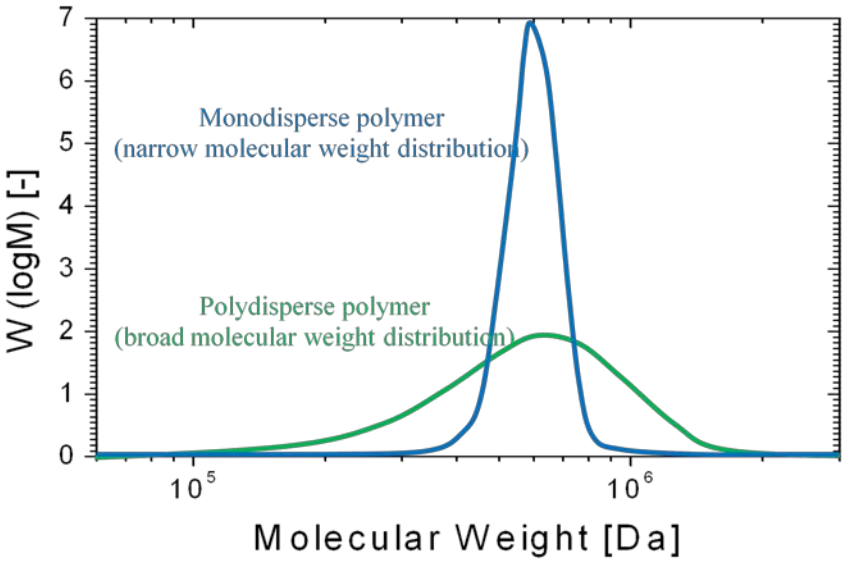

Figure 2.1.1.1. Molecular weight distribution of a polymer.

Therefore, a polymer is called polydisperse when there is a variation of molecular weights of the chain lengths over a wide range. On the contrary, a polymer is called monodisperse when it has a uniform size, shape and molecular weight and in this case $\overline{M}_w \approx \overline{M}_n$ giving rise to a polydispersity index $\overline{M}_w / \overline{M}_n \approx 1$. The fact of being more or less polydisperse depends on the particular synthesis method used.

Polymer properties are determined by its polymeric structure depending mainly on the chemistry of the repeating unit, the chain molecular weight and type, as well as the ending functional groups. In fact, in a polymer having a low molecular weight the effect of a functional end group in many properties is evident, while this effect decreases as molecular weight increases and any property appears to be approaching an asymptotic value [2, 3]. Such behavior is shown below for the glass transition temperature (T_g) of two typical linear polymers [4]:

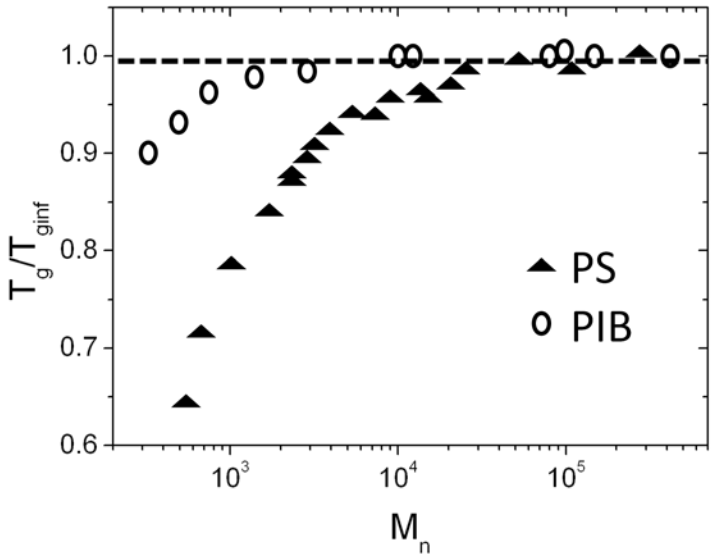

Figure 2.1.1.2. $T_g/T_{g,inf}$ as a function of molecular weight for PS (filled triangles) and PIB (empty circles). $T_{g,inf}$ is the glass-transition temperature of the polymer with infinite molecular weight, 373K for PS and 209.5K for PIB.

It is clear that the glass transition temperature (T_g) depends on the molecular weight. In fact, on decreasing the molecular weight, M_n, the concentration of chain-ends and the mobility increase, which gives rise to a decreasing in T_g. This fact was found to be well described by the so-called Fox-Flory equation [5]:

$$T_g(M) = T_g(\infty) - \frac{K}{\overline{M}_n} \qquad [2.1.1.4.]$$

where $T_g(\infty)$ is the T_g of the polymer with infinite molecular weight and K is a constant.

2.1.2. Dynamical Processes in Polymers

Although the characteristics of the dynamical processes in polymers have been investigated extensively over the last decades, this matter is not still completely resolved. This is because the study of the dynamics of a polymeric material is rather complicated due to the presence of extremely wide range of length scales, from the atomic level to the overall chain scale, and time scales, from picoseconds to hours or even years [6]. This is primarily caused by the chain connectivity, which induces strong correlations between the structural units and, consequently, imposes restrictions in the local molecular motion as well as the overall diffusive behavior. In fact, the main characteristic dynamical processes are vibrations, side-group motions, secondary relaxations, segmental dynamical processes and terminal relaxations.

In general, polymeric materials are characterized by a slow global dynamics giving rise to a practically non-existent or extremely slow crystallization. This is why most polymers show an amorphous behavior instead of a crystalline one. Hence, polymers usually behave as amorphous materials, which are structurally disordered, in the sense that they do not present a long-range order. The amorphous state is often characterized by the glass-transition temperature (T_g), which in the case of polymers refers to the temperature where the material goes from a rubbery/viscous-liquid state to a glassy state, and it can be associated to the ability of the polymer segments to move. In general, the glass transition is associated to the transformation of a liquid (at a temperature below the melting point, T_m) into a disordered solid. Consequently, at T_g the material goes from a super-cooled liquid to a metastable state of a glass, i.e an

amorphous non-crystalline solid [6, 7]**.** This phenomenon occurs when the cooling rate is fast compared to the processes restoring the thermodynamic equilibrium and the reorganization movements typical of the liquid cannot take place. On one hand, the glassy material behaves as a solid due to its deformation resistance, and on the other hand it is amorphous and resembles a liquid where there is no long range order between the structural units. Hence, this transition is characterized by a rather dramatic increase of the second order thermodynamic variables when the glass is heated. Nevertheless, it cannot be characterized as a real thermodynamic transition since the temperature at which it occurs depends on the cooling rate and the glassy state is not a state of thermodynamic equilibrium.

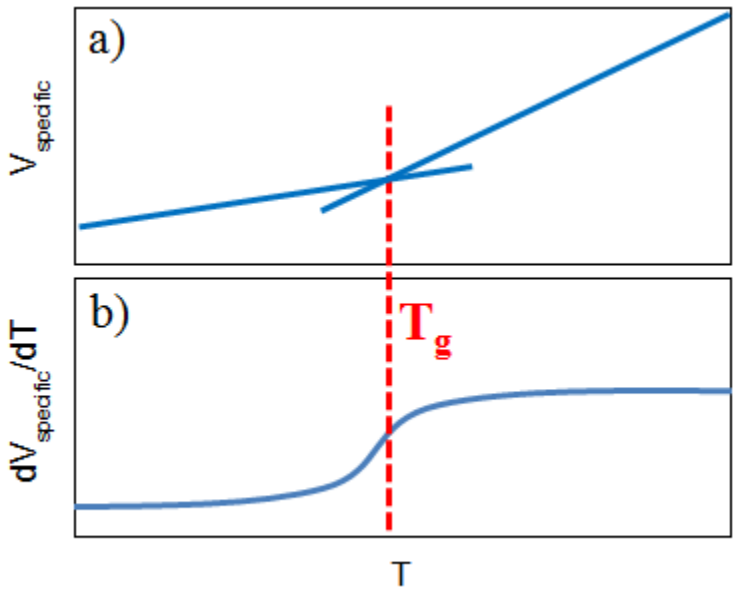

Figure 2.1.2.1. Temperature dependence of the specific volumen ($V_{specific}$) and its derivative ($dV_{specific}/dT$).

The glass transition is directly related to the so-called structural (or α-) relaxation, which is a process that not only takes place in polymers, but in all kind of glass-forming

materials. The α-relaxation is regarded as a cooperative process where the fluctuations of the molecules forming the "cage" around a target molecule cannot be independent from each other, i.e. the motion involves correlated steps with several molecules (e.g. segments, in the case of polymers) that results in complex dynamics. Nevertheless, this structural relaxation, being extensively studied over many years, is still not completely understood and it is considered as one of the main problems to solve in the area of physics [6, 8]. In the case of polymers interesting fundamental questions such as how cooperativity associated with the α-relaxation is affected by chain connectivity arise. Note that for polymeric systems the dynamics of the chain segments involve not only intermolecular but also intramolecular correlations. Related with this, other question still opened is how the dynamics of the chain-end groups are with respect to the inner segments of the chain.

In addition to the α-relaxation, there are other dynamical processes detected as secondary relaxations that can be observed in the glassy state, i.e. below the T_g, which are defined as β-relaxation, γ-relaxation, and so on. Below T_g polymer chains are frozen, and therefore these secondary relaxations cannot be assigned to the long range cooperative movements of the main chain as it occurs for the segmental relaxation. However, there are small movements at the molecular scale that still remain below T_g and therefore are clearly localized since the intermolecular correlations are frozen. They give rise to different loss peaks in the relaxation spectrum (see below), which appear at higher frequencies/lower temperatures than the main α-relaxation. The secondary relaxations are often interpreted as processes that comprise small rotations or vibrations of molecular subgroups not involving the whole molecule [9]. Nevertheless, Johari and

Goldstein [10] characterized some of these processes as universal-like phenomena that could take place even in molecular glasses where the internal conformational changes are very unlikely.

2.1.2.1. Relaxation Phenomena

The basis of many experimental techniques employed to investigate the molecular dynamics, as those used here, is the “Fluctuation-Dissipation Theorem”, which states that when a weak perturbation is applied to a system in thermodynamic equilibrium, its response reflects the internal fluctuations without perturbation [11]. This principle is well applicable for relaxation techniques, which allow studying the polymer dynamics. For instance, with Broadband Dielectric Spectroscopy (BDS) we measure the dielectric properties of a medium as a function of frequency to extract information about the molecular mobility of a polymer since this technique is sensitive to the molecular dipole moment fluctuations. As it is illustrated in the scheme (see Figure 2.1.2.1.1.) when an alternating voltage of very high frequency is applied, molecular dipoles are not able to follow the electric field variation and the dielectric permittivity parameter will be determined from the induced atomic and electronic material polarization. Reducing frequency dipoles are able to partially orientate with the electric field contributing to polarization, so the dielectric permittivity increases. Finally, dipoles will completely orientate with the electric field when the frequency is low enough. This situation gives rise to a low frequency plateau of the dielectric permittivity (static value). There is a range of frequencies where the dielectric permittivity increases and in this range we can

observe the presence of an associated energy dissipation process related to the frictional forzes acting on the dipoles, which is detected as a peak in the imaginary part of the dielectric permittivity, commonly called as “loss peak”.

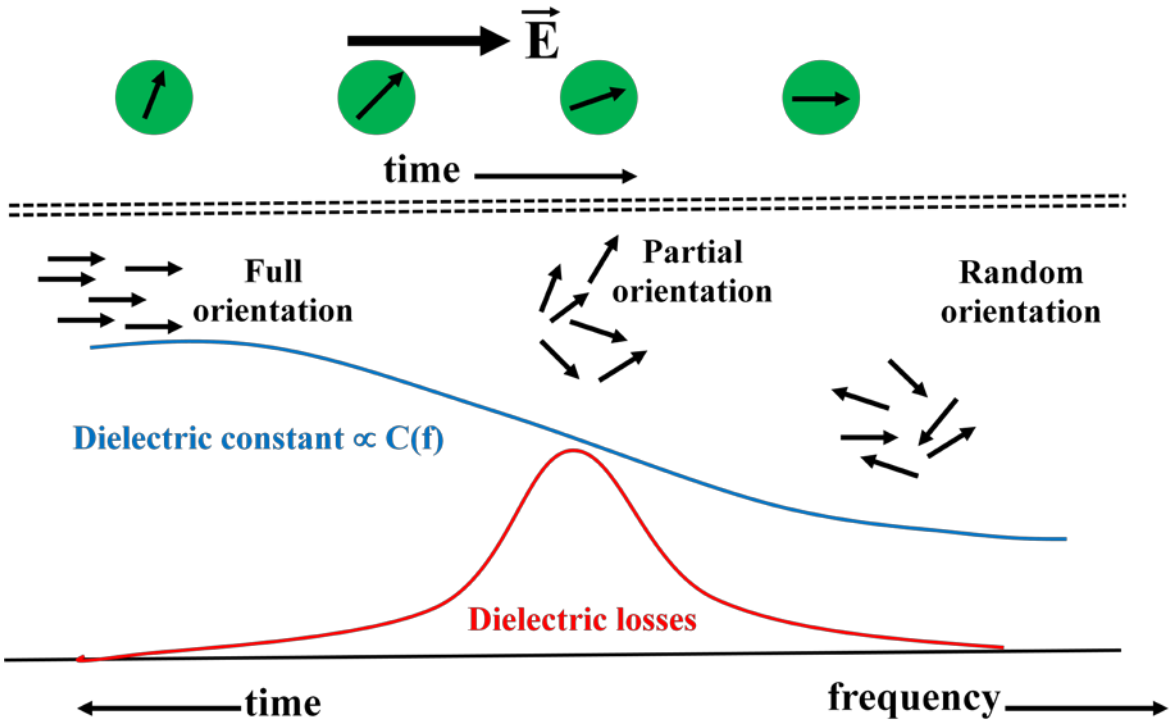

Figure 2.1.2.1.1. Scheme of the orientation of the dipole moments with an applied electric field $\vec{E}$ showing the dielectric losses as a function of the time or frequency.

The characteristic time corresponding to the molecular motions controls the orientation of the molecular dipoles and it can be conveniently determined from the reciprocal of the loss peak frequency.

From an experimental point of view, the obtained quantity is the frequency dependent complex dielectric permittivity:

$$\varepsilon^* = \varepsilon' - i\varepsilon'' \qquad [2.1.2.1.1.]$$

where ε' is the real permittivity, which is proportional to the energy stored reversibly in the system per period, and ε" is the imaginary permittivity, which is proportional to the energy dissipated per period (loss part). Both ε' and ε" contain the same information since they are interrelated by the Kramers/Kronig-relations [12]:

$$\varepsilon'(\omega) - \varepsilon_\infty = \frac{2}{\pi} \int_0^\infty \frac{\omega' \, \varepsilon''(\omega')}{\omega'^2 - \omega^2} \, d\omega' \qquad [2.1.2.1.2.]$$

$$\varepsilon''(\omega) = -\frac{2\omega}{\pi} \int_0^\infty \frac{\varepsilon'(\omega') - \varepsilon_\infty}{\omega'^2 - \omega^2} \, d\omega' \qquad [2.1.2.1.3.]$$

For the case of ideal systems, i.e. systems with a unique time constant (τ_D), a relaxation process can be described through the so-called Debye equation [13]:

$$\varepsilon^*(\omega) = \varepsilon_\infty + \frac{\Delta\varepsilon}{1 + i\omega\tau_D} \qquad [2.1.2.1.4.]$$

where ω is the angular frequency of the alternating electric field, and $\Delta\varepsilon$ is the dielectric strength which can be written as

$$\Delta\varepsilon = \varepsilon_s - \varepsilon_\infty \qquad [2.1.2.1.5.]$$

where

$$\varepsilon_s = \lim_{\omega\tau \ll 1} \varepsilon'(\omega) \qquad [2.1.2.1.6.]$$

and

$$\varepsilon_\infty = \lim_{\omega\tau \gg 1} \varepsilon'(\omega) \qquad [2.1.2.1.7.]$$

being therefore ε_s and ε_∞, respectively, the low- and high-frequency permittivity limiting values.

τ_D (the Debye relaxation time) is straight forwardly related to the position of maximal loss by the following expression

$$\omega_P = \frac{1}{\tau_D} \qquad [2.1.2.1.8.]$$

The Debye relaxation function shows a symmetric loss peak with a narrow width, being the full width at half maximum (FWHM) 1.14 decades [12] (see Figure 2.1.2.1.2.).

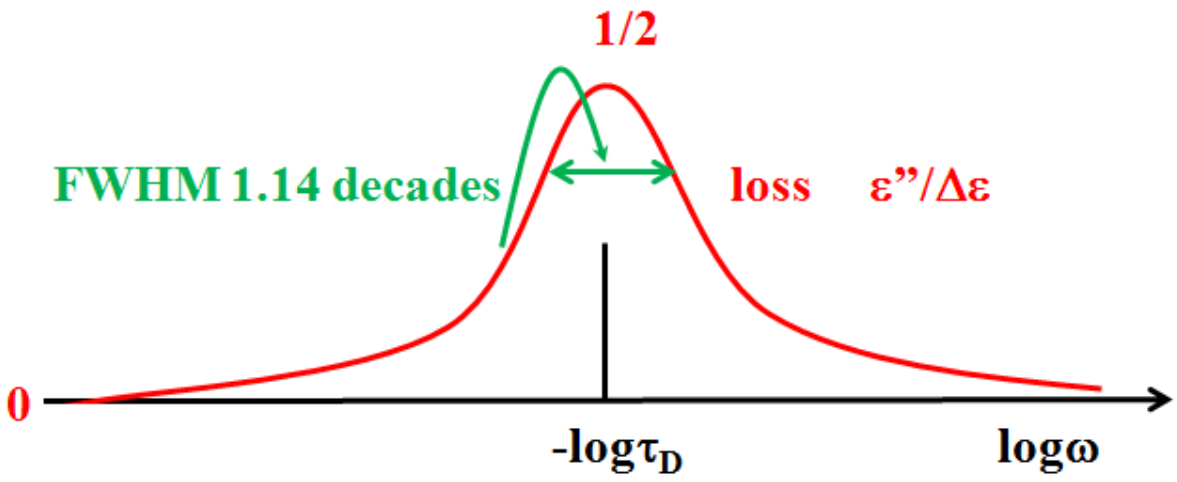

Figure 2.1.2.1.2. Frequency dependence of the dielectric loss permittivity (ε") for a Debye relaxation process.

The Debye relaxation only considers a single relaxation time, in the time domain it therefore corresponds to a single exponential decay of the correlation function of the electric polarization $\Phi(t)$ [6]:

$$\Phi(t) = \exp\left[-\frac{t}{\tau_D}\right] \qquad [2.1.2.1.9.]$$

where t is the time.

However, usually this simple behavior is not found –rather the dynamics is somewhat spread on time or frequencies, i.e. the dynamics can be characterized by a distribution of relaxation times. In most materials the shape of the loss peak is rather asymmetric as well as much broader. This observation of non-Debye behavior has led to define several mathematical models in order to describe dielectric spectra. A general way to account for this behavior is to consider that the measured response arises as a simple superposition of Debye responses, i.e. assuming the existence of a continuous distribution of Debye relaxation times $g(\log \tau_D)$ instead of a single one. In this framework the relaxation function would be given as:

$$\varepsilon^*(\omega) = \varepsilon_\infty + \Delta\varepsilon \int_{-\infty}^{+\infty} g(\log \tau_D) \frac{1}{1 + i\omega\tau_D} d\log \tau_D \qquad \text{[2.1.2.1.10.]}$$

in the frequency domain, and

$$\Phi(t) = \int_{-\infty}^{+\infty} g(\log \tau_D) \exp\left[-\left(\frac{t}{\tau_D}\right)\right] d\log \tau_D \qquad \text{[2.1.2.1.11.]}$$

in the time domain. Although these equations provide a correct mathematical description of the measured response the interpretation of the distribution function often has not a clear physical meaning.

The non-Debye relaxation behavior has been attributed to the existence of cooperative regions having different sizes and relaxation times in agreement with the idea of a relaxation time distribution. However, in the context of the glass transition, other authors and some theories relate such behavior to the correlation between the different relaxing units, which would imply certain homogeneity of the dynamic behavior.

Nevertheless, as the dynamics of super-cooled liquids is not totally understood yet [7, 14, 15, 16, 17, 18, 19, 20], this is still a matter of strong debate.

Other alternative approach for accounting of the measured relaxation functions is by using simple mathematical equations able to describe the data. For the time domain relaxation, a useful model is the Kohlrausch-Williams-Watts (KWW) equation [6, 21, 22, 23, 24, 25]. The KWW function, also called the stretched exponential function, is used to describe the decay of the correlation function in many cases (from experiments as well as from theories and simulations), and is defined as

$$\Phi(t)=\exp\left[-\left(\frac{t}{\tau_{KWW}}\right)^{\beta_{KWW}}\right] \qquad \text{[2.1.2.1.12.]}$$

where β_{KWW} is the so-called stretching parameter ($0 < \beta_{KWW} \leq 1$), and τ_{KWW} is the characteristic relaxation time.

In the frequency domain there is not a simple mathematical expression corresponding to the equation [2.1.2.1.12], thus, other empirical functions are used which include the Cole-Cole equation [26], and Cole-Davidson equation [24, 27] as well as the more versatile and general Havriliak Negami equation. The Havriliak Negami equation [25, 28, 29, 30] is the most general counterpart to the KWW function and is used to describe the asymmetry and broadness of the complex dielectric function by means of the following equation

$$\varepsilon^*(\omega) = \varepsilon_\infty + \frac{\Delta\varepsilon}{\left(1+(i\omega\tau_{HN})^{\beta}\right)^{\gamma}} \qquad \text{[2.1.2.1.13.]}$$

where two new parameters such as β and γ ($\beta, \gamma \leq 1$) describing the asymmetry and the broadness have been added. Debye equation is recovered when $\beta = \gamma = 1$. It should be noted that although this Havriliak Negami (HN) equation provides a value for the characteristic relaxation time (τ_{HN}), this value would depend on the details of the analysis procedure. Thus it is often preferred to characterize the relaxation by means of the peak relaxation time, i.e. that calculated as $\tau^* = 1/\omega_P$. From the HN parameters this characteristic relaxation time τ^* can be determined as

$$\tau^* = \tau_{HN} \left[\sin \frac{\beta \pi}{2 + 2\gamma} \right]^{-1/\beta} \left[\sin \frac{\beta \gamma \pi}{2 + 2\gamma} \right]^{1/\beta} \qquad [2.1.2.1.14.]$$

Moreover, from the HN equation [2.1.2.1.13.] an approximated value of the full-width-half-maximum (*fwhm*) of the loss peak can be determined from the β and γ shape parameters [31] as:

$$fwhm(\beta, \gamma) = -0.516 + \frac{1.058}{\beta} + \frac{0.039}{\gamma} + \frac{0.563}{\beta \gamma} \qquad [2.1.2.1.15.]$$

Finally, some years ago the Alvarez-Alegría-Colmenero (AAC) function [24, 32] was proposed as a modification of the conventional already mentioned Havriliak Negami function [2.1.2.1.13.] that corresponds well with the frequency domain counter part of the KWW function, so reducing the number of free parameters involved. In fact, the AAC function is a variation of the conventional Havriliak Negami equation where the β and γ shape parameters are related in the following way:

$$\gamma = 1 - 0.8121(1 - \beta)^{0.387} \qquad [2.1.2.1.16.]$$

and the corresponding KWW parameters are [33]:

$$\beta_{KWW} = \left(\beta \cdot \gamma\left(\beta\right)\right)^{1/1.23} \qquad [2.1.2.1.17.]$$

$$\log \tau_{KWW} = \log \tau_{HN} - 2.6 \cdot \left(1-\beta\right)^{0.5} \cdot \exp\left(-3\beta\right) \qquad [2.1.2.1.18.]$$

The main dielectric relaxation process in most polymers is the α–relaxation which, as already mentioned, is considered a cooperative process involving segmental motions, thus subjected to interactions of both intra- and intermolecular nature. The temperature dependence of the α-relaxation is different from the more usual Arrhenius law

$$\log \tau = \log \tau_0 + \frac{E_A}{R\,T} \log e \qquad [2.1.2.1.19.]$$

where τ_0 is a preexponential factor, R is the gas constant, and E_A is the activation energy related to rotational barriers. Contrary, the experimental temperature dependence of the characteristic α–relaxation time used to be well described by a Vogel-Fulcher-Tamman (VFT) equation [34, 35]

$$\log \tau = \log \tau_0 + \frac{B}{T - T_0} \qquad [2.1.2.1.20.]$$

where τ_0 use to be close to the reciprocal of an attempt frequency ($\tau_0 = 10^{-11}$-10^{-13} s), B is an energetic parameter and T_0 is the so-called ideal glass transition or Vogel temperature, which typically takes a value of 30-70 K below the experimental T_g. Note that $\tau \to \infty$ when $T \to T_0$ (see Figure 2.3.3.).

In glass-forming systems, fragility determines how quickly the dynamics of a given material slow down as it is cooled towards the glass transition. This can be understood by looking at Figure 2.1.2.1.3. where two different trends can be distinguished depending on the relaxation time temperature dependence.

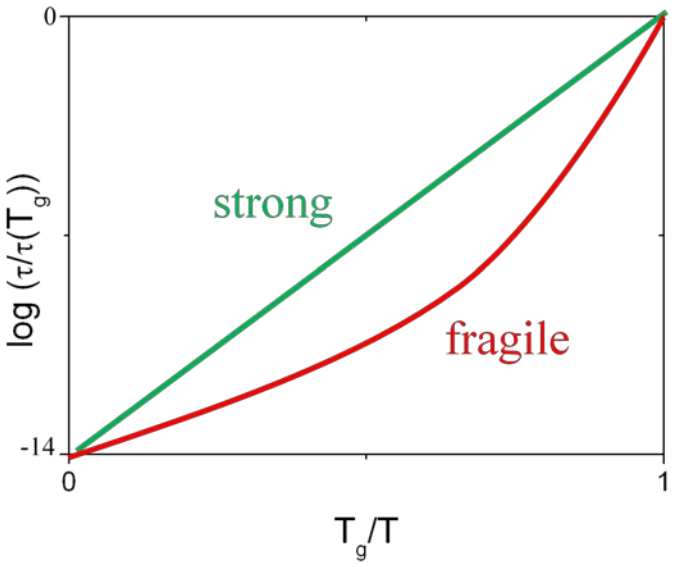

Figure 2.1.2.1.3. Fragility representation.

If it deviates from the Arrhenius behavior [36] the glass-former presents a high fragility and it is called “fragile”, whereas that obeying the Arrhenius behavior exhibits a low fragility and it is called “strong” [18].

The most common definition of fragility characterizes the slope of the relaxation time with temperature as T_g is approached from above:

$$m = \left(\frac{d \log \tau}{d\left(T_g / T \right)} \right)_{T = T_g} \qquad [2.1.2.1.21.]$$

where “m” is the fragility index.

On the other hand, fragility can be also characterized from the B and T_0 Vogel-Fulcher-Tamman (VFT) parameters as

$$D = \frac{B}{T_0} \qquad [2.1.2.1.22.]$$

where "*D*" is a fragility parameter [37, 38]. Hence, the most fragile glass-forming systems are those presenting small "*D*" values.

Equivalent to the above VFT equation [2.1.2.1.20.], Williams-Landel-Ferry law (WLF) [39] is usually used in the polymer field, often to describe the viscosity (η) temperature dependence:

$$\log \eta = \log \eta\left(T_g\right) + \frac{-\frac{C_1}{2.3}\left(T - T_g\right)}{C_2 + T - T_g} \qquad [2.1.2.1.23.]$$

where C_1 and C_2 are the so-called William-Landel-Ferry parameters that for a polymer commonly take values of around 17 and 50 K, respectively [40].

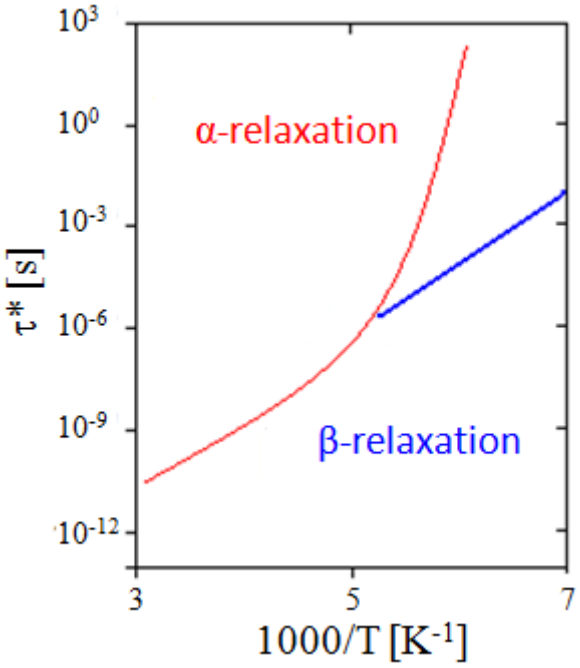

Figure 2.1.2.1.4. Comparison of the characteristic relaxation time temperature dependence for the different relaxation processes.

As already mentioned, many systems exhibit local molecular mobility below T_g, which results in several secondary relaxations where the molecular mechanisms have an intramolecular character in many cases. A general view consists of attributing such secondary dielectric relaxation to localized rotational fluctuations of the dipole vector, which may be due to local conformational rearrangements. The temperature dependence of the time scale for the secondary relaxations is usually well described by an Arrhenius law [2.1.2.1.19.]. In many cases this temperature dependence seems to indicate a merging of the secondary and the α-relaxations (see Figure 2.1.2.1.4.) giving rise to a unique relaxation process, sometimes referred to as αβ-relaxation.

When compared, the shapes of the α and the secondary relaxation functions present some similarities as well as some differences. The common feature refers to the fact that the width of the loss peak, which for the secondary relaxation increases dramatically when the temperature decreases, although in the α-relaxation case this is less dramatic, being the width of the secondary relaxation much larger mainly at low temperatures (see Figure 2.1.2.1.5.). With regard to the asymmetry, the α-loss peak use to be markedly asymmetric whereas the secondary relaxation loss peak is rather symmetric.

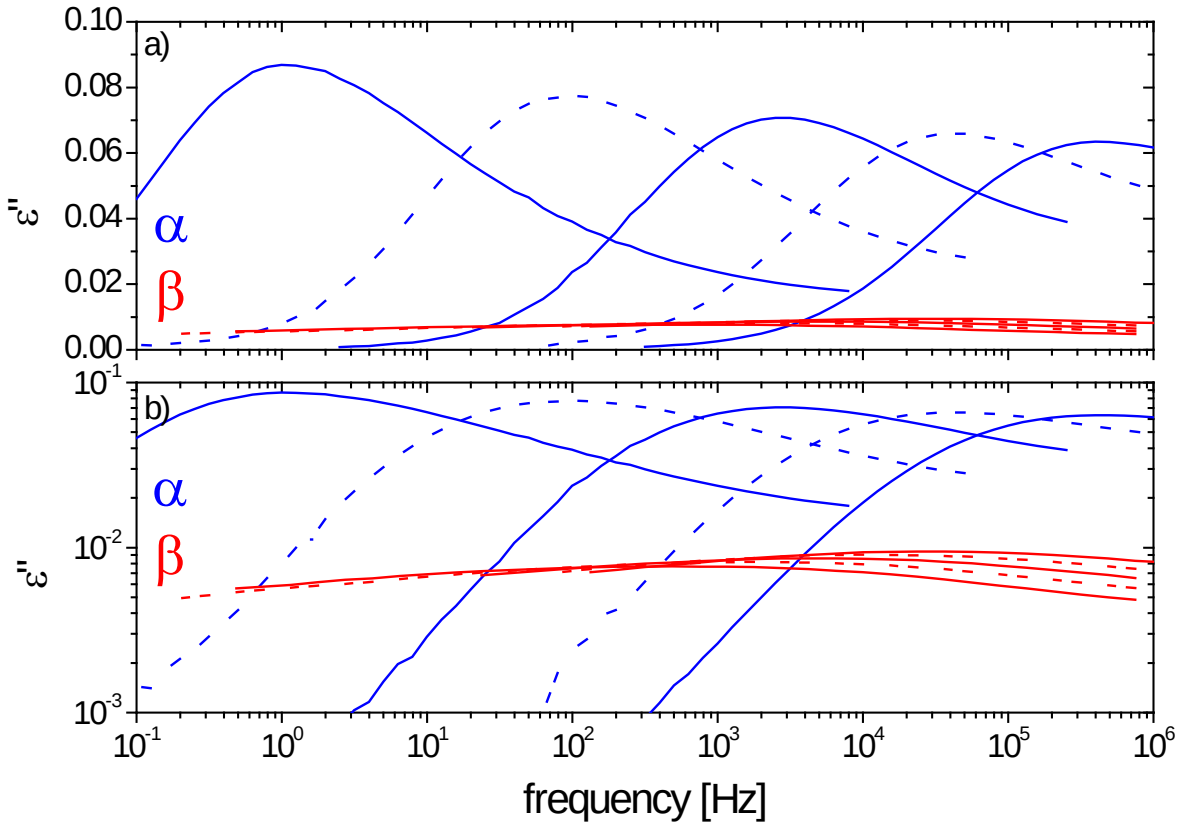

Figure 2.1.2.1.5. Comparison of the loss peak for the α-relaxation and the secondary relaxation processes.

2.2. Polymer Blends

Polymer blends are formed when at least two components are mixed together to create a new polymeric structure with different physical properties. In this way, blending of polymers allows the creation of new materials combining the properties of the polymers involved. As the synthesis of new polymers implies many difficulties, blending the existing polymers to optimize their end-use has been found to be a more successful methodology, turning the study of the polymer blends in general (and its dynamics in particular) into a very important topic.

There are three major types of polymer blends:

- Inmiscible polymer blends (heterogeneous polymer blends): Mixtures that are phase-separated due to the repulsive interaction between the components. They exhibit two different glass-transition temperatures attributed to each of the pure polymers. Most polymer blends belong to this group.
- Partially miscible polymer blends: Mixtures that are phase-separated exhibiting two different glass-transition temperatures intermediate between the pure polymers.
- Miscible polymer blends (homogeneous polymer blends): Mixtures that are presented as single-phase structures. They exhibit a (broad) glass-transition temperature range intermediate between those of the pure polymers.

In particular, for this work the attention has been focused on miscible polymer blends, which are mixtures composed of two different thermodynamically miscible polymers, i. e., a two component system mixed at the molecular level.

Most of the works in miscible polymer blends have been focused on the investigation from the thermodynamical point of view by studying the miscibility conditions and phase diagram. Also the dynamics of polymer blends has been extensively studied during last years [33, 41, 42, 43, 44, 45, 46, 47, 48, 49, 50, 51, 52, 53, 54, 55, 56, 57, 58, 59, 60, 61, 62, 63, 64, 65, 66, 67, 68, 69, 70, 71, 72, 73, 74, 75, 76, 77, 78, 79, 80, 81, 82, 83, 84, 85, 86, 87, 88, 89, 90, 91, 92, 93, 94, 95, 96, 97, 98, 99, 100, 101, 102, 103, 104, 105, 106, 107, 108, 109, 110, 111, 112, 113, 114, 115, 116, 117, 118, 119, 120, 121, 122, 123, 124, 125, 126, 127].

2.2.1. Thermodynamics

The thermodynamic condition for a binary system to be miscible can be define in terms of the Gibbs free energy of the blend (G_m) and its composition and temperature dependence [128, 129, 130]. First, a system will be miscible when the variation of the Gibbs free energy (ΔG_m) is negative:

$$\Delta G_m < 0 \qquad [2.2.1.1.]$$

However, this condition is not enough since miscibility also depends on how G varies with composition. Hence, a second condition is established to avoid phase separation:

$$\left(\frac{\partial^2 \Delta G_m}{\partial \phi_i^2}\right)_{T,P} > 0 \qquad [2.2.1.2.]$$

where ϕ_i is the volume fraction for each component forming the blend.

The Gibbs free energy variation (ΔG_m) is composed by enthalpic and entropic contributions:

$$\Delta G_m = \Delta H_m - T \cdot \Delta S_m \qquad [2.2.1.3.]$$

where ΔH_m and ΔS_m are the enthalpy and the entropy of mixing, respectively.

The theory of Flory-Huggins [131] define the entropy of mixing as:

$$\Delta S_m = - N_{Av}\ K \left(n_A \ln \phi_A + n_B \ln \phi_B \right) \qquad [2.2.1.4.]$$

where N_{AV} is the Avogadro's constant, K is the Boltzmann's constant, n refers to the number of moles and ϕ is the volume fraction, being A and B the two components forming the system.

On the other hand, applying the concept of regular solutions and assuming all pair interactions, the enthalpy of mixing can be defined as:

$$\Delta H_m = N_{Av}\ K\ T\ \chi\ \phi_A\ \phi_B \qquad [2.2.1.5.]$$

where χ refers to the so-called Flory-Huggins binary interaction parameter.

Hence, for a binary system the expression obtained previously for the Gibbs free energy variation (ΔG_m) [2.2.1.3.] can be rewritten as:

$$\Delta G_m = N_{Av}\ K\ T \left[\left(\chi\ \phi_A\ \phi_B \right) + \left(n_A \ln \phi_A + n_B \ln \phi_B \right) \right] \qquad [2.2.1.6.]$$

where the first term refers to the enthalpic contribution and the second to the entropic contribution.

From this expression we can deduce that for polymers having very high molecular weights the entropic contribution becomes very small (low "n" values) and the miscibility or inmiscibility of the binary system mainly depends on the enthalpic contribution. Therefore, for high molecular weights miscibility can only be achieved when the Flory-Huggins interaction parameter (χ) is negative.

Nevertheless, polymer blends do not present the ideal thermodynamic behavior typical of the binary systems due to the macromolecular character of their components and the molecular weights distributions. In fact, a polymer blend exhibits a phase diagram separation, i.e. it can present one or two phases depending on the temperature range.

The phase diagrams more representative are the so-called LCST (Lower Critical Solution Temperature) and UCST (Upper Critical Solution Temperature) phase diagrams. In the LCST phase diagram it can be observed that a monophasic miscible system separates into two phases as temperature increases. However, below the LCST the system will remain as monophasic independently on the composition. Contrary, in the UCST phase diagram, by heating we go from a two phase system (inmiscible) towards a single phase system.

Figure 2.2.1.1. shows a schematic representation of both types of phase diagrams.

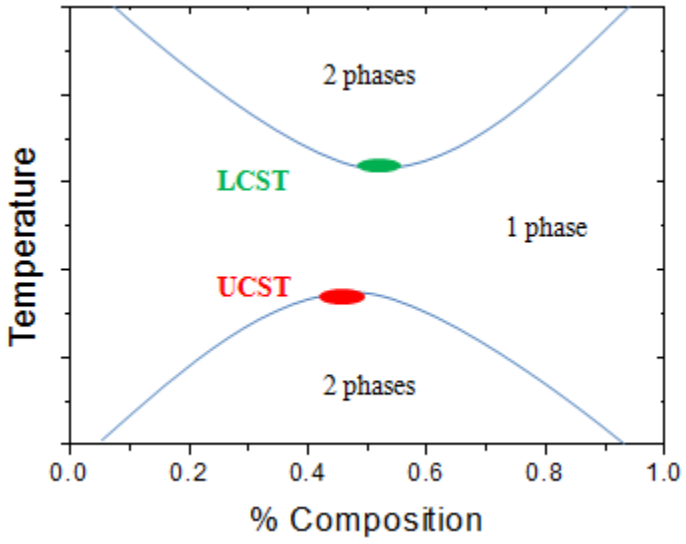

Figure 2.2.1.1. Phase diagram of a binary polymeric system.

On the other hand, the interaction parameter of Flory-Huggins (χ) can be determined also in miscible blends by measuring concentrations fluctuations using scattering techniques. For that, a miscible polymer blend is supposed to be at equilibrium having an average composition of *A* monomers (ϕ). In a small volume formed by "*n*" total monomers with $n_A = n\phi$ *A* monomers, a small fluctuation in composition ($\delta\phi$) can take place spontaneously at equilibrium:

$$\delta\phi \equiv \phi - \bar{\phi} \cdot \qquad [2.2.1.7.]$$

In fact, it can be interpreted as an exchange of *A* and *B* monomers since there is a transfer of *A* monomers (δn_A) to this small volume that occurs simultaneously than a transfer of the same quantity of *B* monomers out of the small volume:

$$\delta n_A = n\delta\phi \cdot \qquad [2.2.1.8.]$$

Hence, the free energy of mixing in this small volume (ΔG_m) can be written in terms of the number of monomers exchanged defining its derivative as the exchange chemical potential:

$$\frac{\partial \Delta G_m}{\partial \phi}\,\delta\phi = \frac{\partial \Delta G_m}{\partial (n\phi)}\,n\delta\phi = \frac{\partial \Delta G_m}{\partial n_A}\,\delta n_A \qquad [2.2.1.9.]$$

Therefore, the free energy change (δG) resulting from such fluctuation is the sum of the free energy change in the small volume and that of the rest of the blend. It should be noted that as the free energy change is of the order of the thermal energy ($\delta G \approx kT$) the mean-squared composition fluctuation can be written as:

$$\left\langle (\delta\phi)^2 \right\rangle \approx kT \left(\frac{\partial^2 \Delta G_m}{\partial \phi^2} \right)^{-1} = \frac{kT}{n} \left(\frac{\partial^2 \Delta \bar{G}_m}{\partial \phi^2} \right)^{-1} \qquad [2.2.1.10.]$$

where $\Delta \bar{G}_m$ refers to the free energy of mixing per site. From this expression it can be deduced that thermally-driven concentration fluctuations decrease as volume increases.

The regime where the study has been focused is that of small wavevector ($q < 1/R$) that is called "Intermolecular regime" and is controlled by concentration fluctuations as a consequence of the difference in the number of chains in a given volume $1/q^3$. Assuming that there are no interactions between the chains, the scattering function can

be defined as the mean-square fluctuation in the number of monomers in the volume $1/q^3$ normalized by the number of monomers n_q in such volume:

$$S(q) = \frac{\left\langle (\delta n_q)^2 \right\rangle}{n_q} \qquad [2.2.1.11.]$$

And by applying equation [2.2.1.8.] the above expression can be rewritten as:

$$S(q) = \frac{\left\langle (\delta n_A)^2 \right\rangle}{n} = n \left\langle (\delta\phi)^2 \right\rangle \qquad [2.2.1.12.]$$

The scattering function (*S(q)*) saturates at small values of the wavevector (*q*) because $\left\langle (\delta\phi)^2 \right\rangle \approx 1/n$. The scattering function when the wavevector tends to zero (*S(0)*) is given through the fluctuation dissipation theorem in statistical physics and gives:

$$S(0) = kT \left(\frac{\partial^2 \Delta\overline{G}_m}{\partial\phi^2} \right)^{-1} \qquad [2.2.1.13.]$$

being related with the second derivative of the free energy of mixing.

By applying the theory of Flory-Huggins in the general case of an asymmetric blend:

$$\frac{\partial^2 \overline{G}_m}{\partial\phi^2} = kT \left[\frac{1}{N_A\phi} + \frac{1}{N_B(1-\phi)} - 2\chi \right] = 0 \qquad [2.2.1.14.]$$

we obtain the following expression that enables determining the interaction parameter of Flory-Huggins (χ):

$$\frac{1}{S(0)} = \frac{1}{kT} \frac{\partial^2 \Delta\overline{G}_m}{\partial\phi^2} = \frac{1}{N_A\phi} + \frac{1}{N_B(1-\phi)} - 2\chi \qquad [2.2.1.15.]$$

It should be noted that the Random-Phase-Approximation (RPA) [132] is a mean-field model and extends the above equation to non-zero wavevectors (*q*) using the form factor of an ideal chain *P(q, N)*:

$$\frac{1}{S(q)} = \frac{1}{N_A \phi P(q, N_A)} + \frac{1}{N_B (1-\phi) P(q, N_B)} - 2\chi \qquad [2.2.1.16.]$$

However, it fails at the equilibrium and a more general model called "Ornstein-Zernike" [133] that is in function of the correlations that exponentially decay can be used.

2.2.2. Dynamics in Polymer Blends

The most extended criterion for polymer miscibility establishes that a miscible polymer blend exhibits a unique glass-transition temperature. Whereas for homopolymers a rather abrupt step in the heat capacity is observed by e.g., Differential Scanning Calorimetry (DSC), for polymer blends usually a monotonous increase extending over a broad temperature range in the interval between the two T_g's of the pure polymers is observed. Due to this broad glass-transition observed for blends [134, 135, 136], an average glass-transition temperature $<T_g>$ is usually determined from its midpoint although this concept has been critically revised.

Dynamics in polymer blends is a very important topic and it has been widely investigated over the past years. Different experimental techniques, like Differential Scanning Calorimetry (DSC), Dielectric Spectroscopy (DS), Nuclear Magnetic Resonance (NMR) and Neutron Scattering have been used to analyze the dynamics of miscible polymer blends. All these investigations reflect not only a markedly broadening of the dynamic response compared to that of the pure components as temperature decreases, but also a dynamic heterogeneity. A system is called as

"dynamically heterogeneous" when two different mean relaxation times (τ^*) are observed, each of them corresponding to the dynamics of each component modified by blending. Therefore, despite these blends seem to be well-mixed at the molecular level, the components in the blend exhibit different dynamical behavior, which is reflected in two distinct relaxation times with different temperature dependences [137, 138, 139]. On the contrary, a system is called as "dynamically homogeneous" when only a single relaxation time (τ^*) is detected for the segmental dynamic relaxation (α-relaxation), which, as aforementioned, is related with the glass transition phenomenon.

Trying to explain both effects, the broadening of the relaxation function and the dynamic heterogeneity, two basic theoretical models have been proposed assuming that the dynamics of one of the blend components is determined by the neighbours located in a finite volume centered on it:

Models based on thermally driven concentration fluctuations (TCF). These models postulate that the thermally driven concentration fluctuations are relevant to calculate the local composition of a blend in a volume V around a segment "i" (ϕ_i). The idea of these models is that the local concentration fluctuations are quasi-stationary near T_g since their average relaxation time is much longer than that of the α–relaxation. Therefore, the sample can be considered as divided into subcells of size V, each of them having a given local composition (ϕ_i) as well as a local T_g ($T_g^i = T_g(\phi_i)$). This fact leads to think about a distribution of local concentrations all over the blend that gives rise to a distribution of characteristic relaxation times concerning the α–relaxation. All this allows understanding the temperature dependence broadening observed for the

relaxation function of each component in the blend compared to that of the pure component. Fischer and co-workers [140, 141] postulated the first model concerning this idea, which gave a quantitative description of this α–relaxation broadening in various miscible blends. This model was improved by Kumar et al. [142, 143, 144, 145, 146, 147] who were able to describe also the two different characteristic relaxation times of the components in the blend.

Roland and Ngai [148, 149, 150, 151, 152, 153, 154] created a model for the blends based on the Coupling Model ideas [155, 156, 157, 158, 159, 160, 161]. Here the local concentration allows determining the coupling parameter as well as the relaxation function shape. As a consequence one obtains a distribution of coupling parameters that gives rise to a distribution of relaxation times using the Coupling Model equation, where both the coupling parameter and the α–relaxation time are correlated.

Summarizing, these models are able to describe the relaxation function broadening as temperature decreases towards $\langle T_g \rangle$. Nevertheless, they fail in some aspects: the size of the relevant volume V that increases too much on approaching $\langle T_g \rangle$ and the impossibility to explain the presence of two different characteristic relaxation times for the components in the blend (dynamic heterogeneity) at T » T_g where it is observed that the pure polymer and the corresponding component in the blend can behave very similar being practically indistinguishable.

Models based on self-concentration (SC). These models consider that the dynamic heterogeneity is mainly determined from the chain connectivity effect [162, 163].

Due to the limitation of the models based on Thermally Concentration Fluctuations (TCF) Chung et al. introduced the "effective concentration" term [162, 164]. The idea is that assuming a blend composed of two polymers *A* and *B*, the local concentration around a segment of polymer *A* will be always richer in this component compared to the bulk composition due to chain connectivity. Then, two different "effective" glass-transitions (T_{geff}) are defined for both components in the blend, which at the same time imply different relaxation times.

Lodge and McLeish (LML) [163] proposed a model where the effective concentration in a volume *V* around a given segment of polymer *A* is defined as:

$$\phi_{eff}^{A} = \phi_{S}^{A} + \left(1 - \phi_{S}^{A}\right)\langle\phi\rangle \qquad [2.2.2.1.]$$

where ϕ_{S}^{A} is the self-concentration of component *A* in the blend and $\langle\phi\rangle$ is the macroscopic composition of the blend. In the original work the self-concentration was calculated in a cubic volume of side equal to the Kuhn length [$\xi \approx l_k$, $V \approx l_k^3$] and therefore can be determined *a priori*. This implies the assumption that at T_g the α-relaxation relevant length scale is of the order of the Kuhn length.

However, the most commonly used method is to consider it as a parameter, which can vary with several factors as temperature, blend components, etc.

In this approach, the effective glass-transition of component A in the blend is calculated by the following expression:

$$T_{geff}^{A} = \langle T_g \rangle (\phi) \Big|_{\phi = \phi_{eff}^{A}} \qquad [2.2.2.2.]$$

where $\langle T_g \rangle$ is the average glass-transition, which depends on concentration, i.e. that determined by DSC for instance.

Apart from this self-concentration concept, this model takes the composition of a volume V as the macroscopic one. All this reflects that only the characteristic relaxation times of each of the blend components are taken into account leaving the distribution of relaxation times concept aside.

Summarizing, these models allow describing the relaxation function dynamic heterogeneity as well as determining an effective glass-transition (T_{geff}) for each of the components in the blend.

In conclusion, both families of models seem to be complementary. Thus, some attemps of combining both approaches have been made, namely [83, 165]. Nevertheless, there is not a completely satisfactory model for accounting the complex dynamical behavior of miscible polymer blends yet.

1. J. Areizaga, M. M. Cortázar, J. M. Elorza and J. J. Iruin, Polímeros. Editorial Síntesis (2002)

2. T. G. Fox and P. J. Flory, J. Appl. Phys., 21, 581 (1950)

3. T. G. Fox and P. J. Flory, J. Polym. Sci., 14, 315 (1954)

4. Y. Ding, , V. N. Novikov, A. P. Sokolov, A. Cailliaux, C. Dalle-Ferrier, C. Alba-Simionesco and B. Frick, Macromolecules, 37, 9264 (2004)

5. J. Mark, K. Ngai, W. Graessley, L. Mandelkern,E. Samulski, J. Koenig and G. Wignall, "Physical properties of polymers "Third Edition

6. G. P. Johari, Plastic Deformation of Amorphous and Semicrystalline Materials, Les Houches Lectures, p. 109, Les Edietions de Physique, France (1982)

7. S. R. Elliot, Physics of Amorphous Materials 2nd Ed., Longman Group UK Limited, Harlow (1990)

8. P. W. Anderson, Science, 267, 1615 (1995)

9. S. Sharifi, D. Prevosto, S. Capaccioli, M. Lucchesi and M. Paluch, J. Non-Cryst. Solids, 353, 4313 (2007)

10. G. P. Johari and M. Goldstein, J. Chem. Phys., 55, 4245 (1971)

11. R. Kubo, J. Phys. Soc. Japan, 12, 570 (1957)

12 . F. Kremer, A. Schönhals, Broadband Dielectric Spectroscopy, Springer-Verlag, Berlín (2003)

13. P. Debye, Polar Molecules, Chem. Catalog., New York (1929)

14. G. Williams, J. Non-Cryst. Sds, 1, 131-133 (1991)

15. M. T. Cicerone, F.R. Blackburn and M.D. Ediger, J. Chem. Phys., 102 (1), 471 (1995)

16. B. Frick and D. Richter, Science, 267, 1939 (1995)

17. C. A. Angell, Proc. Natl. Acad. Sci. USA, 92, 6675 (1995)

18. M. D. Ediger, C.A. Angell and S.R. Nagel, J. Phys. Chem., 100, 13200 (1996)

19. A. P. Sokolov, Science, 273, 1675 (1996)

20. I. Campbell, P.O. Mari, A. Alegría and J. Colmenero, Europhys. News, 29 (2), (1998)

21. R. Kohlrausch, Pogg. Ann. Phys., 91, 179 (1854)

22. G. Williams and D. C. Watts, Trans. Faraday Soc., 66, 80 (1970)

23. C. P. Lindsey and D. G. Patterson, J. Chem. Phys., 73, 3348 (1980)

24. F. Alvarez, A. Alegría and J. Colmenero, J. Phys. Rev. B, 44, 7306 (1991)

25. S. Havriliak, Jr* and S. J. Havriliak, Polymer, Vol. 37 No. 18, pp. 4107 (1996)

26. R. H. Cole and K. S. Cole, J. Chem. Phys., 9, 341 (1941)

27. D. W. Davidson and R.H. Cole, J. Chem. Phys., 19, 1484 (1951)

28. A. Alegría, J. Colmenero, P.O. Mari and I.A. Campbell, Phys. Rev. E, 59, 6888 (1999)

29. S. Havriliak and S. Negami, J. Polym. Sci. Polym. Symp., 14, 89 (1996)

30. S. Havriliak and S. Negami, Polymer, 8, 161 (1967)

31. G. A. Schwartz, J. Colmenero and A. Alegría, Macromolecules, 40, 3246 (2007)

32. F. Alvarez, A. Alegría and J. Colmenero, Phys. Rev. B, 47, 125 (1993)

33 . I. Cendoya, A. Alegría, J. M. Alberdi, J. Colmenero, H. Grimm, D. Richter and B. Frick, Macromolecules, 32, 4065 (1999)

34. H. Vogel, Physik Z., 22, 645 (1921)

35. G. S. Fulcher, J. Am. Ceram. Soc., 8, 339 (1925)

36 . P. G. Debenedetti and F. H. Stillinger, Nature, 410, 259 (2001)

37. C. A. Angell, J. Non-Cryst. Solids, 13, 131 (1991)

38. R. Böhmer, K. L. Ngai, C. A. Angell and D. J. Plazek, J. Chem. Phys., 99, 4201 (1993)

39. M. L. Williams, R. F. Landel and J. D. Ferry, J. Am. Chem. Soc., 77, 3701 (1955)

40. J. D. Ferry, Viscoelastic Properties of Polymers, 3rd Ed, John Wiley & Sons, New York (1980)

41 . M. Shibayama, H. Yang, R. S. Stein and C. C. Han, Macromolecules, 18, 2179 (1985)

42 . D. Schwahn, K. Mortensen and H. Yee-Maderia, Phys. Rev. Lett., 58, 1544 (1987)

43 . D. Schwahn, K. Mortensen, T. Springer, H. Yee-Maderia and R. Thomas, J. Chem. Phys., 87, 6078 (1987)

44 . C. C. Han, B. J. Bauer, B. J. Clark, Y. Muroga, M. Okada, Z. Tran-Cong. and I. C. Sanchez, Polymer, 29, 2002 (1988)

45 . R. H. Colby, Polymer, 30, 1275 (1989)

46 . H. Watanabe, M. Yamazaki, H. Yoshida, K. Adachi and T. Kotaka, Macromolecules, 24, 5365 (1991)

47 . J. Roovers and P. M. Toporowski, Macromolecules, 25, 1096 (1992)

48 . C. Le Menestrel, A. M. Kenwright, P. Sergot, F. Laupretre and L. Monnerie, Macromolecules, 25, 3020 (1992)

49 . O. Urakawa, K. Adachi and T. Kotaka, Macromolecules, 26, 2036 (1993)

50 . O. Urakawa, K. Adachi and T. Kotaka, Macromolecules, 26, 2042 (1993)

51 . A. Alegría, J. Colmenero, K. L. Ngai and C. M. Roland, Macromolecules, 27, 4486 (1994)

52 . J. A. Zawada, G. G. Fuller, R. H. Colby, L. J. Fetters and J. Roovers, Macromolecules, 27, 6861 (1994)

53 . G. C. Chung, J. A. Kornfield and S. D. Smith, Macromolecules, 27, 964 (1994)

54 . G. C. Chung, J. A. Kornfield and S. D. Smith, Macromolecules, 27, 5729 (1994)

55 . B. H. Arendt, R. M. Kannan, M. Zewail, J. A. Kornfield and S. D. Smith, Rheol. Acta, 33, 322 (1994)

56 . K. Adachi, T. Wada, T. Kawamoto and T. Kotaka, Macromolecules, 28, 3588 (1995)

57 . G. Katana, E. W. Fischer, T. Hack, V. Abetz and F. Kremer, Macromolecules, 28, 2714 (1995)

58 . B. T. Poh, K. Adachi and T. Kotaka, Macrommolecules, 29, 6317 (1996)

59 . H. Watanabe, O. Urakawa, H. Yamada and M. L. Yao, Macromolecules, 29, 755 (1996)

60 . H. Takeno, S. Koizumi, H. Hasegawa and T. Hasimoto, Macromolecules, 29, 2440 (1996)

61 . F. Alvarez, A. Alegría and J. Colmenero, Macromolecules, 30, 597 (1997)

62 . C. B. Gell, W. W. Graessley and L. J. Fetters, J. Polym. Sci., Part B: Polym. Phys., 35, 1933 (1997)

63 . C. Lartigue, A. Guillermo, J. P. Cohen-Addad, J. Polym. Sci., Part B: Polym. Phys., 35, 1095 (1997)

64 . A. Kopf, B. Dünweg, W. Paul, J. Chem. Phys., 107, 6945 (1997)

65 . B. H. Arendt, R. Krishnamoorti, J. A. Kornfield and S. D. Smith, Macromolecules, 30, 1127 (1997)

66 . S. Saxena, D. Cizmeciyan and J. A. Kornfield, Solid State Nucl. Magn. Reson., 12, 165 (1998)

67 . R. Mukhopadhyay, A. Alegría, J. Colmenero and B. Frick, J. Non-Cryst. Solids, 233, 235 (1998)

68 . Z. L. Peng, B. G. Olson, R. Srithawatpong, J. D. McGervey, A. M. Jamieson, H. Ishida, T. M. Meier and A. F. Halasa, J. Polym. Sci. Part B: Poly. Phys., 36, 861 (1998)

69 . A. Arbe, A. Alegría, J. Colmenero, S. Hoffmann, L. Willner and D. Richter, Macromolecules, 32, 7572 (1999)

70 . J. Luettmer-Strathmann, J. E. G. Lipson, Macromolecules, 32, 1093 (1999)

71 . J. A. Pathak, R. H. Colby, G. Floudas and R. Jerome, Macromolecules, 32, 2553 (1999)

72 . S. Adams and D. B. Adolf, Macromolecules, 32, 3136 (1999)

73 . J. W. Sy and J. Mijovic, Macromolecules, 33, 933 (2000)

74 . S. Hoffmann, L. Willner, D. Richter, A. Arbe, J. Colmenero and B. Farago, Phys. Rev. Lett., 85, 772 (2000)

75 . M. Doxastakis, M. Kitsiou, G. Fytas, D. N. Theodorou, N. Hadjichristidis, G. Meier and B. Frick, J. Chem. Phys., 112, 8687 (2000)

76 . M. Dionísio, A. C. Fernandes, J. F. Mano, N. T. Correia and R.C. Sousa, Macromolecules, 33, 1002 (2000)

77 . B. Min, X. Qiu, M. D. Ediger, M. Pitsikalis and N. Hadjichristidis, Macromolecules, 34, 4466 (2001)

78 . S. Hoffmann, D. Richter, A. Arbe, J. Colmenero and B. Farago, Appl. Phys. A., 74, S442 (2002)

79 . A. Alegría, D. Gómez and J. Colmenero, Macromolecules, 35, 2030 (2002)

80 . E. Leroy, A. Alegría and J. Colmenero, Macromolecules, 35, 5587 (2002)

81 . S. Salaniwal, R. Kant, R.H. Colby and S. K. Kumar, Macromolecules, 35, 9211 (2002)

82 . Y. Hirose, O. Urakawa and K. Adachi, Macromolecules, 36, 3699 (2003)

83 . E. Leroy, A. Alegría and J. Colmenero, Macromolecules, 36, 7280 (2003)

84 . C. Lorthioir, A. Alegría and J. Colmenero, Phys. Rev. E., 68, 031805 (2003)

85 . J. C. Haley, T. P. Lodge, Y. He, M. D. Ediger, E. D. von Meerwall and J. Mijovic, Macromolecules, 36, 6142 (2003)

86 . T. R. Lutz, Y. Y. He, M. D. Ediger, H. Cao, G. Lin and A. A. Jones, Macromolecules, 36, 1724 (2003)

87 . J. Wolak, X. Jia, H. G. Gracz, E. O. Stejskal, J. L. White, M. Wachowicz and S. Jurga, Macromolecules, 36, 4844 (2003)

88 . S. Kamath, R. H. Colby and S. K. Kumar, Phys. Rev. E, 67. 010801(R) (2003)

89 . S. Kamath, R. H. Colby and S. K. Kumar, Macromolecules, 36, 8567 (2003)

90 . X. Jin, S. Zhang and J. Runt, Macromolecules, 37, 8110 (2004)

91 . K. L. Ngai and C. M. Roland, Macromolecules, 37, 2817 (2004)

92 . S. H. Zhang, X. Jin, P. C. Painter and J. Runt, Polymer, 45, 3933 (2004)

93 . J. C. Haley and T. P. Lodge, J. Rheol., 48, 463 (2004)

94 . J. A. Pathak, S. Kumar and R. H. Colby, Macromolecules, 37, 6994 (2004)

95 . J. C. Haley and T. P. Lodge, Colloid Polym. Sci., 282, 793 (2004)

96 . T. R. Lutz, Y. Y. He, M. D. Ediger, M. Pitsikalis and N. Hadjichristidis, Macromolecules, 37, 6440 (2004)

97 . Y. Y. He, T. R. Lutz and M. D. Ediger, Macromolecules, 37, 9889 (2004)

98 . V. G. Sakai, C. Chen, J. K. Maranas and Z. Chowdhuri, Macromolecules, 37, 9975 (2004)

99 . V. G. Sakai, J. K. Maranas, Z. Chowdhuri, I. Peral and J. R. D. Copley, J. Polym. Sci., Part B: Polym. Phys., 43, 2914 (2004)

100 . E. Jaramillo, D. T. Wu, G. S. Grest and J. G. Curro, J. Chem. Phys., 120, 8883 (2004)

101 . A. Neelakantan and J. K. Maranas, J.. Chem. Phys., 120, 465 (2004)

102 . A. Neelakantan and J. K. Maranas, Macromolecules, 37, 8473 (2004)

103 . A. Neelakantan and J. K. Maranas, J. Chem. Phys., 120, 1617 (2004)

104 . S. Koizumi, J. Poly. Science Part B:Polym. Phys., 42, 3148 (2004)

105 . D. Cangialosi, G. A. Schwartz, A. Alegría and J. Colmenero, J. Chem. Phys., 123, 144908 (2005)

106 . K. Mpoukouvalas, G. Floudas, S. H. Zhang and J. Runt, Macromolecules, 38, 552 (2005)

107 . E. Krygier, G. Lin, J. Mendes, G. Mudankela, D. Azar, A. A. Jones, J. A. Pathak, R. H. Colby, S. Kumar, G. Floudas, R. Krishnamoorti and R. Faust, Macromolecules, 38, 7721 (2005)

108 . J. H. Lee, L. J. Fetters, L. A. Archer and A. F. Halasa, Macromolecules, 38, 3917 (2005)

109 . T. R. Lutz, Y. Y. He and M. D. Ediger, Macromolecules, 38, 9826 (2005)

110 . H. Cao, G. Lin and A. A. Jones, J. Polym. Sci., Part B: Polym. Phys., 43, 2433 (2005)

111 . Y. Y. He, T. R. Lutz, M. D. Ediger, M. Pitsikalis, N. Hadjichristidis and E. D. von Meerwall, Macromolecules, 38, 6216 (2005)

112 . J. Wolak and J. L. White, Macromolecules, 38, 10466 (2005)

113 . A. C. Genix, A. Arbe, F. Alvarez, J. Colmenero, L. Willner and D. Richter, Phys. Rev. E, 72, 031808 (2005)

114 . B. Farago, C. Chen, J. K. Maranas, S. Kamath, R. H. Colby, A. J. Pasqualeand T. E. Long, Phys. Rev. E, 72, 031809 (2005)

115 . A. Neelakantan, A. May and J. K. Maranas, Macromolecules, 38, 6598 (2005)

116 . D. Bedrov and G. D. Smith, Macromolecules, 38, 10314 (2005)

117 . J. Luettmer-Strathmann, J. Chem. Phys., 123, 014910 (2005)

118 . Y. Miwa, K. Usami, K. Yamamoto, M. Sakaguchi, M. Sakai and S. Shimada, Macromolecules, 38, 2355 (2005)

119 . D. Cangialosi, A. Alegría and J. Colmenero, Macromolecules, 39, 7149 (2006)

120 . C. M. Roland, K. J. McGrath and R. Casalini, Macromolecules, 39, 3581 (2006)

121 . O. Urakawa, T. Ujii and K. Adachi, J. Non-Cryst. Solids, 352, 5042 (2006)

122 . R. Pérez Aparicio, A. Arbe, J. Colmenero, W. Schweika, W. Richter, L. J. Fetters, Macromolecules, 39, 1060 (2006)

123 . M. Tyagi, A. Arbe, J. Colmenero, B. Frick and J. R. Stewart, Macromolecules, 39, 3007 (2006)

124 . A. J. Moreno and J. Colmenero, J. Chem. Phys., 124, 184906 (2006)

125 . D. Bedrov and G. D. Smith, Macromolecules, 39, 8526 (2006)

126 . J. Luettmer-Strathmann and M. Mantina, J. Chem. Phys., 124, 174907 (2006)

127 . A. F. May and J. K. Maranas, J. Chem. Phys., 125, 024906 (2006)

128. "Polymer Blends", D. R. Paul and J. W. Barlow (Eds), Academic Press, New York (1978)

129. "Polymer-Polymer Miscibility", O. Olabisi, L. M. Robeson and M. T. Shaw, Academic Press, New York (1979)

130. "Polymer Blends and Mixtures" NATOS ASI Series E 89, Martinus Nijhoff. Publishers. Dordrecht (1985)

131. P. J. Flory, "Principles of Polymer Chemistry", Cornell University Press, Ithaca (1953)

132 . P. G. De Gennes, "Scaling Conecpts in Polymer Physics", Cornell University Press (1982)

133 . J. S. Higgins and H. C. Benoit, "Polymers and Neutron Scattering", Clarendon Press, Oxford (1994)

134 . C. A. Trask and C. M. Roland, Macromolecules, 22, 256 (1989)

135 . J. Roovers and P. M. Toporowski, Macromolecules, 25, 3454 (1992)

136 . J. Roovers and P. M. Toporowski, Macromolecules, 1096, 25 (1992)

137 . J. B. Miller, K. J. Mcgrath, C. M. Roland, C. A. Trask and A. N. Garroway, Macromolecules, 23, 4543 (1990)

138 . J. Kanetakis, G. Fytas, F. Kremer and T. Pakula, Macromolecules, 25, 3484 (1992)

139 . G. C. Chung, J. A. Kornfield and S. D. Smith, Macromolecules, 27, 964 (1994)

140 . A. Zetsche and E. Fischer, Acta Polym., 45, 168-175 (1994)

141 . G. Katana, E. W. Fischer, T. Hack, V. Abetz and F. Kremer, Macromolecules, 28, 2714 (1995)

142 . S. K. Kumar, R. H. Colby, S. H. Anastasiadis and G. J. Fytas, Chem. Phys., 105, 3777 (1996)

143 . S. Salaniwal, R. Kant, R. H. Colby and S. K. Kumar, Macromolecules, 35, 9211 (2002)

144 . S. Kamath, R. H. Colby and S. K. Kumar, Phys. Rev. E, 67, 010801(R) (2003)

145 . S. Kamath, R. H. Colby and S. K. Kumar, Macromolecules, 36, 8567 (2003)

146 . S. Kamath, R. H. Colby, S. K. Kumar, K. Karatasos, G. Floudas, G. Fytas and J. E. L. Roovers, J. Chem. Phys., 111, 6121 (1999)

147 . R. Kant, S. K. Kumar and R. H. Colby, Macromolecules, 36, 10087 (2003)

148 . C. M. Roland and K. L. Ngai, Macromolecules, 24, 2261 (1991)

149 . C. M. Roland and K. L. Ngai, Macromolecules, 25, 363 (1992)

150 . C. M. Roland and K. L. Ngai, J. Rheol., 36, 1691 (1992)

151 . C. M. Roland, K. L. Ngai, J. M. O´Reilly and J. S. Sedita, Macromolecules, 25, 3906 (1992)

152 . A. Alegría, J. Colmenero, K. L. Ngai and C. M. Roland, Macromolecules, 27, 4486 (1994)

153 . K. L. Ngai and C. M. Roland, Macromolecules, 28, 4033 (1995)

154 . C. M. Roland and K. L. Ngai, Macromolecules, 33, 3184 (2000)

155 . K. L. Ngai and C. M. Roland, Macromolecules, 26, 6824 (1993)

156 . K. L. Ngai and C. M. Roland, Macromolecules, 27, 2454 (1994)

157 . K. L. Ngai and D. J. Plazek, Rubber Chem Technol., 68, 376 (1995)

158 . P. G. Santagelo, K. L. Ngai and C. M. Roland, Macromolecules, 29, 3651 (1996)

159 . R. Casalini, K. L. Ngai, C. G. Robertson and C. M. Roland, J. Poly. Sci. Phys. Ed., 38, 1841 (2000)

160 . K. L. Ngai and D. J. Plazek, Macromolecules, 35, 9136 (2002)

161 . K. L. Ngai and C. M. Roland, Polymer, 43, 567 (2002)

162 . G. C. Chung, J. A. Kornfield and S. D. Smith, Macromolecules, 27, 5729 (1994)

163 . T. P. Lodge and T. C. B. McLeish, Macromolecules, 33, 5278 (2000)

164 . G. C. Chung, J. A. Kornfield and S. D. Smith, Macromolecules, 27, 964 (1994)

165 . S. Shenogin, R. Kant, R. H. Colby and S. K. Kumar, Macromolecules, 40, 5767 (2007)

3. Experimental Section

3.1. Synthesis of Functionalized Polymers

3.1.1. Synthesis Methodology

All the functionalized polymers used for this thesis work have been synthesized by the group of Professor Roderic P. Quirk of the University of Akron in USA.

The synthesis technique used to produce the functionalized polymers investigated here consisted of combining living anionic polymerization with transition metal-catalyzed hydroxylation reaction, which allows the addition of several polar groups of varying polarities precisely placed via a silyl hydride functionality. The resulting product was a well-defined and pre-determined polymer designed with high precision in the position of the functional groups, and the molecular weight.

Scheme 3.1.1.1. shows the overall polymer synthesis in detail followed for the chain-end and in-chain functionalized polystyrenes.

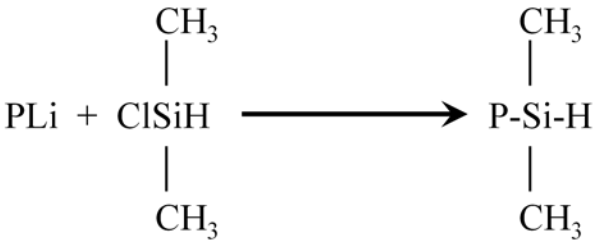

a)

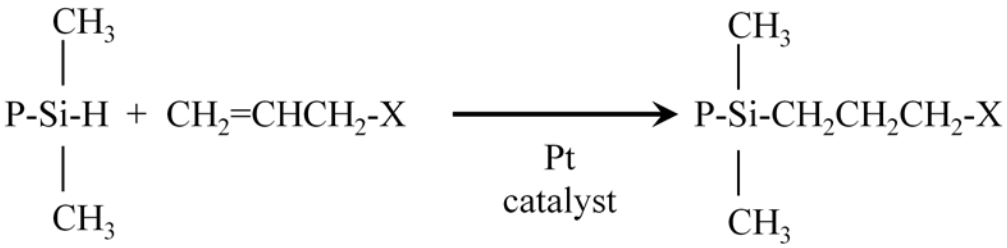

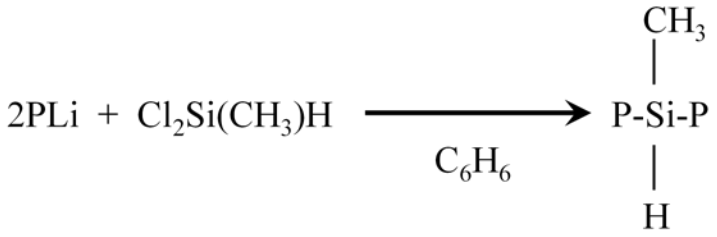

b)

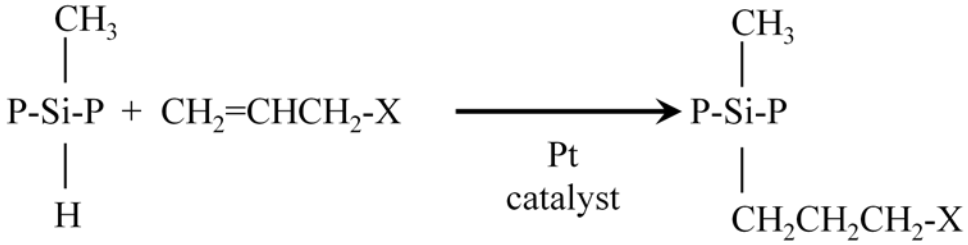

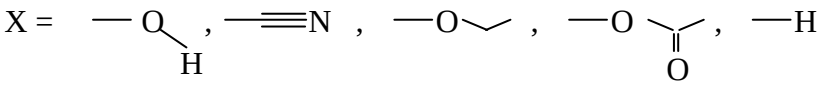

Scheme 3.1.1.1. Methodology for the synthesis of chain-end functionalized polymers (a) and in-chain functionalized polymers (b)

where we can distinguish two steps. First, the termination of the living poly(styryl)lithium with chlorodimethylsilane gives rise to the chain-end or in-chain silyl hydride-functionalized polystyrene, depicted in Scheme 3.1.1.1. a) and b) , respectively.

This can then react with a large variety of substituted alkenes in order to achieve the desired chain-end or in-chain functionalized polystyrene, i.e. when *one* functional group is added at the end or in the middle of the chain, respectively.

Using this method it was possible to synthesize chain-end and in-chain functionalized polymers where the functional group is the only variable [1, 2, 3]. The polymer selected

here was polystyrene mainly due to its weak dielectric relaxation and its well-known properties. This work was focused on the study of the H/CN pair of functionalized PS, which are found to provide a very similar overall dynamical behavior [4, 5].

Table 3.1.1.1. shows the different PS samples used for the study with their corresponding characteristics.

polymer	M_n [g/mol]	M_w /M_n
PS-H 2k	2200	1.05
PS-CN 2k	2200	1.05
PS-H 4k	4200	1.04
PS-CN 4k	4200	1.04
PS-H-PS 2k	2300	1.02
PS-CN-PS 2k	2300	1.02
PS-H-PS 4k	4100	1.05
PS-CN-PS 4k	4100	1.05
PVME	74000	1.49

Table 3.1.1.1. Molecular weights and the polydispersity indexes of the investigated polymers.

3.1.2. Stabilization, Cleaning and Characterization of Samples

In general, cleaning procedure has been critical in order to remove any impurities from the samples. First, the Karstedt's catalyst (in ppm amounts) used in the hydrosilation reaction was carefully removed by extraction of the hydrocarbon reaction solution with water, filtration through an activated silica gel column and treatment for 24 h with QuadraPure® TU, which is an effective scavenger of platinum (ref Aldrich Catalog). All of the chain-end and in-chain functionalized polymers were prepared from the same

batch of silyl hydride-functionalized polymer and were characterized by FTIR (Fourier Transform Infrared Spectroscopy), ^{13}C and ^{1}H NMR (Nuclear Magnetic Resonance Spectroscopy) spectroscopy and MALDI-TOF (Matrix-Assisted Laser Desorption/Ionization- Time-Of-Flight) mass spectrometry. Furthermore, before the experiments, those samples having the lowest molecular weight (2000 g/mol) were dried in the oven at 403 K for 24 h, while the samples having a larger molecular weight (4000 g/mol) were dried in the oven at 413 K for more than 24 h. Furthermore, in the case of 4 kg/mol samples a problem of stabilization was detected during the experiments, which was the reason of carrying out another type of procedure for solvent removal and purification. These chain-end 4 kg/mol samples were first dissolved in benzene and subsequently precipitated in methanol. This methodology was found useful to extract the residual components from the samples. Then, the samples were placed in a vacuum oven at room temperature overnight and heated at 413 K for a period of 24 h, under reduced pressure. After this heating period, the samples were allowed to cool to room temperature over a period of at least 12 h prior to exposure to the atmosphere, which was shown a way to avoid any sample decomposition detectable by ^{1}H NMR spectroscopy and DSC.

3.2. Preparation of PS/PVME Blends

For the preparation of the polymer blends 2k protonated and deuterated in-chain functionalized polystyrenes (PS-X-PS and dPS-X-PS, respectively) were synthesized. They were mixed with a (protonated) commercial poly(vinyl methyl ether) (PVME) obtained from Sigma Aldrich to prepare the PS/PVME miscible blends. Such commercial PVME was also characterized by Size Exclusion Cromatography (SEC or GPC) and the obtained parameters are given in Table 3.1.1.1.

Three polymer blend concentrations, containing 75% PS and 25% PVME (PS/PVME 75/25), 50% PS and 50% PVME (PS/PVME 50/50) and 25% PS and 75% PVME (PS/PVME 25/75) were prepared by dissolving the two components in toluene and by evaporating with an Argon (Ar) current. In the case of samples used for dielectric and calorimetric measurements, casting was carried out directly on the electrodes used for BDS measurements. The polymer blends were maintained at 353 K under vacuum conditions for 48 h to remove the solvent completely. In the case of deuterated samples used for Small Angle Neutron Scattering (SANS) measurements an analogue procedure was followed although here blend films were directly prepared on the hellma cells.

The miscibility of the investigated polymer blends was checked by microscopic techniques and it was found that they were miscible without problems when looking for phase separation. In fact, phase separation was not detected likely because PS molecular weights were significantly small.

3.3. Experimental Techniques

The main idea of our approach is to use the polymer functionalization as a route for the investigation of the dynamics of selective molecular groups. The study has been done using a combination of techniques such as Broadband Dielectric Spectroscopy (BDS), Rheology and Differential Scanning Calorimetry (DSC), since Rheology and Differential Scanning Calorimetry are sensitive to the overall dynamical properties whereas Broad-band Dielectric Spectroscopy is selective to dipole moment fluctuations. Structural features of the blends were characterized by means of Small Angle Neutron Scattering (SANS) experiments.

3.3.1. Broad-band Dielectric Spectroscopy (BDS)

Dielectric spectroscopy technique is used as a tool to study relaxation processes, which are caused by the rotational fluctuations of molecular dipoles. Therefore, this type of measurement will provide us with selective information about the dynamical processes accessing to a characteristic part of a molecule or system.

The technique is based on the application of an external field $\vec{E}$ to the sample, so the molecular dipole system is weakly perturbed from the equilibrium until the field is removed [6]. Once it takes place, the dipole system is able to return to the equilibrium supplying information concerning the spontaneous fluctuations in the system. This technique is usually implemented by measuring the dielectric properties of a medium as

a function of the frequency of the external oscillating field. However, it offers also the possibility of studying the system response in the time domain.

The typical experiment (the one used by us) would consist in using the sample as the insulator of a parallel plate capacitor:

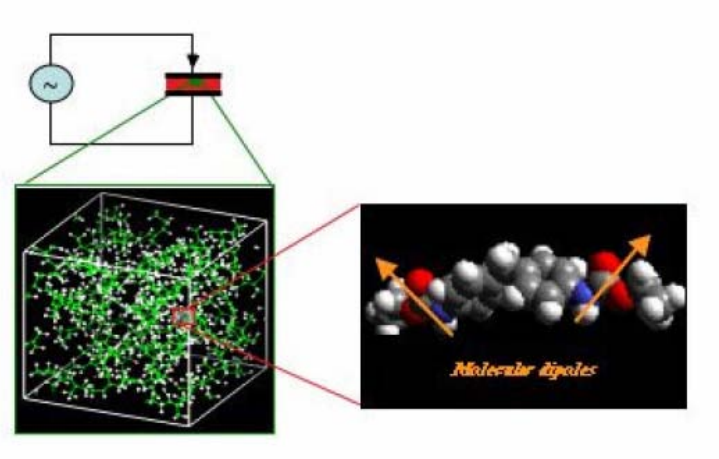

Figure 3.3.1.1. Scheme of the methodology used to measure the molecular motions by means of Dielectric Spectroscopy.

Since the capacitor is subjected to a sinusoidal voltage the responding current oscillates, after a few cycles, with the same frequency than that of the voltage, but with a phase shift as it is shown in Figure 3.3.1.2.

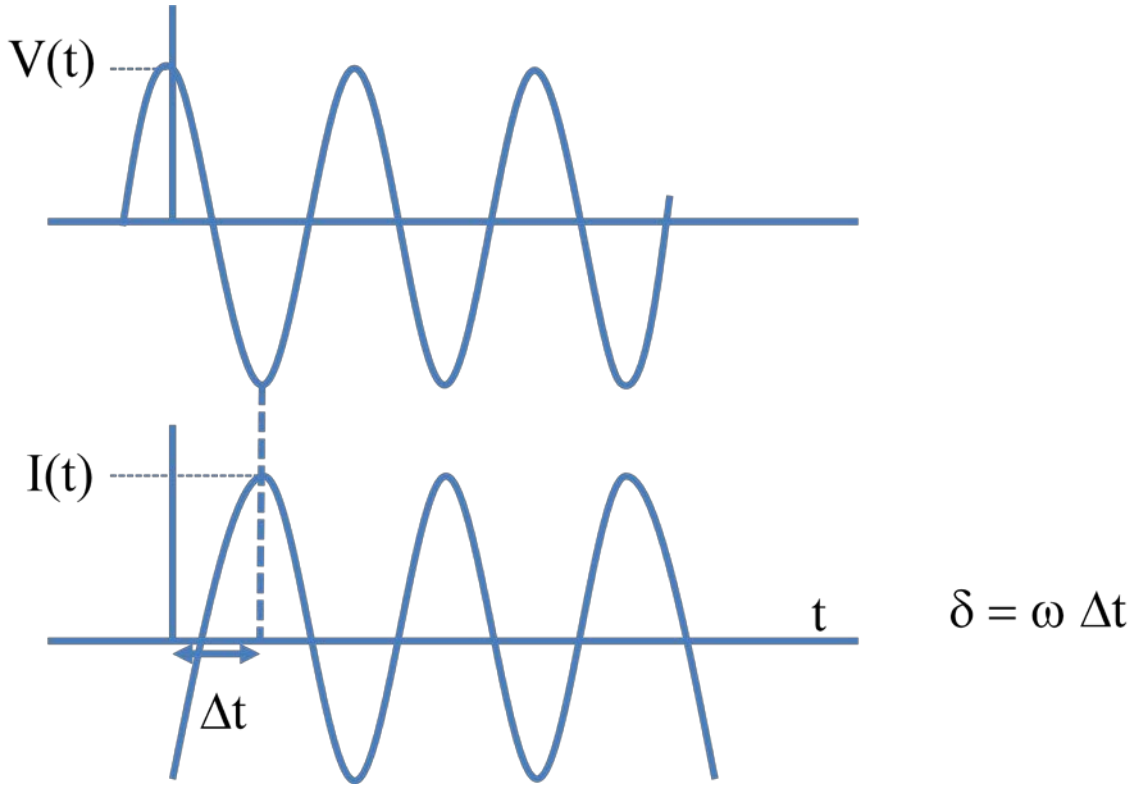

Figure 3.3.1.2. The time dependence of the voltage and the current functions.

The resulting time dependent functions would be:

$$V(t) = V_{max} \cos(\omega t) \Rightarrow V^*(\omega) = V_{max} \qquad [3.3.1.1.]$$

$$I(t) = I_{max} \cos(\omega t - \delta) \Rightarrow I^*(\omega) = I_{max}\, e^{-i\delta} = I_{max} \cos\delta - i\, I_{max} \sin\delta \qquad [3.3.1.2.]$$

where the * refers to the complex character of the quantity and *i* is the imaginary number ($i^2 = -1$).

For a capacitor filled with a given material the relative complex dielectric permittivity is calculated as:

$$\varepsilon^*(\omega) = \varepsilon'(\omega) - i\, \varepsilon''(\omega) = \frac{C^*(\omega)}{C_0} \qquad [3.3.1.3.]$$

where C^* is the complex capacitance of the measured system and C_0 is the capacitance of the same arrangement without the sample. In this way, the dielectric permittivity is directly related with the capacitance, which at the same time is inversely related with the impedance (Z^*) by

$$C^*(\omega) = \frac{i}{\omega\, Z^*(\omega)} = i\frac{I^*(\omega)}{\omega\, V^*(\omega)} \qquad [3.3.1.4.]$$

where I^* is the measured current, V^* is the applied voltage and ω its angular frequency.

The basic measuring principle is shown below

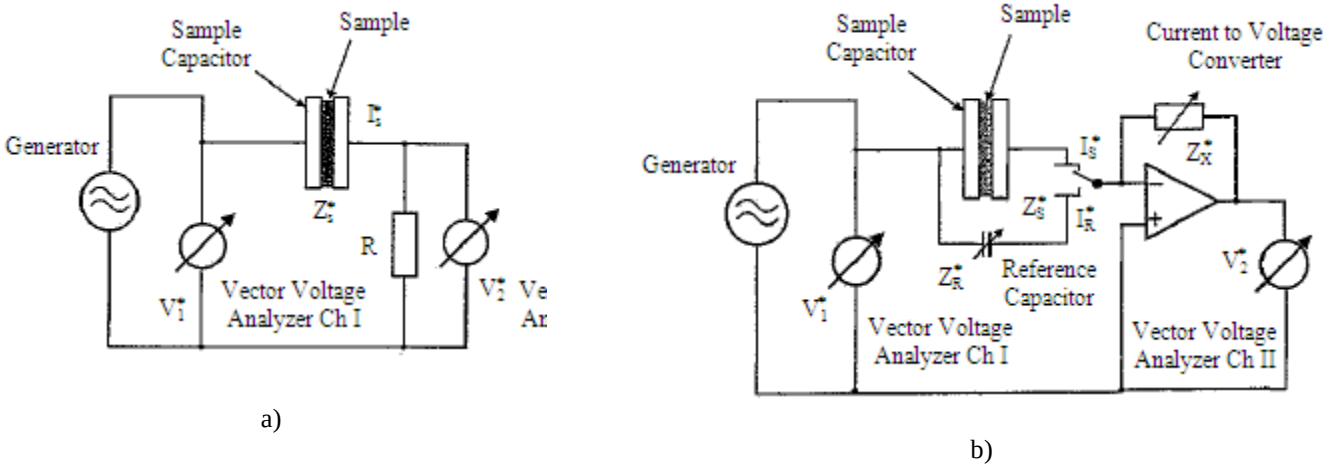

Figure 3.3.1.3. Scheme of a Fourier Correlation analyzer (a) and Scheme of a dielectric converter in the low-frequency range with electrometer amplifier and variable reference capacitor (b).

where a sinusoidal voltage $V_1(t)$ with frequency $f = \omega/2\pi$ is applied to the sample by means of a generator (see Figure 3.3.1.3.a). The resistor R converts the sample current $I_s(t)$ into a voltage $V_2(t)$. Then, both voltages, $V_1(t)$ and $V_2(t)$, are analyzed with respect to the amplitudes and phases of their harmonic Fourier base waves $V_1^*(\omega)$ and $V_2^*(\omega)$ using two sensitive sine wave correlators.

To improve the accuracy, the measuring method used to be more sophisticated (see Figure 3.3.1.3.b). A reference capacitor and a current to voltage converter are introduced, the latter allowing low frequency measurement where the capacitor impedance is extremely high.

In this set-up, if $Z_X^*(\omega)$ is an impedance, which varies with resistance and capacitance, the sample impedance $Z_S^*(\omega)$ is calculated as

$$Z_S^*(\omega) = \frac{V_{1S}^*(\omega)}{I_S^*(\omega)} = -\frac{V_{1S}^*(\omega)}{V_{2S}^*(\omega)} Z_X^*(\omega) \qquad [3.3.1.5.]$$

Therefore, the accuracy of the measurement is restricted by the amplitude and phase errors in the current to voltage converter and the correlators.

Under the very same conditions a reference capacitor with impedance similar to that of the sample is measured, improving the sensitivity. Thus, the reference impedance is obtained by

$$Z_R^*(\omega) = \frac{V_{1R}^*(\omega)}{I_R^*(\omega)} = -\frac{V_{1R}^*(\omega)}{V_{2R}^*(\omega)} Z_X^*(\omega) \qquad [3.3.1.6.]$$

And the sample impedance is finally calculated from the two above equations as:

$$Z_S^*(\omega) = \frac{V_{1S}^*(\omega)}{V_{2S}^*(\omega)} \frac{V_{2R}^*(\omega)}{V_{1R}^*(\omega)} Z_R^*(\omega) \qquad [3.3.1.7.]$$

which does not depend on the linear amplitude or phase errors.

All this is implemented in the Novocontrol high-resolution dielectric analyzer (Alpha-analyzer), which allows high accuracy measurements ($\tan\delta < 10^{-4}$) in a broad frequency range of $10^{-2} – 10^{7}$ Hz (see Figure 3.3.1.4.).

Figure 3.3.1.4. Equipment used for the dielectric measurements.

Sample's Preparation:

Samples were prepared directly on two gold-plated electrodes with diameters of 20 and 30 mm forming the parallel plate capacitor (see Figure 3.3.1.5.). For preparing the sample capacitor the sample on the lower electrode was maintained at 403 K for 24 h in a vacuum oven for the case of functionalized polymers and at 353 K for 48 h for the case of PS/PVME blends.

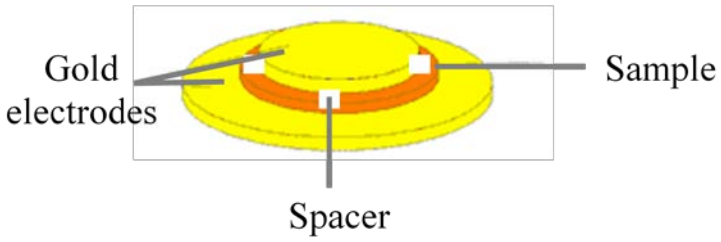

Figure 3.3.1.5. Sample placed between two gold-plated electrodes for the dielectric Measurements.

Then, when the sample was already hot, a thin star-shaped spacer 0.1 mm thick made of Teflon was placed between the electrodes before compressing the sample. Subsequently the sample was kept in the oven for some minutes in order to remove possible bubbles

and stored under vacuum at room temperature. Finally, the sample was inserted into the dielectric analyzer, and measured in a broad temperature range typically between 110-413 K.

3.3.2. Differential Scanning Calorimetry (DSC)

DSC is a thermoanalytical technique that consists in measuring the difference in the amount of heat required to increase the temperature of a sample and a reference as a function of the temperature, being both subjected to the same temperature program. In DSC the glass-transition is detected when a change occurs in the sample heat capacity (C_P) increasing from the glassy state, where configurational degrees of freedom are frozen, to the liquid state.

The instrument used was a Q2000 TMDSC (Temperature Modulated Differential Scanning Calorimetry) from TA Instruments [7] (see Figure 3.3.2.1.).

Figure 3.3.2.1. Equipment used for the calorimetrical measurements.

In contrast to the conventional DSC, the temperature modulated technique does not use a linear temperature profile (dT/dt=const.). Instead, the heating ramp is superimposed by a sinusoidal temperature perturbation of amplitude (A_T); i.e,

$$T(t) = T_i + \beta\, t + A_T \sin(\omega t) \qquad [3.3.2.1.]$$

where T_i is the initial temperature, β is the underlying heating rate and ω is the angular frequency. From the above equation we can calculate the instantaneous heating rate as

$$q = \frac{dT}{dt} = \beta + A_T\, \omega \cos(\omega t) \qquad [3.3.2.2.]$$

Conventional DSC measurements try to maintain the heating rate constant. On the contrary, in a MTDSC experiment there is a change in the heating rate. Thus, in this later type of measurement instead of using the heat flow and the heating rate to evaluate the sample thermal properties, the amplitudes of oscillation of these quantities are computed. Therefore, one of the main advantages of MTDSC technique consists on the possible separation of kinetic and heat capacity related effects. To correct the asymmetry of the sample/reference system arising from some factors as a small difference in the pans and the aluminium pan weights a standard procedure of online correction for the DSC Q2000 (TzeroTM method) was used.

Sample's Preparation:

Concerning the experimental details, the sample mass required for this measurement was about 5-10 mg, a small amount, which is a clear advantage of this thermal analysis technique. This allows a uniform temperature distribution as well as a high resolution to be achieved. Samples are encapsulated in standard hermetic aluminum pans with the

thermocouple sensors just below them and a Helium gas flow was used for thermalization.

The program used for the calorimetric analysis consisted of a modulated temperature experiment where an average ramp rate of 3 ºC/min and a temperature oscillation, with amplitude of 0.5 ºC every 60 s, superimposed.

3.3.3. Viscosity Measurements

For the mechanical measurements an ARES (Advanced Rheological Expansion System) has been used to study the deformation and flow of the sample under the influence of an applied torsional stress.

Figure 3.3.3.1. Equipment used for the rheological measurements.

A dynamical mechanical experiment consists in the application of an oscillatory strain to the sample. The principle is similar to that explained before for the BDS technique since here the material is subjected to a sinusoidal strain (or stress) and the responding stress (or strain) oscillates sinusoidally at the same frequency but with a phase lag δ:

$$\gamma(t) = \gamma_{max} \cdot \sin(\omega t) \qquad [3.3.3.1.]$$

$$\sigma(t) = \sigma_{max} \cdot \sin(\omega t + \delta) \qquad [3.3.3.2.]$$

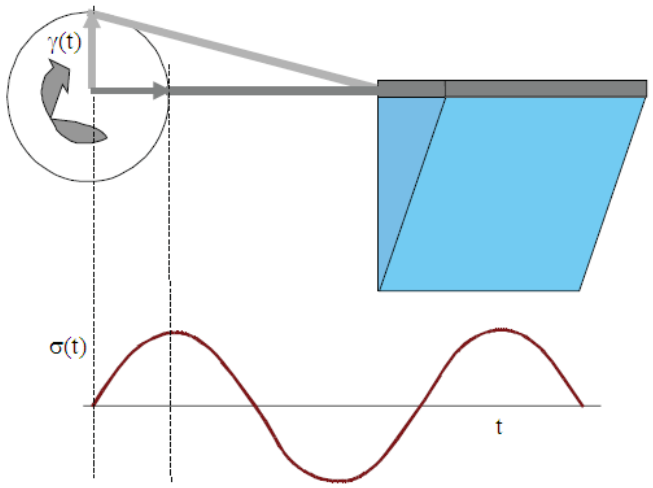

Figure 3.3.3.2. Scheme of the experiment principle.

Then, in parallel with the treatment of the dielectric measurements, the measured stress signal can be written as the sum of two oscillations with the same frequency where one is in phase and the other is out of phase:

$$\sigma(t) = \sigma'(t) + \sigma''(t) = \sigma'_{max} \cdot \sin(\omega t) + \sigma''_{max} \cdot \cos(\omega t) \qquad [3.3.3.3.]$$

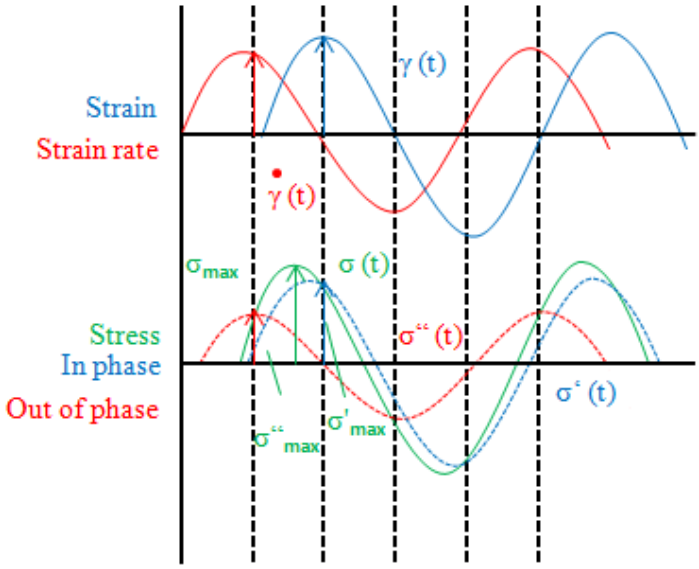

Figure 3.3.3.3. The time dependence of the strain and stress functions.

The strain and stress functions can be written as complex functions in the following way:

$$\gamma^* = \gamma_{max} \qquad [3.3.3.4.]$$

$$\sigma^* = \sigma_{max} \cdot e^{i\delta} \qquad [3.3.3.5.]$$

Dividing the complex stress by the complex strain the complex modulus (G^*) is obtained:

$$G^* = \frac{\sigma^*}{\gamma^*} = \frac{\sigma_{max} \cdot e^{i\delta}}{\gamma_{max}} = \frac{\sigma_{max}}{\gamma_{max}} \cdot \cos\delta + i \cdot \frac{\sigma_{max}}{\gamma_{max}} \cdot \sin\delta = |G^*| \cdot \cos\delta + i \cdot |G^*| \cdot \sin\delta = G' + i \cdot G''$$

[3.3.3.6.]

G' and *G"* are the real and the imaginary parts of the complex modulus and they are named as the elastic or storage modulus and the viscous or loss modulus, respectively.

The complex viscosity (η^*) can be determined from the complex modulus by means of the following equation:

$$\eta^* = \frac{G^*}{\omega} \qquad [3.3.3.7.]$$

All the experiments performed here correspond to the linear regime, i.e. where the result does not depend on the deformation rate.

The experiments have been carried out using parallel plate geometry (see Figure 3.3.3.4.).

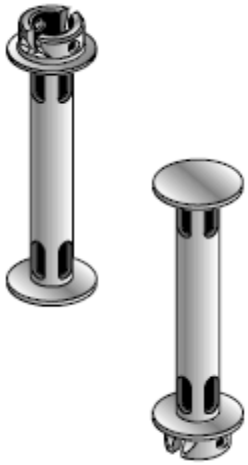

Figure 3.3.3.4. Parallel plates used for the rheological measurements.

The lower plate is driven by a motor, which works in the dynamic oscillatory mode, and it is in charge of exerting the deformation while the upper plate is connected to the transducer, which is in charge of measuring the torque and the normal force parameters. According to the parallel plate's geometry, the upper plate remains fixed while the lower plate moves at a certain rate as a consequence of being subjected to a force. The movement of the plate gives rise to a rate gradient on the fluid.

One of the advantages of the instrument is the absence of inertia effects at least in the lower region since we cannot avoid the inertia effects coming from the sample and the transducer.

The polystyrene-based samples used for rheological measurements have been formed into discs using a Teflon mold in a vacuum oven at 373 K. Before starting the measurement, the sample was heated and dried at 403 K for 24 h.

First of all, before placing the sample between the plates, it was necessary to set the gap when there was no sample in order to control it. Once it was done, we separated both plates around 15 mm being the suitable distance to place the sample. It is said that the sample is already prepared when the gap is around 1-2 mm and the sample fills completely the gap as illustrated in Figure 3.3.3.5.

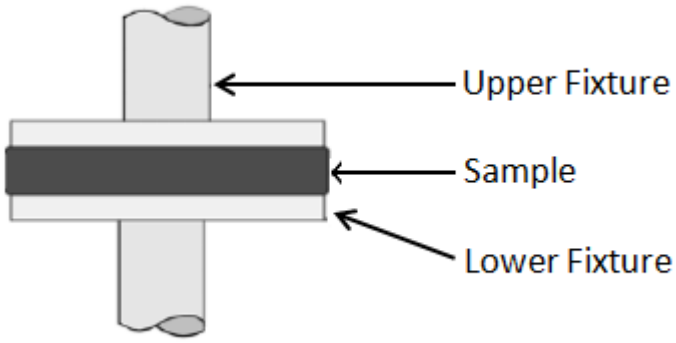

Figure 3.3.3.5. Parallel plates with the sample loaded.

3.3.4. Small Angle Neutron Scattering (SANS)

SANS is a characterization technique used for investigating the structure of a material on a length scale of 10 to 1000 Å. In particular, it allows to study the shapes and sizes of the particles that are dispersed in an homogeneous medium, or any type of nano-structure providing the required contrast.

SANS involves the fundamental four steps followed for any scattering experiment: monochromation, collimation, scattering and detection. Scheme 3.3.4.1. shows how this SANS technique works.

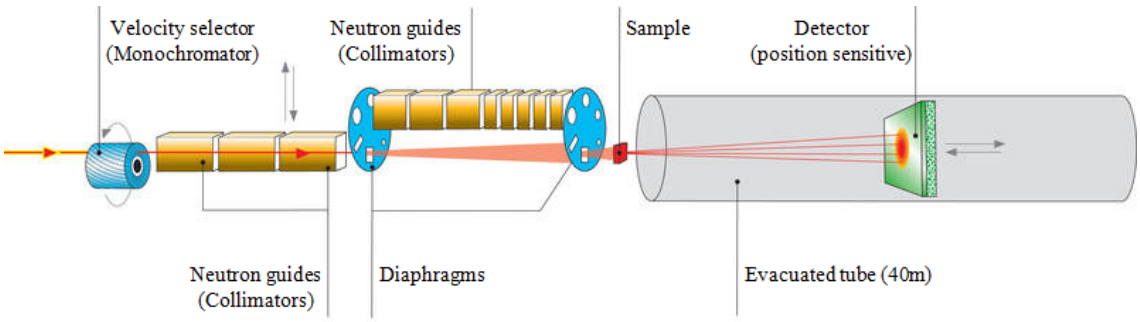

Scheme 3.3.4.1. Representation of the SANS technique.

The experiments were performed at the Institut Laue-Langevin in France using the D11 equipment which is a neutron diffraction technique able to access to large-scale structures.

The measurements were carried out at 13 temperatures in the range 260 K$\leq$ T $\leq$ 370 K with two sample-to-detector distances, namely 8m (collimation length: 8 m) and 1.2 m (collimation length: 2.5 m).

The wavelength was set to 6Å. In this way the Q-range covered was from 0.072 to 0.52 $Å^{-1}$. For some selected temperatures (267, 311, 328 and 361 K) measurements with 34 m for sample-detector distance and collimation length were also performed, extending the covered Q-range down to 0.0017 $Å^{-1}$. Detector sensitivity corrections were made with water, which was also used as secondary standard. Empty cell scattering and the background signal arising from electronic noise, γ radiation and fast unmoderated neutrons were subtracted using standard procedures. The background noise was determined using cadmium to block the primary beam. All background subtraction was done directly pixel by pixel on the two- dimensional detector intensity image. After radial averaging the intensities were treated for dead time effects in order to yield the absolute normalized macroscopic differential scattering cross sections $(d\Sigma/d\Omega)(Q)$ in absolute units of cm^{-1}.

1 . R. P. Quirk, H. Kim, M. J. Polce and C. Wesdemiotis, Macromolecules, 38, 7895 (2005)

2. R. P. Quirk, J. Janoski, S. R. Chowdhury, C. Wesdemiotis and D. E. Dabney, Reaxa Quadrapure User Guide, Manchester, U.K. (2006)

3 . H. L. Hsieh and R. P. Quirk, "Anionic Polymerization: Principles and Practical Applications", Marcel-Dekker, New York (1996)

4 . R. Lund, S. Plaza-García, A. Alegría, J. Colmenero, J. Janoski, S. R. Chowdhury and R. P. Quirk, Macromolecules, 42, 8875 (2009)

5 . R. Lund, S. Plaza-García, A. Alegría, J. Colmenero, J. Janoski, S. R. Chowdhury and R. P. Quirk, Journal of Non-Cryst. Solids, 356, 676 (2010)

6 . F. Kremer and A. Schönhals, (eds.) Broadband Dielectric Spectroscopy, Springer-Verlag, Berlín (2003)

7 . G. W. H-Höhne, W. F. Hemminger and H. J. Flammersheim, Differential Scanning Calorimetry 2nd Edition, Springer (2003)

4. Functionalized PS: Chain-End vs. In-Chain Functionalization

In this chapter experimental results of functionalized polystyrenes having the functional group located at the end of the chain (chain-end functionalized PS) or in the middle of the chain (in-chain functionalized PS) will be presented establishing a comparison between them to remark the importance of the functionalization site. In such a way on one hand we will determine the most convenient functionalization for the investigation of component dynamics in PS/PVME blends. Moreover, we will probe the site-dependent segmental dynamics.

4.1. DSC Results

Differential Scanning Calorimetry was a useful tool to determine the glass-transition temperature (T_g) for the various functionalized polymers:

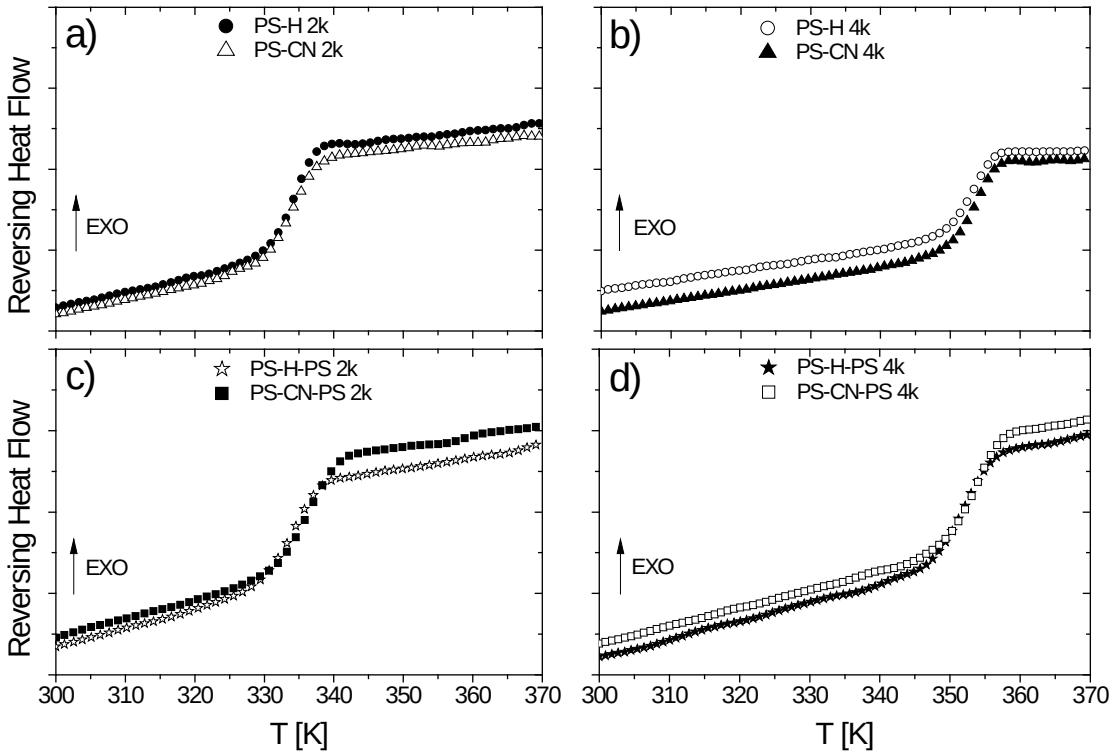

Figure 4.1.1. The reversing heat flow as a function of temperature, a) and b) for the chain-end 2k and 4k, respectively; and c) and d) for the in-chain 2k and 4k, respectively.

Figure 4.1.1. shows the reversing C_p as a function of the temperature in order to analyze the glass-transitions of each of the functionalized polymers. For all cases, both chain-end (see Figure 4.1.1. a) and b)) and in-chain functionalized polymers (see Figure 4.1.1. c) and d)), a well defined jump is observed in the heat capacity, which is directly related to the glass-transition temperature (T_g).

Defining the glass-transition temperatures as the inflection point of the DSC heating trace, we determined the calorimetric T_g values for each of the polymers which are shown in the table 4.1.1.

polymer	M_n [g/mol]	M_w /M_n	T_g [K]
PS-H 2k	2200	1.05	334
PS-CN 2k	2200	1.05	334
PS-H 4k	4200	1.04	354
PS-CN 4k	4200	1.04	354
PS-H-PS 2k	2300	1.02	329
PS-CN-PS 2k	2300	1.02	331
PS-H-PS 4k	4100	1.05	350
PS-CN-PS 4k	4100	1.05	351

Table 4.1.1. Molecular weights, the polydispersity indexes and the glass transition temperatures of the investigated polymers.

DSC results show as expected from previous studies [1] that T_g increases with increasing molecular weight. Concerning functionalization with –H and –CN groups, it is observed that it does not significantly affect thermal properties since the T_g are very similar for each pair. Now, comparing the chain-end and the in-chain functionalized polymers one can see if there is an effect on placing the functional group at the end of the chain or in the middle of the chain. Looking at the results we see that there is no evidence of a mayor effect due to functionalization site. Therefore, these DSC results show that –H and –CN functionalized polymers have essentially identical thermal properties, that are unspecific of the functional group (they are indistinguishable from those of a conventional PS with similar molecular weight). As it is shown in Figure 4.1.1. this fact was checked using such functionalized polymers with a higher molecular weight (4000 g/mol) coming to the same conclusion [2]. Trying to confirm this interesting result with other kind of properties, viscosity measurements were performed.

4.2. Viscosity Measurement Results

Viscosity measurements were done for both molecular weights (2000 g/mol and 4000 g/mol) with the aim of verifying that there are no changes in the overall polymer properties when comparing these two functional groups over a broad temperature range.

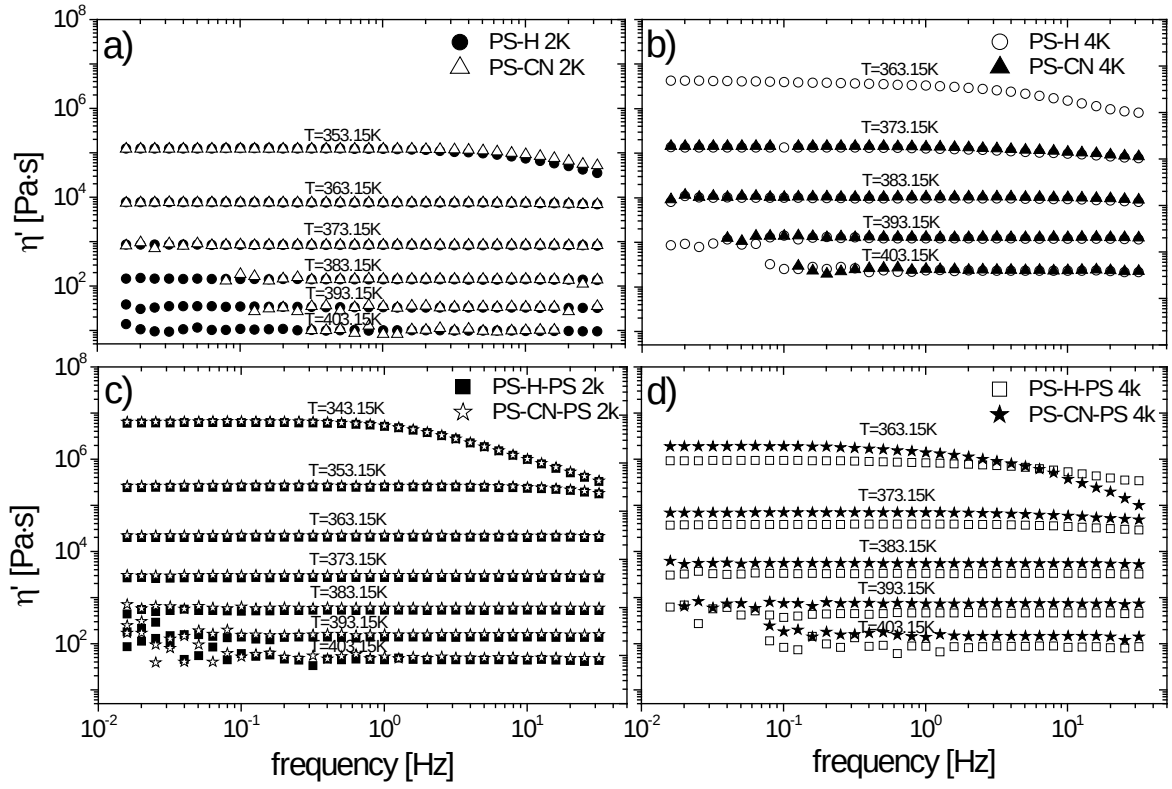

Figure 4.2.1. Comparison of the complex viscosity (η^*) as a function of angular frequency at different temperatures, a) and b) for the chain-end 2k and 4k, respectively; and c) and d) for the in-chain 2k and 4k, respectively.

Figure 4.2.1. shows the frequency dependence of the viscosity (η') for both cyanide-functionalized polystyrene and H-functionalized polystyrene, having a molecular weight of 2k and 4k respectively. The experiments have been done for a range of temperatures of 403-333 K. The temperature dependence of the sample Newtonian

(ω→0) viscosity was determined for each of the temperatures from the low frequency data (frequency independent range) and it is shown in Figure 4.2.2.

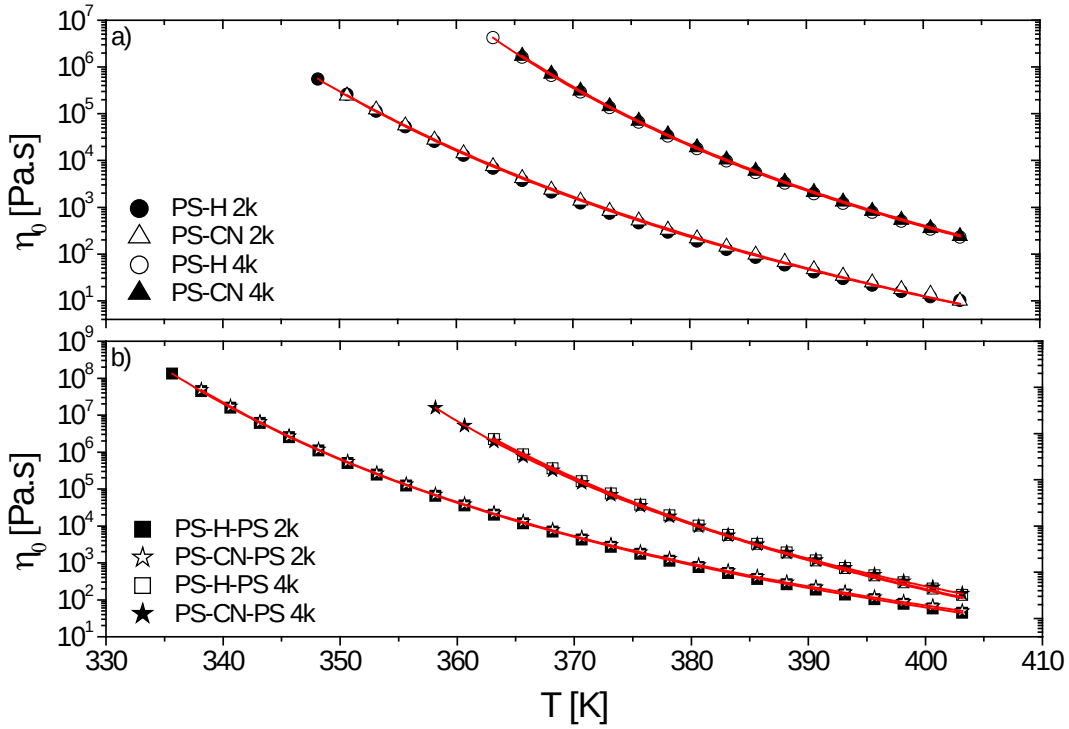

Figure 4.2.2. Comparison of the plateau viscosity (η_0) temperature dependence for the –cyano functionalized polystyrenes (PS-CN) and the reference polystyrenes (PS-H), a) for chain-end; and b) for in-chain.

As can be seen the decrease of the viscosity (η) with increasing temperature is well-described by the William-Landel-Ferry (WLF) equation [3]. The resulting values, determined for each functionalized polymer, are summarized in table 4.2.1.

X	polymer	C_1	C_2
H	PS-H 2k	14.3	64.2
CN	PS-CN 2k	14.5	68.0
H	PS-H 4k	12.8	53.9
CN	PS-CN 4k	12.8	54.0
H	PS-H-PS 2k	14.5	54.1
CN	PS-CN-PS 2k	14.3	51.9
H	PS-H-PS 4k	14.6	57.4
CN	PS-CN-PS 4k	13.1	50.9

Table 4.2.1. The parameters obtained from the WLF fits of the viscosity data of the investigated polymers.

The obtained parameters again confirm that the -CN and -H functionalization of PS does not affect much the overall dynamics since they are comparable with the WLF parameters (corresponding to a conventional PS) taken from the literature [4], which are C_1 =13.7 and C_2 = 50.0 K.

These results show clearly that the sample viscosity does not change between the –CN and –H functionalization providing that the molecular mass remain the same.

Therefore, it was clearly observed from DSC and viscosity measurements that overall properties of the cyano-functionalized polymer and that of the –H functionalized are the same since they exhibit a similar T_g as well as a similar viscosity [2]. These results confirm that the H/CN polystyrenes are identical from an overall behavior point of view, at least in the temperature range between T_g and T_g+50K. This is a key result that has made it possible to investigate the two main issues of this PhD work, namely, i) the site-specific contributions to the segmental polymer dynamics, and, ii) the slow component dynamics in PS/PVME miscible polymer blends. In both cases, the

comparison of the dielectric relaxation experiments performed in samples with cyanide- and -H functionalized PS allowed to probe selectively the dynamics of the cyanide-containing molecular groups.

4.3. BDS Results

Now, we will focus on the results obtained from BDS measurements since they provide detail information about the contributions of the different functional groups to the dynamics. Three different ranges of temperatures were used to observe the relaxation processes occurring in each of the polymers. First, BDS measurements were done using a range of temperatures above the glass-transition temperature (T_g) where it was possible to observe the α–relaxation, which is directly related with T_g.

Figure 4.3.1. and Figure 4.3.2. show the frequency dependence of the dielectric loss ε'' on the chain-end and in-chain functionalized polymers, respectively, on a temperature range of 388-338 K in the case of 2k and on a temperature range of 398-358 K in the case of 4k.

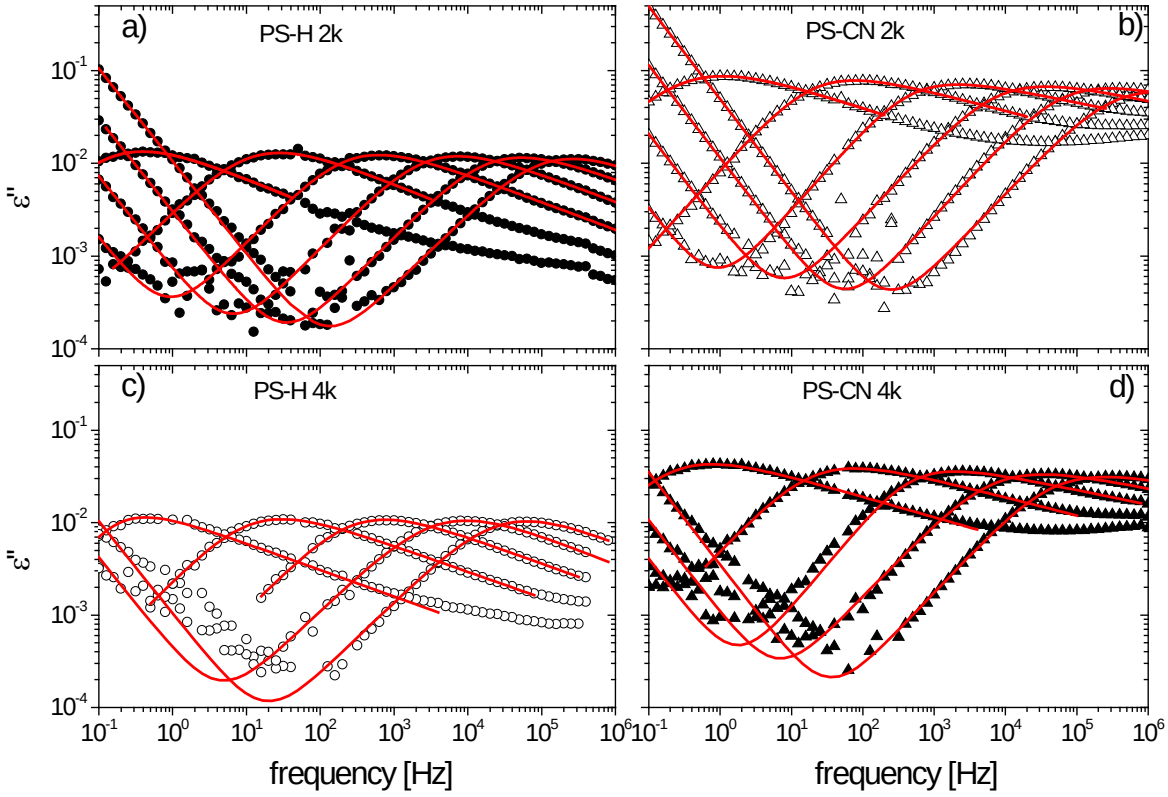

Figure 4.3.1. Dielectric segmental relaxation spectra showing the loss permittivity (ε") as a function of frequency for the chain-end functionalized polystyrenes (10 K interval from right to left starting from 388 to 338 K in the case of 2k and from 398 to 358 K in the case of 4k).

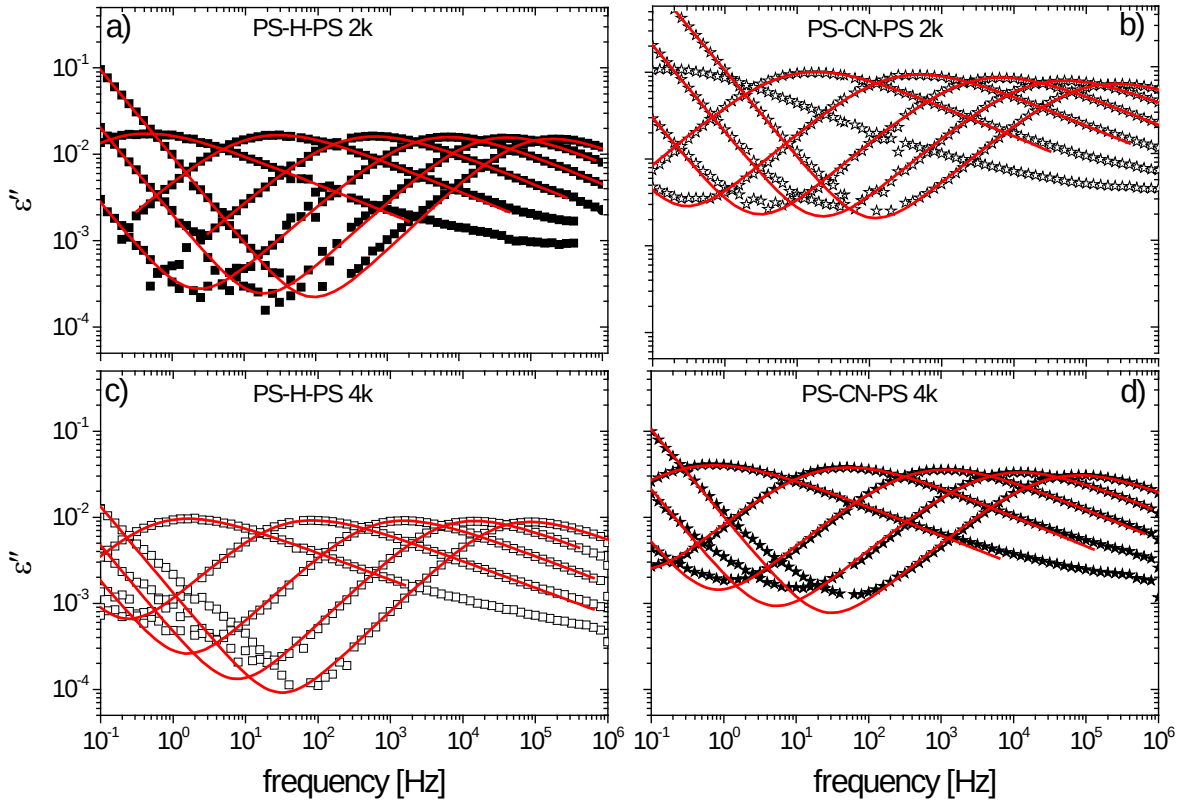

Figure 4.3.2. Dielectric relaxation spectra showing the dielectric loss permittivity (ε“) as a function of frequency for the in-chain functionalized polystyrenes (10 K interval from right to left starting from 388 to 338 K in the case of 2k and from 398 to 358 K in the case of 4k)..

Using these spectra we have calculated the characteristic relaxation time (τ*) for each of the temperatures, which has been obtained from the maximum frequency (f_{max}) corresponding to the peak of the dielectric loss spectra as:

$$\tau^* = \frac{1}{2\pi f_{\max}} \qquad [4.3.1.]$$

Figure 4.3.3. shows the resulting temperature dependence of τ* for the various functionalized polymers.

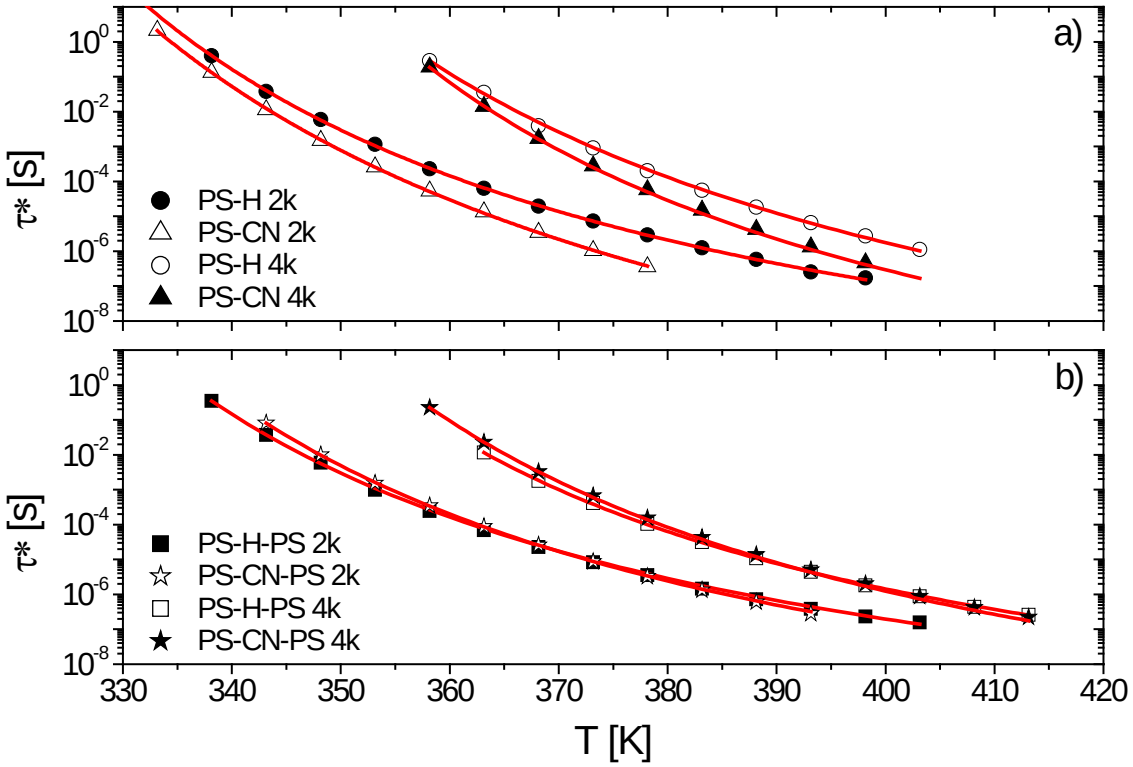

Figure 4.3.3. Typical relaxation time corresponding to the peak maximum (τ^*) of the α-relaxation as a function of temperature, a) for chain-end; and b) for in-chain.

Lines correspond to the fitting of the characteristic relaxation time associated with the α-relaxation process using the "Vogel-Fulcher-Tamman" equation [2.1.2.1.20.].

Looking at Figures 4.3.1. and 4.3.2. it is clear that a main relaxation process is observed, which corresponds to the α-relaxation although a high frequency tail is also evident in all cases, more evidently for the chain-end –CN functionalized PS samples. Lines correspond to the fitting of the main process using the "Havriliak Negami" mathematical equation [2.1.2.1.13.] in order to describe the dielectric relaxation for each of the temperatures, but not accounting for the relatively high frequency data (f $>10^3$ f_{max}). The parameters obtained from the fitting are shown in Table 4.3.1.

Polymer	T [K]	C	p	Δε	τ_{HN} [s]	β	γ
PS-H 2k	388.15	0.066	1	0.046	1.57E-6	0.793	0.425
	378.15	0.019	1	0.050	8.73E-6	0.816	0.365
	368.15	0.0045	1	0.051	6E-5	0.827	0.425
	358.15	9.8E-4	1	0.053	7.4E-4	0.834	0.358
	348.15	6E-5	1	0.054	0.015	0.809	0.401
	338.15	0	1	0.056	1.055	0.800	0.415
PS-CN 2k	388.15	0.309		0.391	5.56E-7	0.812	0.2
	378.15	0.072		0.397	2.93E-6	0.840	0.2
	368.15	0.013		0.423	2E-5	0.823	0.2
	358.15	0.002		0.440	3.9E-4	0.871	0.186
	348.15	0		0.424	0.009	0.848	0.238
	338.15	0		0.443	0.53	0.739	0.34
PS-H 4k	398.15	0.007	1	0.043	6.621E-6	0.786	0.421
	388.15	0.003	1	0.045	5.000E-5	0.774	0.416
	378.15	0	1	0.047	6.400E-4	0.823	0.355
	368.15	0	1	0.048	0.016	0.827	0.342
	358.15	0	1	0.045	1.013	0.996	0.289
PS-CN 4k	398.15	0.022	1	0.212	4.010E-6	0.823	0.180
	388.15	0.007	1	0.218	3.000E-5	0.806	0.195
	378.15	0.003	1	0.220	4.000E-4	0.933	0.170
	368.15	0	1	0.217	0.010	0.815	0.241
	358.15	0	1	0.224	0.839	0.811	0.273
PS-H-PS 2k	388.15	0.059	1	0.059	1.835E-6	0.788	0.476
	378.15	0.012	1	0.063	8.025E-6	0.763	0.476
	368.15	0.002	1	0.067	6E-5	0.732	0.476
	358.15	0	1	0.070	6E-4	0.721	0.476
	348.15	0	1	0.073	0.013	0.719	0.476
	338.15	0	1	0.077	0.921	0.706	0.476
PS-CN-PS 2k	388.15	0.658	1	0.326	1.54E-6	0.704	0.487
	378.15	0.129	1	0.353	7.905E-6	0.705	0.487
	368.15	0.019	1	0.379	6E-5	0.712	0.487
	358.15	0.002	1	0.407	7.8E-4	0.716	0.487
	348.15	0	1	0.435	0.022	0.718	0.487
PS-H-PS 4k	398.15	0.008	1	0.036	4.957E-6	0.815	0.407
	388.15	0.003	1	0.038	2.909E-5	0.805	0.407
	378.15	0.001	1	0.039	2.830E-4	0.788	0.407
	368.15	4.4E-4	1	0.040	0.005	0.768	0.407
	358.15	0	1	0.042	0.274	0.777	0.407
PS-CN-PS 4k	398.15	0.065	1	0.135	4.786E-6	0.699	0.504
	388.15	0.013	1	0.146	3.144E-5	0.695	0.504
	378.15	0.003	1	0.156	3.4E-4	0.696	0.504
	368.15	4.9E-4	1	0.167	0.007	0.693	0.504
	358.15	0	1	0.187	0.556	0.660	0.504

Table 4.3.1. Havriliak Negami parameters obtained for the α–relaxation characterization for the various functionalized polymers.

It should be emphasized that the value τ_{HN} does not correspond to the value of τ^*. In fact, τ^* is the most widely used of both parameters to describe the characteristic relaxation time since it is a parameter more independent of the analysis procedure as it was explained in Section 2.1.2.1.

The average values over the temperature range investigated of the parameters obtained from the Havriliak Negami mathematical model, and the Vogel-Fulcher-Tamman parameters describing the temperature dependence of the characteristic relaxation time are summarized in Table 4.3.2.

Polymer	$\Delta\bar{\varepsilon}$	$\bar{\gamma}$	$\bar{\beta}$	τ_{VFT} [s]	B	T_0 [K]	T_{gD} [K]
PS-H 2k	0.052	0.382	0.818	7.10E-14	1735.8	279.0	332.5
PS-CN 2k	0.42	0.223	0.825	7.00E-14	1430.9	287.4	331.3
PS-H 4k	0.042	0.365	0.82	9.16E-15	2067.7	291.6	351.3
PS-CN 4k	0.217	0.214	0.828	5.8E-15	1726.8	302.6	351.8
PS-H-PS 2k	0.067	0.476	0.741	2.03E-13	1640.0	280.0	332.0
PS-CN-PS 2k	0.387	0.487	0.711	9.78E-14	1653.4	282.9	333.9
PS-H-PS 4k	0.037	0.407	0.805	2.19E-14	2021.0	288.0	347.9
PS-CN-PS 4k	0.148	0.504	0.694	5.76E-14	1691.3	299.8	351.4

Table 4.3.2. Parameters obtained from the Havriliak Negami model and the Vogel-Fulcher-Tamman equation.

From the VFT description, what is known as the 'dielectric glass transition temperature', T_{gD}, has been evaluated as $\tau^*(T_{gD})=10$ s. The resulting values for each sample are also included in the table.

As Figures 4.3.1. and 4.3.2. show the α-peaks can be superimposed with other significant contributions at the high frequencies. In order to access to this signal in more detail it was convenient to extend the dielectric experiments also to an intermediate range of temperatures, going from a temperature below the T_g to the room temperature. The obtained data are depicted in Figures 4.3.4. and 4.3.5., for the chain-end and in-chain functionalized polymers, respectively.

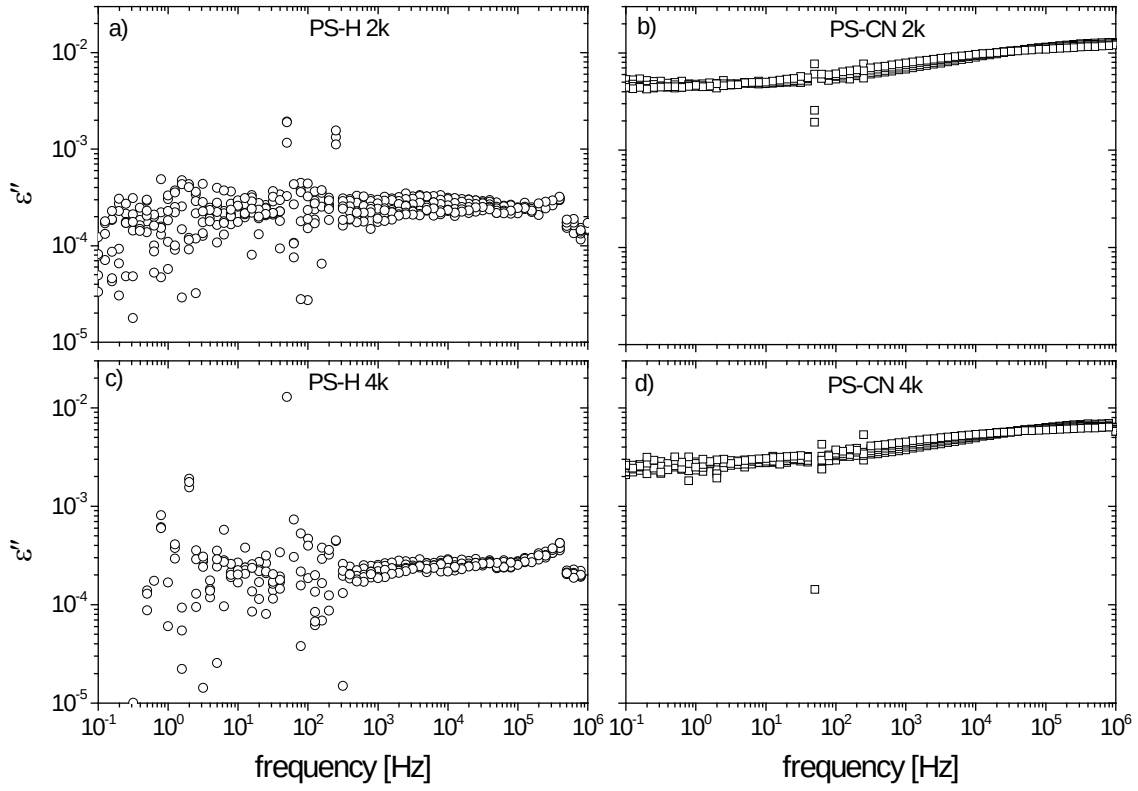

Figure 4.3.4. The dielectric loss permittivity (ε'') as a function of frequency for all the chain-end functionalized polymers for an intermediate range of temperatures (10 K interval starting from 293 to 243 K in the case of 2k and from 293 to 253 K in the case of 4k).

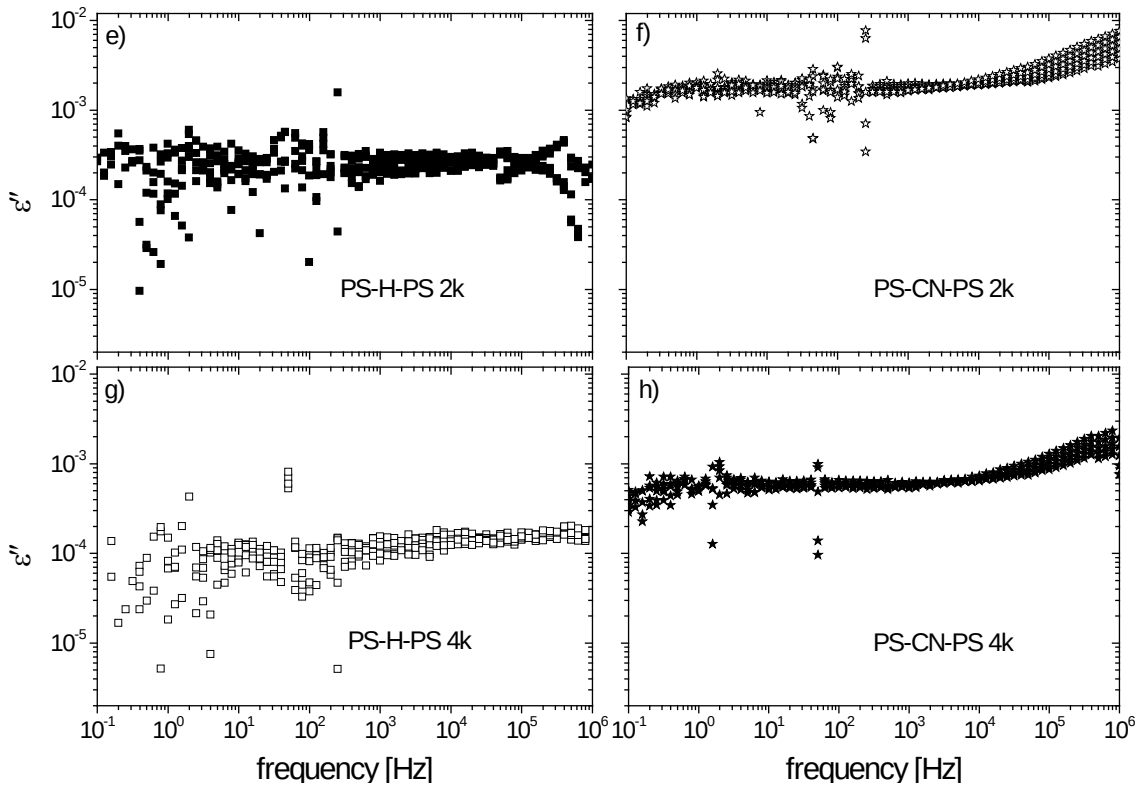

Figure 4.3.5. The dielectric loss permittivity (*ε''*) as a function of frequency for all the in-chain functionalized polymers for an intermediate range of temperatures (10 K interval starting from 293 to 243 K in the case of 2k and from 293 to 253 K in the case of 4k).

As we can observe it is evident the absence of any well resolved relaxation loss peak in all polymers. Trying to find any signature of dielectric secondary relaxations in these polymers the lowest temperature regime (T > 110K) was investigated.

Figure 4.3.6. shows the frequency dependence of the dielectric loss *ε''* on the chain-end and in-chain functionalized polystyrenes 2k and 4k using a range of temperatures of 110-140 K. A well resolved peak is found for all –CN functionalized polymers and not for the reference ones (PS-H 2k, PS-H 4k, PS-H-PS 2k and PS-H-PS 4k).

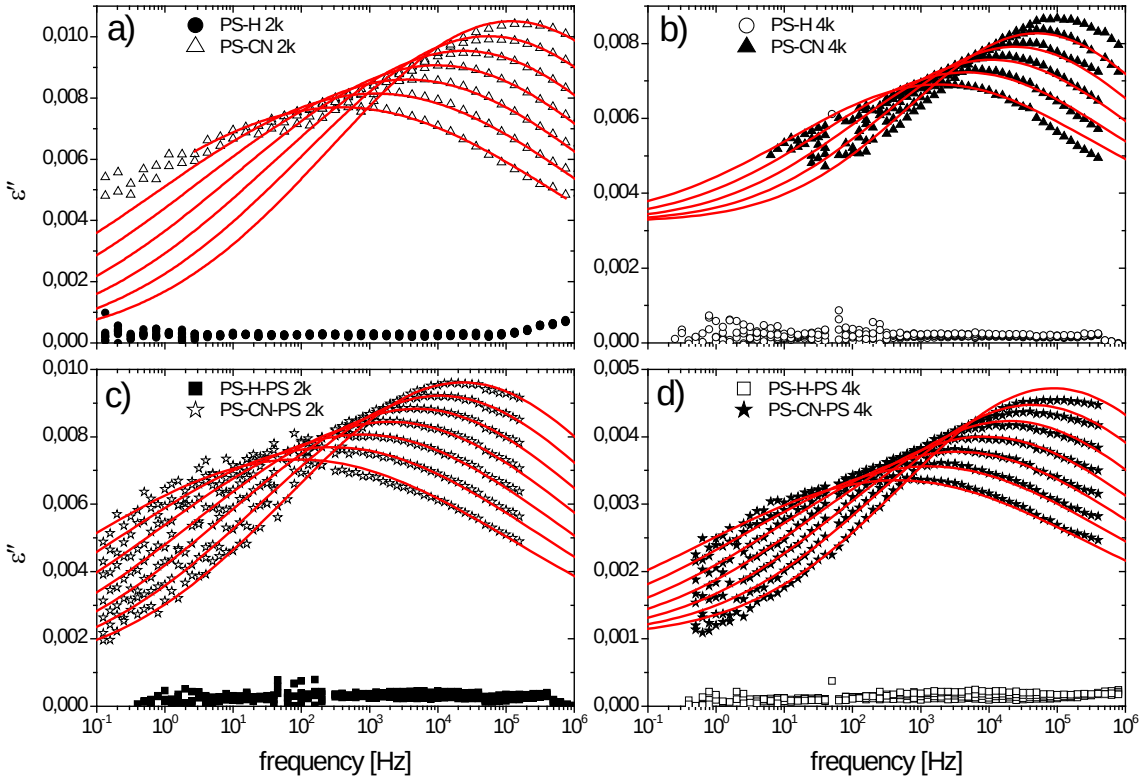

Figure 4.3.6. The secondary relaxation from the dielectric relaxation functions obtained from the isothermal measurements for all the functionalized polymers, a) and b)for the chain-end 2k and 4k, respectively; and c) and d) for the in-chain 2k and 4k, respectively.

Using these spectra we have calculated the characteristic relaxation time (τ^*) for each of the temperatures, which has been obtained by applying the equation [4.3.1]. The resulting temperature dependence of these secondary relaxations is shown in Figure 4.3.7.

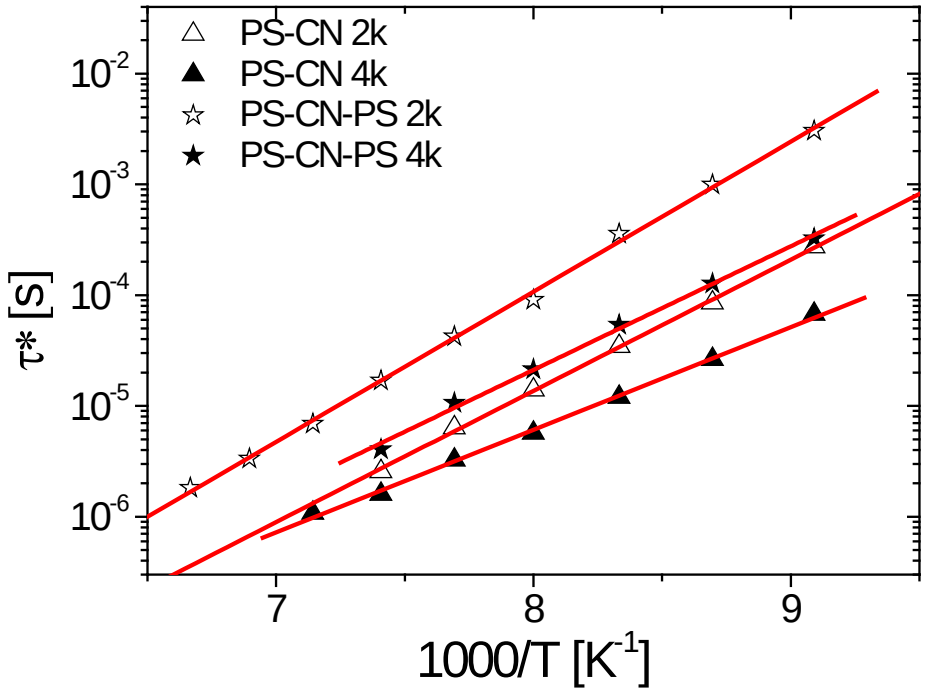

Figure 4.3.7. Temperature dependence of the secondary relaxation process for the chain-end and in-chain –CN functionalized polymers. Here the logarithm of the characteristic relaxation time is plotted versus the inverse temperature in a so-called Arrhenius representation.

In order to describe also the shape of the secondary relaxation processes it has been useful to use a mathematical model based on the superposition of individual Debye processes (single relaxation time). Since the relaxation times follow Arrhenius behavior, i.e. $\log\tau = \log\tau_0 + E\log e/KT$, the distribution of relaxation times g(logτ) appearing in Equation [2.1.2.1.10.] has been assumed to arise from a Gaussian distribution of the activation energies, i.e.:

$$g(E_A) = \frac{1}{\sqrt{2\pi\cdot\sigma_{E_A}{}^2\cdot\langle E_A\rangle^2}}\exp\left(-\frac{(E_A-\langle E_A\rangle)^2}{2\cdot\sigma_{E_A}{}^2\cdot\langle E_A\rangle^2}\right) \qquad [4.3.2.]$$

being σ_{E_A} the relative width and $<E_A>$ the mean activation energy, both assumed to be temperature independent. Consequently,

$$g(\log\tau) = g(E_A)\,dE_A/d\log\tau = g(E_A)\,KT/\log e \qquad [4.3.3.]$$

Therefore, the total contribution to the relaxation can be written as

$$\varepsilon''(\omega) = \Delta\varepsilon(T)\int g(E_A)\frac{\omega\,\tau(E_A)}{1+\omega^2\,\tau(E_A)^2}\,dE_A \qquad [4.3.4.]$$

where $\Delta\varepsilon(T)$ is defined as

$$\Delta\varepsilon(T) = \Delta\varepsilon_0 + A\,T \qquad [4.3.5.]$$

being A and $\Delta\varepsilon_0$ numerical coefficients.

Using this model it has been possible to describe the shape and the width of the dielectric relaxation function over the temperature range where the loss peak is detectable. The parameters so obtained are shown in Table 4.3.3.

polymer	$\langle E_A \rangle$ [kJ/mol]	σ_{EA}	$\tau_0{}^s$ [s]	$\Delta\varepsilon_0$	A [K^{-1}]
PS-CN 2k	24.5 ± 0.5	0.28 ± 0.03	9.20E-16	0.0646	2.80E-4
PS-CN 4k	19.8 ± 0.1	0.31 ± 0.23	3.57E-14	0.062	1.2E-4
PS-CN-PS 2K	25.9 ± 0	0.26 ± 0.01	1.13E-15	0.049	2.50E-4
PS-CN-PS 4K	21.3 ± 0	0.3 ± 0.01	2.39E-14	0.017	1.36E-4

Table 4.3.3. Parameters obtained from the theoretical model explained above in order to caracterize the secondary relaxation process for the various functionalized polymers.

4.4. Discussion of Functionalized PS Results

4.4.1. Secondary Relaxation Process

In the section we will focus on the detected dielectric secondary relaxations processes, which take place at temperatures well below T_g and can be assigned to local conformational rearrangements involving the –CN group. Obviously BDS was the single technique used to study these local processes. In Figure 4.3.6. we have the dielectric relaxation spectra for a given range of temperatures obtained for all CN/H functionalized polystyrenes. We focus our attention on the spectra obtained for a given temperature (120K) in order to compare the responses in a more clearly way as seen in Figure 4.4.1.1.

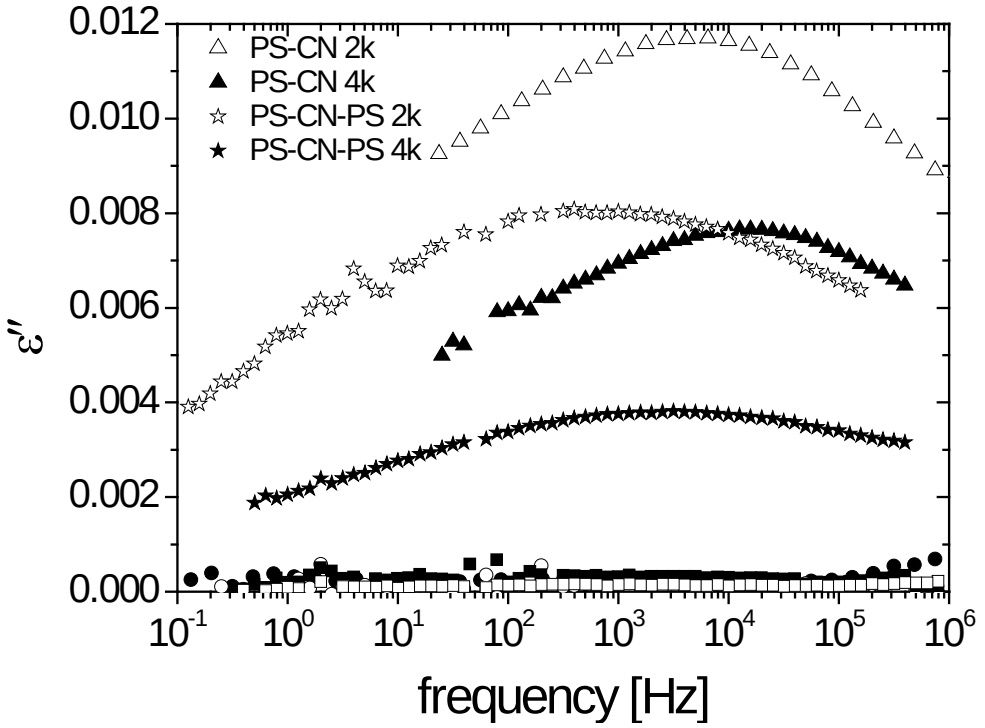

Figure 4.4.1.1. Dielectric relaxation at low temperatures showing the frequency dependence of the dielectric loss permittivity (ε“) at a temperature of 120 K for the chain-end and in-chain functionalized polymers.

As expected, it can be observed that all the references (PS-H; PS-H-PS) do not show a significant signal, which can be seen in the lower part of the dielectric spectra. In contrast, we see that all the -CN functionalized polystyrenes (PS-CN; PS-CN-PS) present a significant dielectric loss. Hence, these secondary relaxation processes seem to have their origin on the rather localized motion of the –CN group.

Concerning the intensity of the loss peak, the spectra show that the polymers with lower molecular weight (2k) exhibit a higher dielectric signal, observing a difference in intensity approximately of a factor of 2 between the 2k and the 4k functionalized polymers. This feature can be assigned to the dilution of polar groups when the molecular weight is doubled. Functionalization site also affects the loss peak intensity observing a higher intensity when the functional group is added at the end of the chain. This suggests less steric restrictions in this case.

Now regarding the shape and the peak position of the dielectric spectra the above results show that, whereas the shape is not much affected, dynamics become faster for the higher molecular weights (4k) as well as for the chain-end functionalized polystyrenes.

These results indicate that both molecular weight and functionalization site play an important role in the dynamics of these functionalized polymers. This is corroborated by looking at the temperature dependence of the relaxation time (τ_0^s) shown in Figure 4.3.7. where it can be observed that the dynamics become faster for the higher molecular weights (4k) and also when the –CN functional group is added at the end of the chain.

In order to compare the responses of these local processes we can have a look on Table 4.3.3. where values obtained from the fitting of the dielectric spectra (see

Figure 4.3.6.) and from the fitting of the temperature dependence of the relaxation time (see Figure 4.3.7.) are given. Before analyzing the obtained results it should be noted that in the polymer that we are investigating a dielectrically active movement can only take place via a CH_2-CH_2 bond rotation. Due to the linearity of the C-CN unit the rotation around this end group is not dielectrically active.

Now concerning the activation energy, which is expected to be related to the available volume around of the functional group and to increase with increasing the relative unit-size, the values obtained show a slight but significant difference when comparing the two different molecular weight samples. In fact, the activation energy is higher for the lower molecular weights (2k) and this effect can be interpreted as a difference in the local packing around the –CN functional group. Also there is an effect due to functionalization site getting a slightly higher value of the activation energy when the functional group is added in the middle of the chain. These two facts suggest that this activation energy is not only controlled by the rotational barriers within the whole functional group: Si-CH_2-CH_2-CH_2-CN.

Concerning the values obtained for the relaxation loss peak width, it can be observed that the width is only slightly larger for the higher molecular weights (4k). Here, functionalization site plays a role giving rise to a slightly larger width when the –CN functional group is placed at the end of the polymer chain.

4.4.2. α–Relaxation Process

In the previous chapter we have presented the calorimetric, viscosity and dielectric properties of chain-end and in-chain CN/H functionalized polystyrenes (PS-X ; PS-X-PS), i.e. when *one* CN/H functional group is added at the end or in the middle of

the chain, respectively, using two different molecular weights of 2k and 4k. To study the dynamics of these polymers we used the combination of such a precise functionalization with BDS, selective to dipole moments, as well as other complementary techniques like DSC and Viscosity measurements, both sensitive to overall polymer properties. First of all, we will focus on the results obtained by means of DSC (Table 4.1.1.) where we can observe that the T_g for the CN-functionalized polymers (PS-CN 2k; PS-CN-PS 2k) take practically the same value as that of the references (PS-H 2k; PS-H-PS 2k), what is somehow surprising. This behavior has been confirmed for the polymers having higher molecular weights (4k) providing additional support. Then, it seems that for a given molecular weight functionalization with –H and –CN functional groups does not affect much the overall dynamics. What is also observed is that as expected T_g increases with increasing molecular weight, which is usually attributed to the free volume induced by the chain-ends that decrease in quantity as chain length increases. Now comparing the chain-end and in-chain functionalized polymers, it is observed that functionalization site does not seem to affect significantly T_g noticing values of T_g slightly smaller for the in-chain than for the chain-end functionalized polymers despite that the molecular weight is slightly larger for the in-chain. This small difference could be attributed to the additional flexibility of the –C-Si-C- group placed in the middle of the chain for the in-chain functionalized polymers.

The viscosity measurements performed extending the study of the overall dynamics to higher temperatures ($T > T_g$) confirmed that the CN/H pairs exhibit the same overall dynamical behavior. Looking at Figure 4.4.2.1. we see that not only the corresponding samples have the same viscosity but also nearly the same storage and loss modulus are found for both the –CN functionalized polystyrenes (PS-CN; PS-

CN-PS) and the reference polystyrenes (PS-H; PS-H-PS). This finding was obtained for the two molecular weights (2k and 4k) as well as for the two different functionalization sites (chain-end and in-chain).

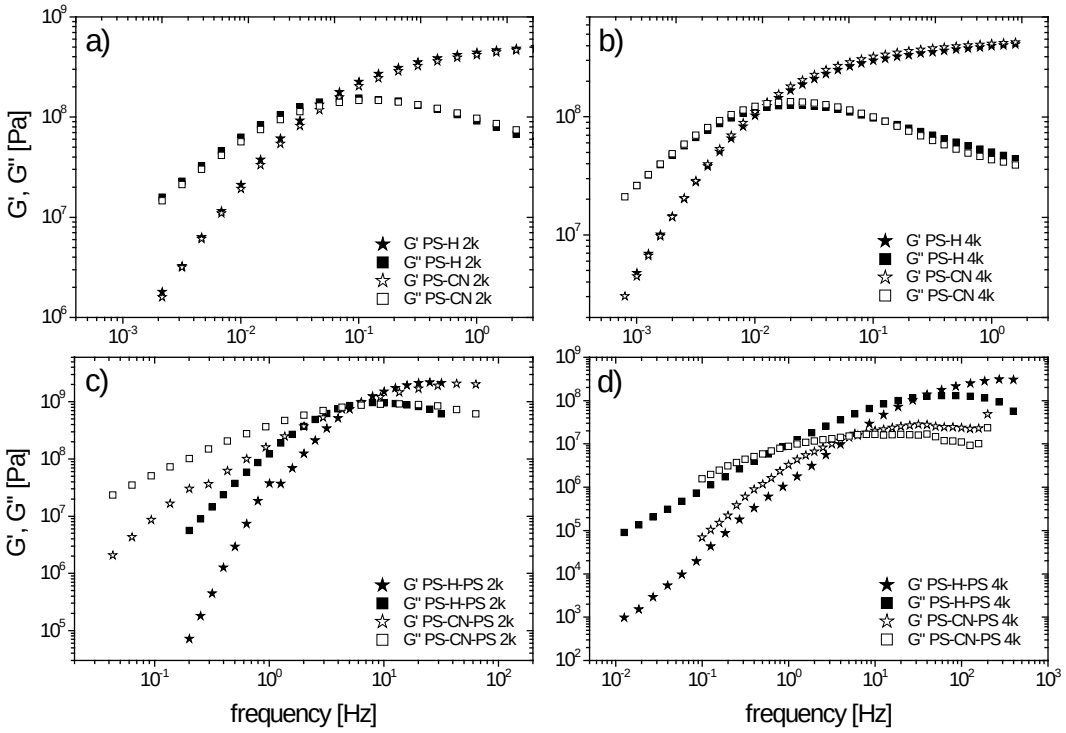

Figure 4.4.2.1. Frequency dependence of the shear storage modulus (G') and the loss modulus (G") for the –cyano functionalized polystyrenes (PS-CN) and the reference polystyrenes (PS-H) pairs.

In fact that CN/H pairs of functionalized polystyrenes exhibit the same overall dynamical behavior is likely related with the low concentration and small size of both functional groups and is consistent with previous results [5, 6] where it was observed that T_g was actually affected when a bulkier or interacting functional group (hydroxyl, acetate or ethyl ether) was introduced in the polystyrene matrix leading to a decrease of T_g.

The similar behavior observed for the CN/H functionalized polystyrenes allows BDS to be used as a selective tool to determine the specific contributions to the

polymer segmental dynamics from the sites where the polar entities (-CN) are located. Considering the two types of polymers investigated here, it is evident that for the -CN functionalized polystyrenes the dipole moment around the –CN functionalized segments is large and dominant over the styrene repeating units. On the other hand, the resulting matrix contributions to the dielectric relaxation of the –CN functionalized polystyrenes will be given by the –H functionalized polystyrenes being the references.

When considering the intensity of the loss peak in Figures 4.3.1. and 4.3.2., the spectra show that all the –CN functionalized polystyrenes (PS-CN; PS-CN-PS) exhibit much stronger dielectric signals almost one order of magnitude higher than the corresponding references (PS-H; PS-H-PS) independently of the molecular weight and the functionalization site (chain-end and in-chain). Moreover, this difference in intensity increases as molecular weight decreases observing approximately a factor of 2 between the signals of the low molecular weight (2k) and the high molecular weight (4k) polymers. Such effect can be attributed to the "dilution effect" as already mentioned when the secondary relaxation process has been discussed. Then, these results reflect that in the case of the chain-end functionalized polystyrenes the PS-CN dielectric losses are dominated by the fluctuating chain-ends, while in the case of the in-chain functionalized polystyrenes the PS-CN-PS dielectric losses are mainly assigned to the fluctuations in the middle of the chain.

Now regarding the shape of the dielectric spectra in Figure 4.3.1. it can be seen that the responses for the –CN functionalized polystyrenes become broad showing a high frequency tail contribution more prominent for -CN end-functionalization, which cannot be resolved as a peak at lower temperatures. The behavior observed for the

chain-end functionalized polystyrenes is not so clear for the case of the in-chain functionalized polystyrenes (see Figure 4.3.2.) where the –CN functionalized polymers exhibit a response similar in shape to the corresponding references (-H functionalized polymers). In addition, this feature only seems to depend on the functionalization site and not on the molecular weight. All this suggests that the high frequency tail reflects mainly the end-group fluctuations.

If we now look at the temperature dependence of the characteristic α-relaxation time (τ^*) shown in Figure 4.3.3., a general trend is found for all the CN/H functionalized polystyrenes independently of the location of the functional group in the polymer chain where the characteristic relaxation time decreases with decreasing molecular weight. Thus, this effect just is mainly attributed to the corresponding changes in T_g. Focusing on chain-end functionalized polymers (see Figure 4.3.3.a)) we can observe that PS-CN polymers exhibit a lower characteristic relaxation time comparing with the references (PS-H polymers). Furthermore, it is shown that the time scale is well separated at high temperatures, whereas at low temperatures they seem to approach each other in agreement with the close T_g values. However, the behavior obtained for the in-chain functionalized polymers (see Figure 4.3.3.b)) differs from that of the chain-end functionalized polymers observing that at low temperatures the time scale of the PS-CN-PS polymers is slightly larger comparing with the references (PS-H-PS). Nevertheless, as temperature increases both time scales approach each other.

Summarizing, the results concerning the chain-end functionalized polymers show that the peak positions shift to higher frequency and the shape of the dielectric spectra becomes broader reflecting a faster and more heterogeneous dynamics for

the –CN chain-end functionalized PS (PS-CN) comparing with the reference (PS-H) [2, 5, 6]. In contrast, the results concerning the in-chain functionalized polymers show a similar time scale and shape of the dielectric spectra indicating the presence of a more homogeneous dynamics similar to the backbone (PS-H-PS) [2].

4.4.2.1. α–Relaxation Process: Specific Contributions to the Dynamics

The couple of polymers PS-H/PS-CN and PS-H-PS/PS-CN-PS allow investigating the specific contributions to the segmental dynamics (α-relaxation by BDS) of the sites where the functional groups are located, which will be most sensitive to the fluctuations of the strong polar groups located at the chain-ends or at the mid-chains, respectively. The approach we applied consists of extracting the "pure" chain-end and in-chain fluctuation dynamics (-CN dynamics) from the overall dynamics by directly subtracting the dielectric response of the reference polymer (PS-H; PS-H-PS) from the -CN functionalized polymer (PS-CN; PS-CN-PS) dielectric response. The idea behind this procedure is that the dielectric signal coming from the corresponding reference (PS-H; PS-H-PS) reflects only the contribution of the overall dynamics, i.e. those associated to the segment fluctuations in the polystyrene chains. However, this is not the case for the CN-functionalized polymers (PS-CN; PS-CN-PS) whose dielectric signal is dominated by the fluctuation of the functional group, making the dielectric relaxation to be much stronger. This subtraction methodology was used for both functionalization sites and molecular weights.

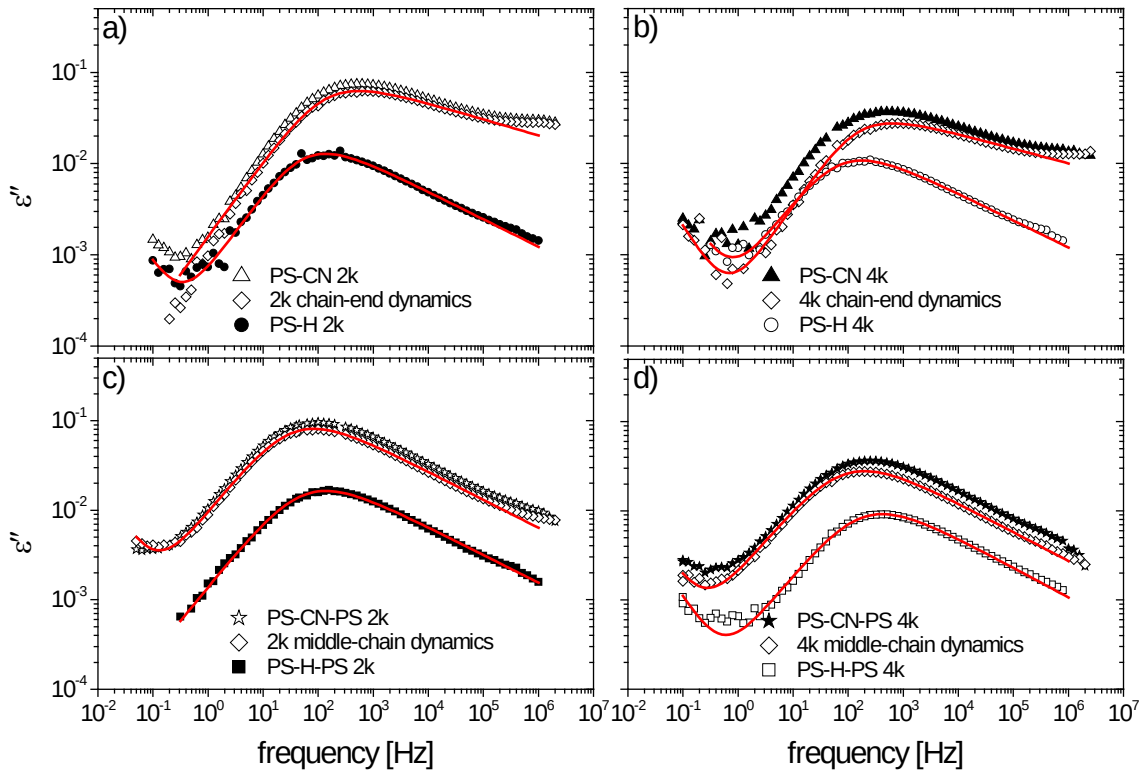

Figure 4.4.2.1.1. Comparison of the dielectric spectra of the –CN functionalized polystyrenes, the corresponding references (-H functionalized polystyrenes) and the subtracted spectrum (-CN dynamics), which corresponds to the specific signal of the chain-end or in-chain fluctuations, e.g. the fluctuations of the segments connected to the –CN group.

Figure 4.4.2.1.1. shows the frequency dependence of the loss peak of the CN-functionalized polymers, the corresponding references (-H functionalized polymers) and the subtracted response (-CN dynamics), which corresponds to the specific signal of the chain-end or in-chain fluctuations. To facilitate comparisons, the results are displayed at temperatures that correspond to about 20 K above T_g being the chosen temperatures 353 K and 373 K for the 2k and 4k, respectively. As clearly seen from Figures 4.4.2.1.1. a) and b) where the chain-end functionalization is presented, most of the signal of the –CN chain-end functionalized polystyrene (PS-CN) comes from the fluctuations of the –CN chain-end groups. Hence, this subtraction procedure allows observing chain-end fluctuations in a direct way. It is found that the chain-ends show a faster and more heterogeneous dynamics

compared with the main chain (average) response showing a high frequency tail whose contribution cannot be resolved as a peak even at lower temperatures. The case of the in-chain functionalization observed in Figures 4.4.2.1.1. c) and d) is contrary since the shapes of the dielectric spectra of the –CN in-chain functionalized polymers (PS-CN-PS) are very similar to their references (PS-H-PS) despite having –CN functional groups contributing again to most of the detected signal.

In order to compare the response coming from the in-chain, chain-end and the overall dynamics shown in Figure 4.4.2.1.1. the dielectric responses were analyzed using the "Havriliak Negami" equation [2.1.2.1.13.] in addition to a conductivity term [$\varepsilon_{cond} \propto 1/\omega$]. Lines in Figure 4.4.2.1.1. correspond to the fitting results of the dielectric spectra, providing a good-description of the curves over the whole frequency range at least for the in-chain fluctuations. However, for the chain-end fluctuations, which exhibit an asymmetric broadening at the high frequency regime reflected in a tail-like contribution (specific of the chain-end fluctuations), this simple equation is not enough to describe the measured data in that region. The obtained parameters are given in Table 4.4.2.1.1.

polymer	$\Delta\varepsilon$	β	γ	fwhm DECADES
PS-H 2k	0.054	0.85	0.35	2.70
End-chain 2k	0.372	0.83	0.21	4.12
PS-H 4k	0.047	0.80	0.37	2.81
End-chain 4k	0.171	0.88	0.18	4.39
PS-H-PS 2k	0.072	0.77	0.40	2.78
Middle-chain 2k	0.353	0.77	0.40	2.74
PS-H-PS 4k	0.039	0.76	0.44	2.66
Middle-chain 4k	0.123	0.74	0.44	2.74

Table 4.4.2.1.1. Fit parameters and related quantities extracted from an analysis of the dielectric loss spectra shown in Figure 4.4.2.1.1. using a Havriliak-Negami function. Last column present the full with at half maximum (*fwhm*) of the fitting peak loss determined from the shape parameters. [7].

As seen in the above table, very similar values for the shape are obtained when comparing middle-chain and whole dynamics (reference –H functionalized polymer). However, for the chain-end signal the parameters are clearly different and the full-width-half-maximum (*fwhm*) markedly larger. This makes it clear that the chain-end fluctuations have very significant contributions to high frequencies that persist even below T_g as already discussed.

Concerning the main relaxation rate, Figure 4.4.2.1.2. shows a comparison of the site dependent characteristic relaxation time in a temperature scaled representation canceling the variations produced by T_g changes. In this way, all the data have been normalized to the T_{gD} of the corresponding reference polymer. This procedure has been done for both molecular weights, 2k and 4k. In such representation all the reference polymers present the same dynamics, and as a consequence the dielectric relaxation times perfectly superimpose (see x and + symbols in the figure) despite of the clear difference between the corresponding glass transition temperatures. So any minor difference between T_g values associated to the site where the functional group is located will not be relevant in the comparison. Consequently, Figure 4.4.2.1.2. highlights the differences in dynamics originated by the chain-site where the polar functional group is located.

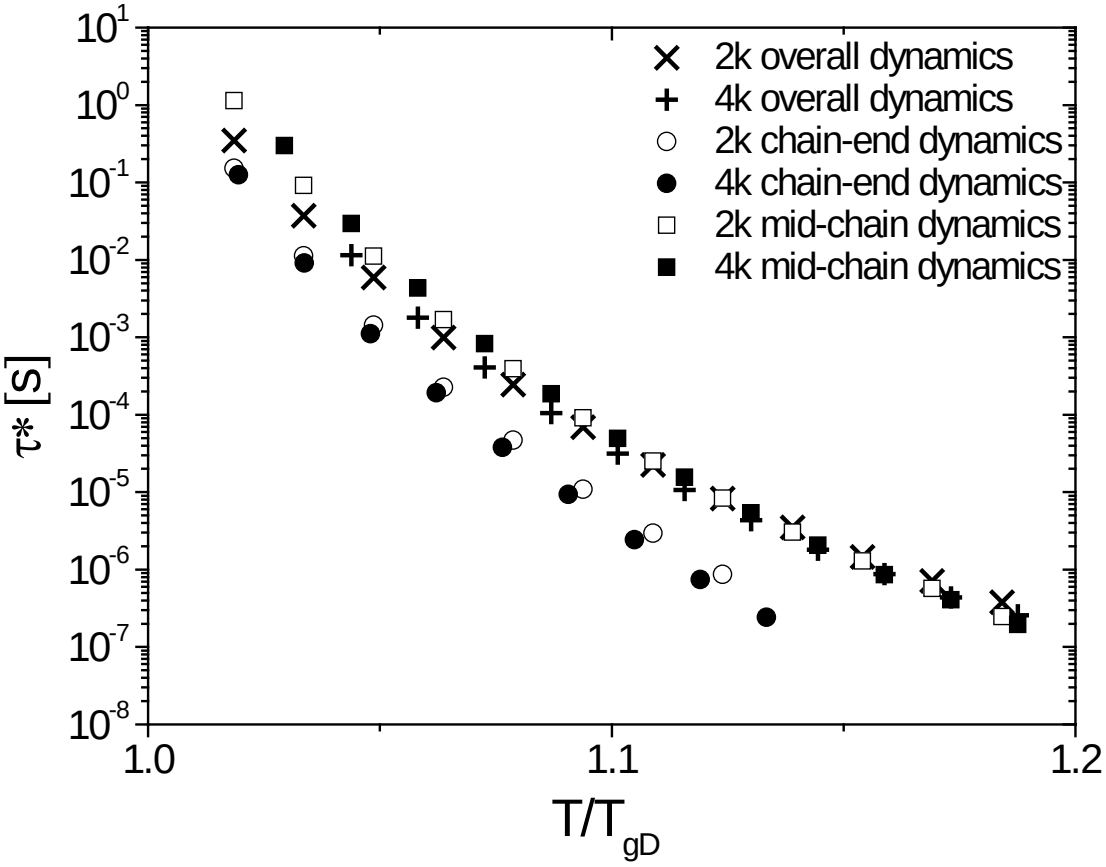

Figure 4.4.2.1.2. Scaled temperature dependence of the characteristic relaxation time (τ*) for overall dynamics as compared with the timescale of the chain-end segments fluctuations and middle-chain segments fluctuations.

Focusing on the chain-end dynamics both polymers (2k and 4k) show similar behavior, it can be seen an evident faster decreasing of these time scales by increasing temperature. This evidences a considerably faster than average motions of the end segments, mainly at high temperatures. Nevertheless, as temperature gets closer to T_g it seems that the time scale of the chain-end fluctuations start approaching that reflecting the overall dynamics. Now having a look at the in-chain dynamics, it can be observed that at high temperatures the time scales of the middle-chain fluctuations of both polymers (2k and 4k) appear to be almost identical to those of the overall dynamics, but at low temperatures (about T/T_{gD}<1.1) the time

characteristic of the fluctuations occurring at the middle of the chain becomes noticeable larger than that of the average dynamics.

Therefore, the above results can be interpreted by the existence of a variable segmental mobility along the polymer chain. As it has already shown, at the high temperature regime the chain-ends tend to move clearly faster than the overall dynamics, whereas the mid-chains segments exhibit a dynamics really similar to the overall. In this way, the faster dynamics found for the chain-ends seems to be also reflected in the high frequency wing decoupled from the overall dynamics, which is observed for the PS-CN samples and consequently for the –CN signal. As this extra contribution only appears for the chain-end functionalized polymers and not for the in-chain functionalized polymers we cannot assigned it to the specific dynamics of the functional group. This finding leads us to associate such an extra wing-like contribution to an intrinsic dynamic aspect of the chain-ends. Nevertheless, at progressively lower temperatures, the two time scales corresponding to the chain-ends and the overall dynamics seem to merge towards a common value, i.e. a common dynamic glass-transition temperature. This relevant result can be interpreted in terms of growing cooperativity regions, named Cooperative Rearranging Regions (CRR), upon a temperature decrease, which coincides with the ideas proposed by Adam & Gibbs [8]. The idea behind it is that at low temperatures the dynamics reflect an average over many types of segments, including chain-ends, since the cooperativity volume is large. As temperature increases this cooperativity volume gradually decreases and the motion gradually reflects single segment motion. In the Adam & Gibbs framework the typical diameter of the CRR was found to be of the order of 1-3 nm depending on the temperature around T_g [9, 10]

being compatible with our results. It has to be remarked that the size corresponding to the molecular volume of the end-group must be the lower limit to the CRR, i.e. the size of the CRR must be larger than that of the end-group, which is approximately of the order of 0.5 nm. Hence, only at temperatures corresponding to CRR smaller in size than 0.5 nm we can expect to observe the independent motion of the end-group. This reasoning of the CRR leads to think that the time scale for the chain-ends is more slowed-down than the overall dynamics as we get closer to T_g from above. All this can be explained in the sense that at low temperatures the dynamics reflects a cooperative motion of many types of segments together with those of the chain-ends rather than the specific part where the –CN functional group is selectively located. However, the dynamics observed at this low temperature regime for the in-chain functionalization is different since in this case the mid-chains segments exhibit a dynamics that is slightly slower than the overall. This effect can be interpreted as a consequence of the local surrounding of the middle of the polymer chain, where less chain-ends than in the overall are found. Then, it gives rise to have a slower mid-chain dynamics contributing to the whole segmental dynamics.

Figures 4.4.2.1.1. and 4.4.2.1.2. have been used to visualize how the dynamics at the end of the chain and in the middle of the chain are as compared with the overall behavior. Summarizing, it has been observed that in terms of the shape the dielectric spectra for the dynamics of the –CN group when it is located at the center of the chain is very similar to the backbone [2]. Moreover, for the chain-end the dynamics have been found to be extremely heterogeneous with faster motions that persist well below T_g [2, 5, 6]. These important findings show also that contributions from the end of the chain influence significantly in the overall dynamics leading to a larger

degree of heterogeneity, namely close to T_g, which could explain the change in the width observed for the α–relaxation with decreasing molecular weight [11]. On the contrary, the specific middle of the chain contributions does not seem to have a relevant influence in the overall dynamics [2].

1 . Y. Ding, V. N. Novikov, A. P. Sokolov, A. Cailliaux, C. Dalle-Ferrier, C. Alba-Simionesco and B. Frick, Macromolecules, 37, 9264 (2004)

2 . S. Plaza-García, R. Lund, A. Alegría, J. Colmenero, J. Janoski and R. P. Quirk, Macromolecules, 44, 7810 (2011)

3 . M. L. Williams, R. F. Landel and J. D. Ferry, J. Am. Chem. Soc., 77, 3701 (1955)

4 . J. D. Ferry, Viscoelastic Properties of Polymers, 3rd Ed., John Wiley & Sons, New York (1980)

5 . R. Lund, S. Plaza-García, A. Alegría, J. Colmenero, J. Janoski, S. R. Chowdhury and R. P. Quirk, Macromolecules, 42, 8875 (2009)

6 . R. Lund, S. Plaza-García, A. Alegría, J. Colmenero, J. Janoski, S. R. Chowdhury and R. P. Quirk, Journal of Non-Cryst. Solids, 356, 676 (2010)

7 . G. A. Schwartz, J. Colmenero and A. Alegría, Macromolecules, 40, 3246 (2007)

8 . G. Adam and J. H. Gibbs, J. Chem. Phys., 43, 139 (1965)

9 . E. Hempel, G. Hempel, A. Hensel, C. Schick and E. Donth, J. Chem. Phys., 104, 2460 (2000)

10 . D. Cangialosi, A. Alegría and J. Colmenero, Phys. Rev. E., 76, 011514 (2007)

11 . J. Mattsson, R. Bergman, P. Jacobsson and L. Börjesson, Phys. Rev. Lett., 90, 075702 (2003)

5. Polystyrene/Poly (vinyl methyl ether) (PS/PVME) Blends Results

In this chapter polymer blend dynamics will be investigated requiring the use of different experimental techniques. One of the main goals of most of the experimental studies carried out on polymer blends has been to resolve the dynamics of the individual components in the blend. In the past many systems have been investigated trying to characterize the segmental relaxation dynamics of the components forming the blend. Within all the polymer blends investigated, one of the most extensively studied systems has been the PS/PVME blend. This particular system has been investigated by several techniques but the component that has been investigated in depth has been PVME and there is not so detailed information about PS dynamics in the blends. One major reason for this is that by using dielectric spectroscopy the response of the blend is largely dominated by the fluctuation of the dipole moment associated to PVME. Furthermore, when using neutron scattering techniques the fact that deuterated PVME was not available makes the NS investigation of this blend system to be also focused on the PVME component only.

For this study the most useful technique has been Broad-band Dielectric Spectroscopy (BDS), which in combination with these PS/PVME blends made of in-chain functionalized polystyrenes allows accessing to the PS component dynamics as well as the already studied PVME component dynamics as it will be shown in the following. Also, the use of Differential Scanning Calorimetry as a complementary technique has been needed to characterize these blends.

The study of the dynamics of these PS/PVME blends has been carried out on different compositions (75/25, 50/50 and 25/7575 wt%) covering the whole range.

5.1. DSC Results

DSC was employed to determine the glass-transition temperatures (T_g) corresponding to the three different types of PS/PVME blends investigated. This technique allowed studying the miscibility on this kind of systems and in particular checking that it is not significantly affected by functionalization as it will be reflected in the obtained results. In fact, to prove it polymer blends prepared with a conventional PS as a reference (PS2300 / PVME) and with the same compositions than the blends made of H- and CN- functionalized PS were included in this study. Namely, the samples investigated in this work where: PSHPS2k / PVME 75/25 – PSCNPS2k / PVME 75/25, PSHPS2k / PVME 50/50 – PSCNPS2k / PVME 50/50 and PSHPS2k / PVME 25/75 – PSCNPS2k / PVME 25/75. Figure 5.1.1. shows the temperature dependence of the normalized heat capacity derivative (dC_p/dT) for these polymer blends.

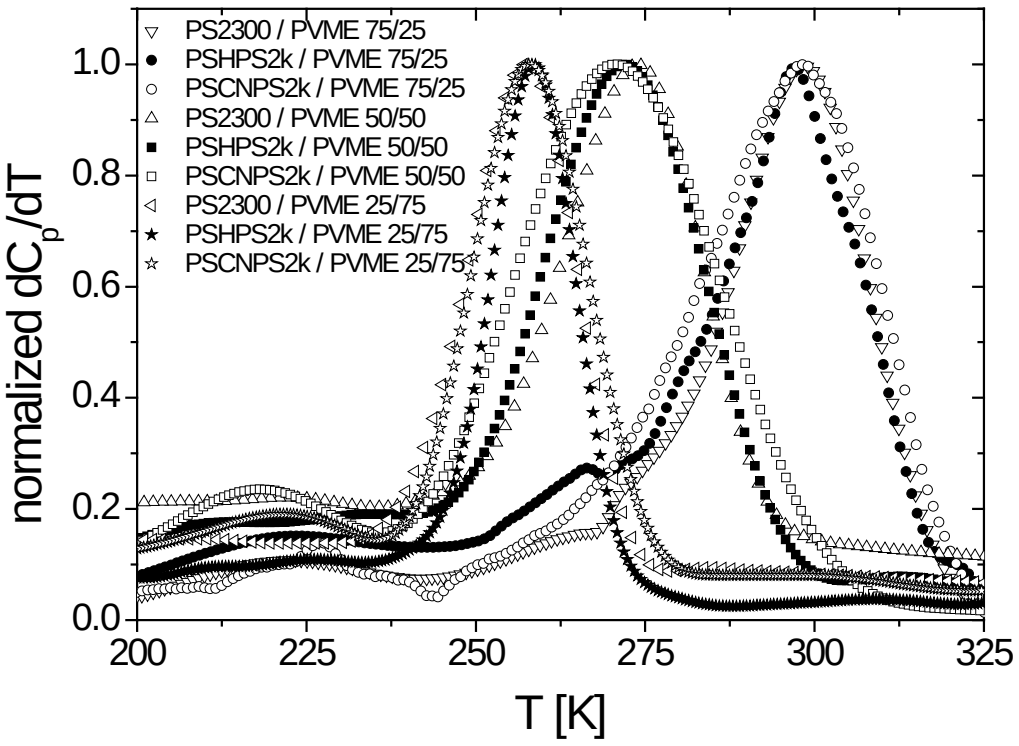

Figure 5.1.1. Comparison of the normalized heat capacity derivative (dC_p/dT_{norm}) as a function of the temperature for the conventional polystyrene blends and the three different pairs of functionalized polymer blends having a composition of 75/25, 50/50 and 25/75.

Polymer blend Code	T_g [K]
PS2300/PVME 75/25	298 ± 1
PS-H-PS 2k / PVME 75/25	297 ± 1
PS-CN-PS 2k / PVME 75/25	298 ± 1
PS2300/PVME 50/50	274 ± 1
PS-H-PS 2k / PVME 50/50	272 ± 1
PS-CN-PS 2k / PVME 50/50	271 ± 1
PS2300/PVME 25/75	257 ± 1
PS-H-PS 2k / PVME 25/75	258 ± 1
PS-CN-PS 2k / PVME 25/75	258 ± 1

Table 5.1.1. Glass-transition temperatures (T_g) for the various polystyrene blends.

The effect of functionalization can be checked by comparing within a same composition, 75/25 for instance, the –H functionalized PS blend ((PSHPS2k / PVME 75/25) with the conventional PS blend (PS2300 / PVME 75/25). Looking at Figure 5.1.1. it seems that functionalization does not affect miscibility since the T_g's (peak positions) are practically indistinguishable. The same result is obtained for the other two compositions, 50/50 and 25/75.

Now comparing functionalization with –H and –CN groups, it can be observed that when these functionalized PS, having a –H or a –CN group located in the middle of the chain, are mixed with poly (vinyl methyl ether), T_g is essentially unaffected being very similar for each pair of polymer blends. Such finding could be expected since in the previous section it was shown that both H/CN in-chain functionalized PS (PSHPS2k and PSCNPS2k) exhibited the same T_g not having a significant effect due to the type of functionalization [1]. However, looking at the width of the glass-transition it can be clearly seen that all –CN functionalized PS blends exhibited a slightly wider glass-transition compared to the –H functionalized PS blends (references) independently of the composition. This effect of functionalization on width can be observed in detail in Figure 5.1.2. where we present the width of the glass-transition corresponding to each of the blends defined by the full-width at half-maximum (*fwhm*) of the peaks shown previously in Figure 5.1.1.. As seen the glass-transition of the CN-functionalized PS blends (PSCNPS2k / PVME) is always distinctly wider than that of the references (PSHPS2k / PVME). Nevertheless, the effect is not very pronounced and therefore miscibility can be considered not significantly affected by the type of functionalization. Extra support for this conclusion will be given below.

Moreover, comparing the –H functionalized PS blend (PSHPS2k / PVME) with the conventional PS blend (PS2300 / PVME) it can be observed that there are no significant differences in width, which is in agreement with the previous results evidencing that this kind of functionalization does not affect miscibility.

Now regarding composition it can be observed that as PVME content increases in the polymer blend T_g takes a value progressively smaller from 75/25 to 50/50 and from 50/50 to 25/75 as expected. This can be even more clearly seen in Figure 5.1.2. where the average T_g corresponding to each of the blends is shown as a function of its PS percentage in the blend.

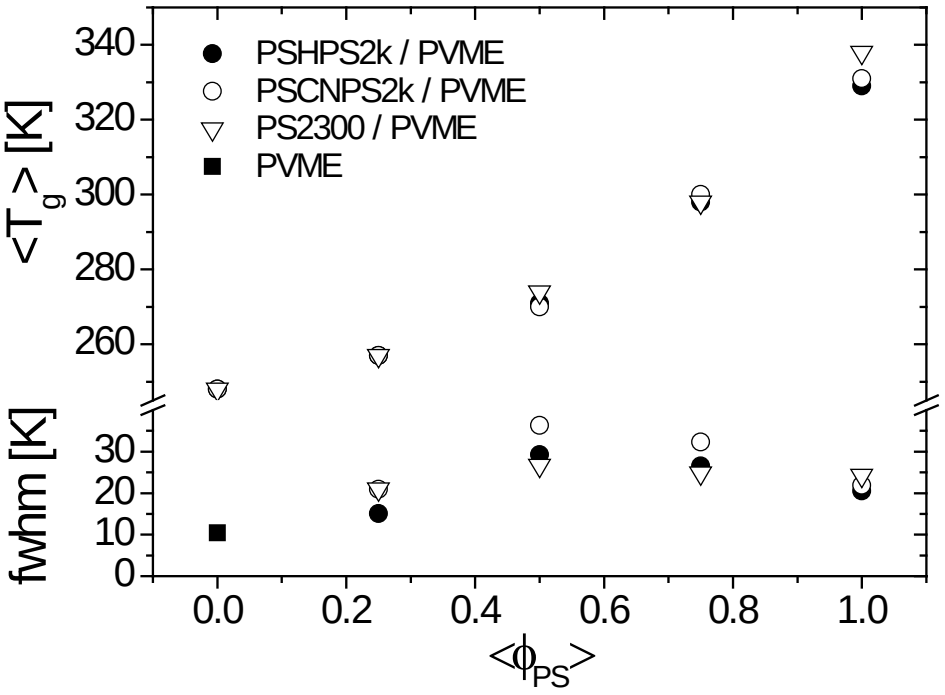

Figure 5.1.2. The average T_g and the full-width at half-maximum (*fwhm*) as a function of the PS content in the blends.

Summarizing, it should be remarked that functionalization does not affect practically miscibility and –H and –CN functionalized PS behave very similar at

least from the calorimetric point of view and also similar to a conventional PS of the same molecular weight.

5.2. BDS Results

5.2.1. 75/25 PS/PVME Blends

Now, we will focus our attention on BDS measurements to continue studying the dynamics of these polystyrene blends. As it has been already explained the combination of BDS and the proper PS functionalization opens the route for the investigation of the PS dynamics in this blend that has been intensively investigated in the past but focusing the attention on the study of the PVME component. In the following section we will start presenting the data of PS/PVME blends with the lowest PVME content where resolving the dynamics of PS is easier.

Figure 5.2.1.1. shows the frequency dependence of the loss peak comparing the dielectric losses (ε“) of the -H functionalized PS blend (PS-H-PS2k/PVME) with the conventional PS blend (PS2300/PVME).

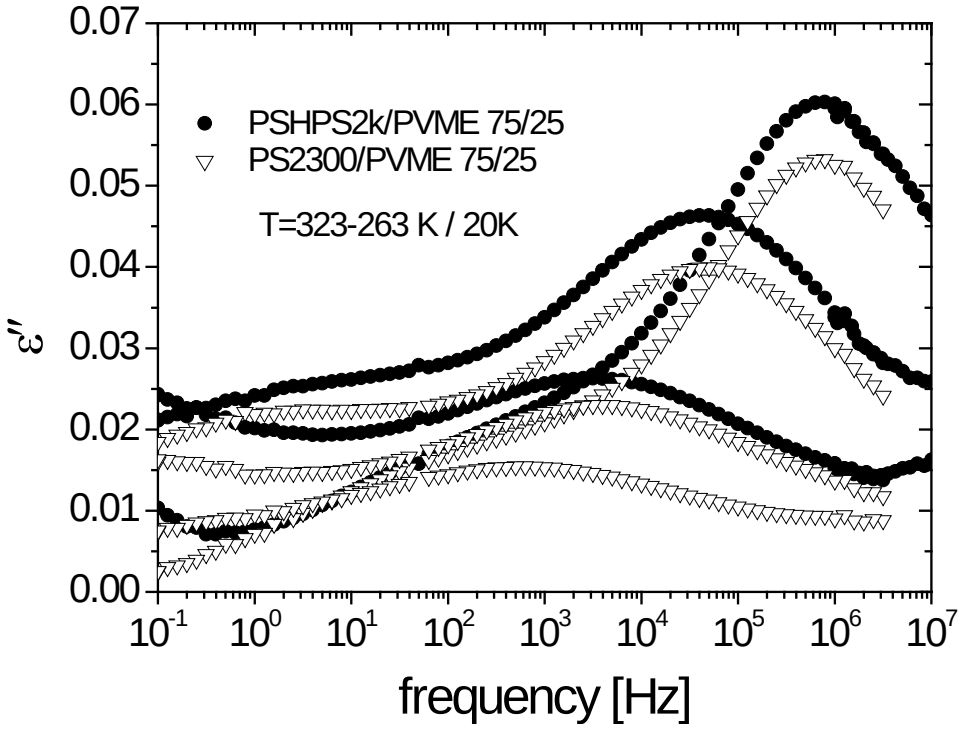

Figure 5.2.1.1. Dielectric segmental relaxation spectra showing the loss permittivity as a function of frequency for the –H functionalized PS blend (PS-H-PS2k/PVME) and the conventional PS blend (PS2300/PVME) at a given range of temperatures.

From this plot we can observe a similar dynamics for the poly(vinyl methyl ether) using both functionalized and conventional PS. The minor differences in intensity would be attributed to the typical uncertainty in the sample capacitor geometry. This result is in agreement with the DSC results where it was shown that both samples present essentially the same glass transition process. Nevertheless, the present dielectric results are a much more detailed test although mainly reflects the behavior of the polar component, i.e. PVME. Thus, both BDS and DSC results evidence that blends made with functionalized PS and PVME are directly comparable with those made by mixing conventional PS and PVME, provided the molecular mass is similar.

Now we compare both functionalized PS blends as seen in Figure 5.2.1.2.

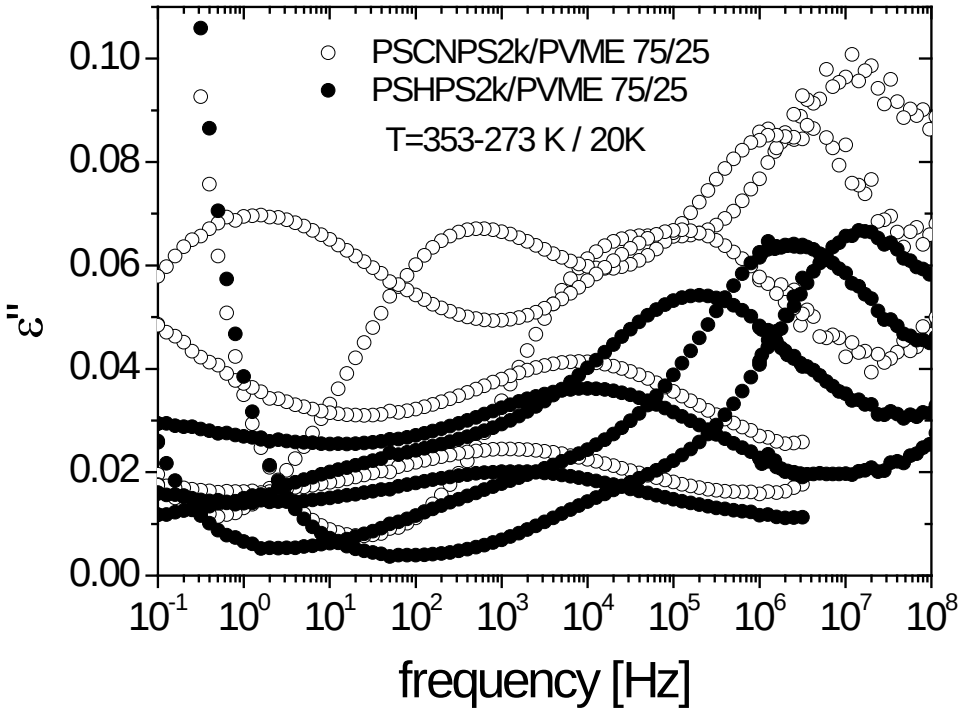

Figure 5.2.1.2. Dielectric segmental relaxation spectra showing the loss permittivity (ε") as a function of frequency for the –H functionalized PS blend (PS-H-PS2k/PVME) and the –CN functionalized PS blend (PS-CN-PS2k/PVME) at a given range of temperatures.

Due to the similar overall behavior observed for these two functionalized PS blends by DSC, they can be used together to resolve PS and PVME component dynamics since in the case of the –H functionalized PS blend (PSHPS2k / PVME) what is mainly reflected by dielectric relaxation is the response of the PVME component, whereas in the –CN functionalized PS blend (PSCNPS2k / PVME) both PS and PVME contributions are well observed. The approach followed to separate these two dynamic contributions consists namely of subtracting the response of the –H functionalized PS blend (reference) from the response of the –CN functionalized PS blend. However, this subtraction requires the use of two factors. A factor (f_1), which comes from the superposition of the two H/CN functionalized PS blends at a very low temperature where only the PVME contribution can be observed, compensates

minor differences in the sample capacitor geometry not properly accounted in the raw data.

Accordingly we can write:

$$\varepsilon''_{PSCNPS\,2k/PVME} \cdot f_1 = \varepsilon''_{PSCNPSblend} + \varepsilon''_{PVMEblend}$$

$$\varepsilon''_{PSHPS\,2k/PVME} = \varepsilon''_{PSHPSblend} + \varepsilon''_{PVMEblend} \qquad [5.2.1.1.]$$

A second factor (f_2) is used to account for the ratio between the contributions of H- and CN- functionalized PS in the blends, i.e. $\varepsilon''_{PSHPSblend} = f_2 \bullet \varepsilon''_{PSCNPSblend}$. The value f_2 was obtained from the superposition of the dielectric losses from the two functionalized homopolymers at a given temperature where their responses are well centered (see Figure 4.3.2.). In this way, we will take into account that there is a small but relevant contribution to the dielectric losses coming from the H-functionalized PS (mainly in the blends with low PVME concentration).

Therefore, the equations used with this procedure to resolve component dynamics were the following:

$$\varepsilon''_{PSCNPSblend} = \frac{\left(\varepsilon''_{PSCNPS/PVME} \cdot f_1\right) - \varepsilon''_{PSHPS/PVME}}{(1 - f_2)} \qquad [5.2.1.2.]$$

$$\varepsilon''_{PVMEblend} = \varepsilon''_{PSHPS/PVME} - \left(f_2 \cdot \varepsilon''_{PSCNPSblend}\right) \qquad [5.2.1.3.]$$

Figure 5.2.1.3. shows the frequency dependence of the loss peak for both H/CN functionalized PS blends, which are the measured signals, as well as PS and PVME contributions obtained by this procedure at a representative temperature (313 K).

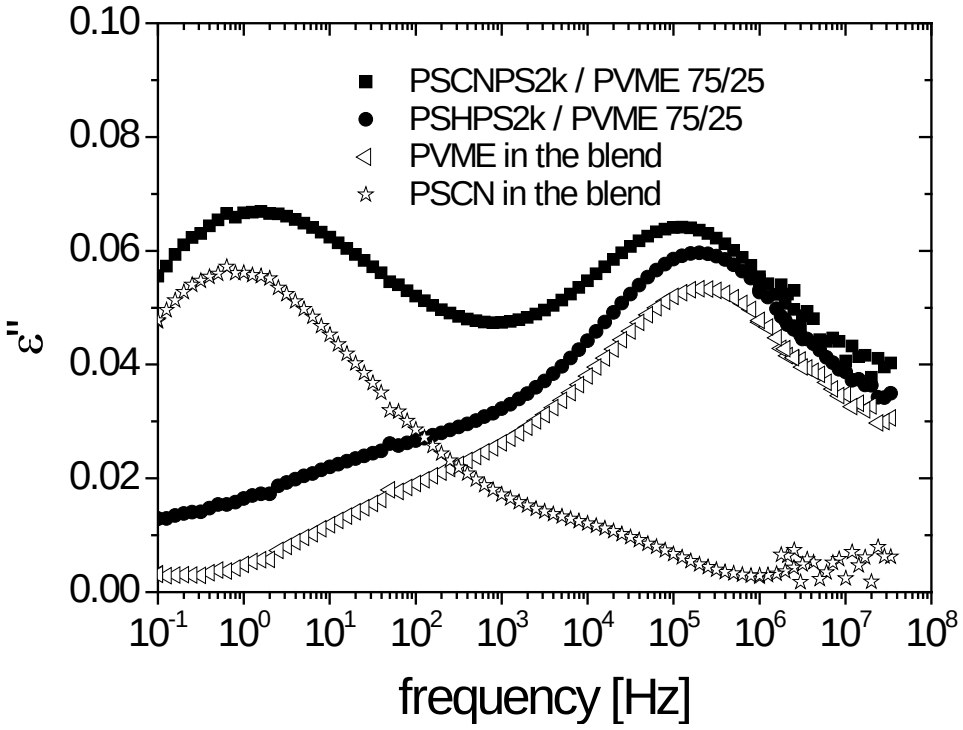

Figure 5.2.1.3. Dielectric segmental relaxation spectra showing the loss permittivity (ε") as a function of frequency for the H/CN functionalized PS blends, PSHPS2k/PVME 75/25 and PSCNPS2k/PVME 75/25, respectively, and their PVME and PSCN component dynamics at 313 K.

Concerning the response of the PSCN in the blend we can observe at first sight a main peak appearing at the low frequency regime, which would correspond to the PS component dynamics in the conventional blend.

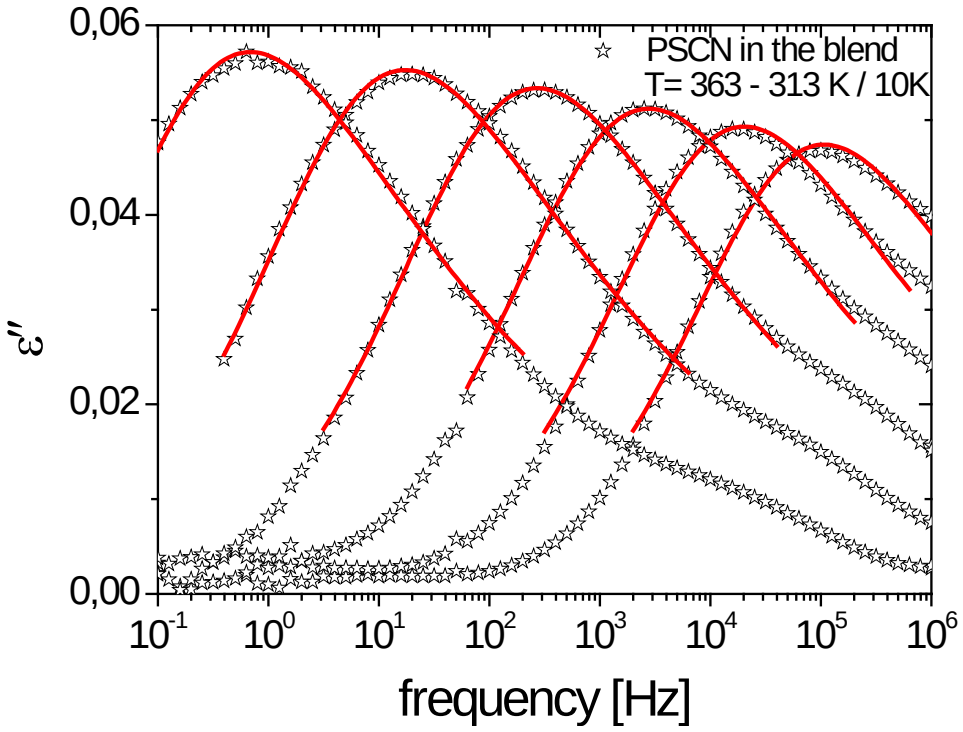

Figure 5.2.1.4. Comparison of the frequency dependence of the dielectric loss (ε") for the PSCN contribution in a PS/PVME 75/25 blend where the fitting is focused on the main loss peak.

Looking in detail at the shape of the PSCN component dielectric losses over a broad temperature range (see Figure 5.2.1.4) an extra contribution with a shoulder-like shape appearing at the high frequency regime can be clearly observed. The fact of obtaining this fast contribution for the PSCN component in the blend is not consequence of an inappropriate separation of responses during the procedure since it was performed within a precise control. In fact, this high-frequency tail would be attributed also to the PS dynamics. What it happens is that although the average PS is getting frozen, there are always PS segments moving faster, although likely with small amplitude, once PVME component starts moving and this generates a PS dielectric response in some way related with the PVME motions. As a first approach we tried to describe the segmental relaxation process of the PSCN component focusing only on the main loss peak observed in Figure 5.2.1.4. not including the

high frequency contribution. For that the Alvarez-Alegría-Colmenero (AAC) function [2.1.2.1.16.] was used for the fitting instead of using a conventional Havriliak Negami equation [2.1.2.1.13.] since the former is a more restricted equation where there is only one shape free parameter involved.

The so obtained parameters are given in the following table 5.2.1.1. In the same table characteristic relaxation time ($\tau^*=1/\omega_{max}$) obtained from the HN parameters as well as the full-width-half-maximum (*fwhm*) [2.1.2.1.15.] parameter are included.

Note that τ^* and *fwhm* values are very much representative of the experimentally resolved loss peak and therefore will be not much dependent on the selected fitting strategy.

T [K]	Δε	τ_{HN} [s]	B	γ	τ* [s]	fwhm DECADES
363.15	0.282	6.06E-6	0.579	0.419	1.49E-6	3.726
353.15	0.300	3.34E-5	0.57	0.414	7.85E-6	3.822
343.15	0.319	2.56E-4	0.561	0.409	5.73E-5	3.920
333.15	0.338	2.71E-3	0.554	0.406	5.88E-4	3.988
323.15	0.361	0.045	0.543	0.400	0.009	4.123
313.15	0.375	1.114	0.546	0.402	0.231	4.083

Table 5.2.1.1. Havriliak Negami parameters obtained for the α–relaxation characterization of the PSCN contribution in the PSCNPS2k / PVME 75/25 blend when only the main loss peak is considered.

In order to obtain a more complete description of these same data a much more detailed analysis of the data was strictly required. In this case the fitting of the two peaks together was performed using a conventional Havriliak Negami equation

[2.1.2.1.13.] to describe the main loss peak of the PSCN component appearing at the low frequency regime and a Cole-Cole function (γ=1 in the HN equation 2.1.2.1.13.) to describe the shoulder in the high frequency tail. The result is shown in Figure 5.2.1.5. and the parameters obtained from the fitting are given in Table 5.2.1.2.

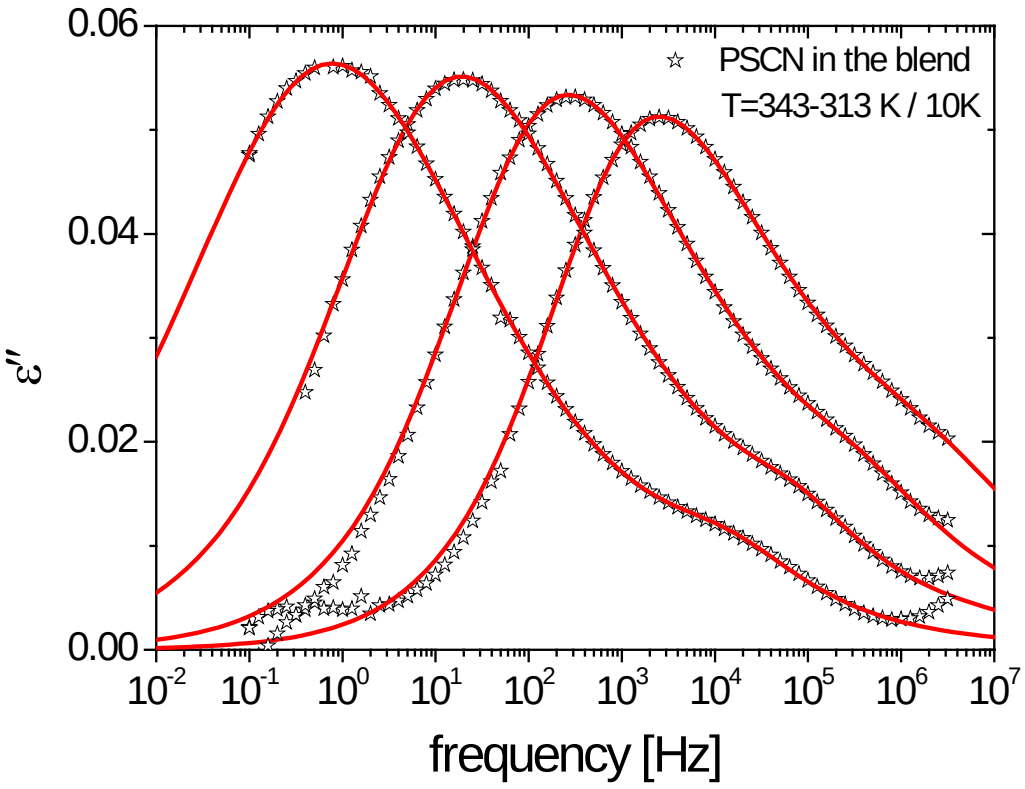

Figure 5.2.1.5. Comparison of the frequency dependence of the dielectric loss (ε“) for the PSCN contribution in a PS/PVME 75/25 blend where the fitting involves both the mean loss peak and the high frequency tail.

T [K]	$\Delta\varepsilon_1$	τ_{HN1} [s]	β_1	γ_1	τ_1^* [s]	$fwhm_1$ DECADES
343.15	0.299	2.57E-4	0.578	0.429	6.54E-5	3.678
333.15	0.328	2.36E-3	0.54	0.456	5.98E-4	3.820
323.15	0.355	3.16E-2	0.494	0.502	8.38E-3	3.969
313.15	0.382	0.444	0.408	0.721	0.205	4.044

T [K]	$\Delta\varepsilon_2$	τ_{HN2} [s]	β_2	γ_2	τ_2^* [s]	$fwhm_2$ DECADES	$\Delta\varepsilon_{total}$
343.15	0.028	7.33E-8	0.561	1	7.33E-8	2.411	0.327
333.15	0.015	4.27E-7	0.674	1	4.27E-7	1.929	0.343
323.15	0.009	2.04E-6	0.830	1	2.04E-6	1.475	0.365
313.15	0.013	1.09E-5	0.715	1	1.09E-5	1.789	0.395

Table 5.2.1.2. Parameters obtained using a combination of a Havriliak Negami equation and a Cole-Cole function to describe the α–relaxation of the PSCN contribution in the PSCNPS2k / PVME 75/25 blend when the total response is considered, being (1) the main loss peak and (2) the high frequency tail . In addition, the characteristic relaxation time (τ^*) obtained from the HN parameters as well as the full-width-half-maximum parameter (*fwhm*) and the total dielectric strength ($\Delta\varepsilon_{total}$) are included in the table.

A combination of these two procedures used to describe the α–relaxation processes for the PSCN contribution in the blend, the first focused only on the main loss peak response and the second one being more exhaustive describing the dielectric response as a whole, is shown in Figure 5.2.1.6. As seen the first methodology is applied for the high temperatures when only the main peak is observed, whereas the second one can be only applied when the shoulder is clearly observed in the spectra.

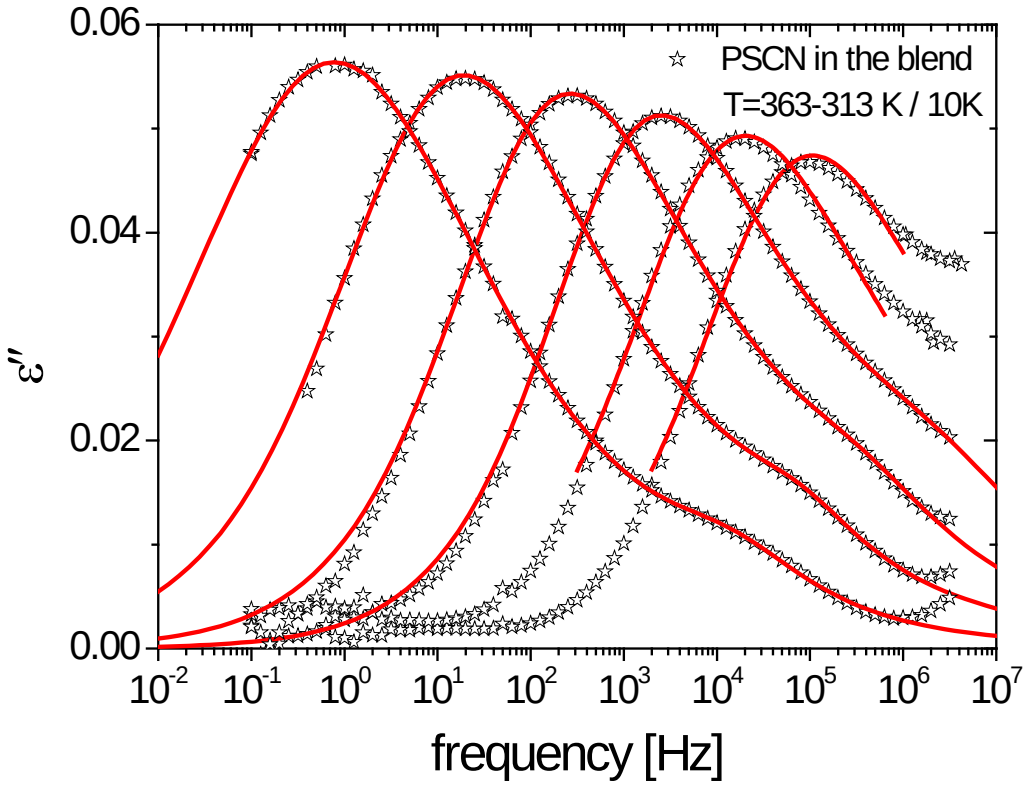

Figure 5.2.1.6. Dielectric segmental relaxation spectra showing the loss permittivity (ε") as a function of frequency for the PS contribution in the -CN functionalized PS blend using a simple HN equation for the highest temperatures and a double HN equation for the rest of the temperature range.

In Figure 5.2.1.7.a) it is represented the temperature dependence of the dielectric strength ($\Delta\varepsilon$) determined directly from the fitting with a single peak of the main losses (see Figure 5.2.1.4.) as well as the total dielectric strength value ($\Delta\varepsilon_{total}$) determined as the sum of the two dielectric strengths obtained when the fitting is carried out including the shoulder (see Figure 5.2.1.5.). They are represented in the plot with open squares and X, respectively. As expected the values obtained for the dielectric strength ($\Delta\varepsilon$) when the fitting is focused only on the main loss peak match well with those obtained when the dielectric response is taken as a whole including the losses visible as a shoulder at the high frequency regime ($\Delta\varepsilon_{total}$), because the weakness of this component. The dielectric strength of the PS component in the blend depicted a temperature dependence similar to that in the homopolymer with a

moderated decreasing as temperature increases. On the other hand Figure 5.2.1.7.b) shows also the temperature dependence of *fwhm*. Here it is observed that the loss peak width decreases markedly with increasing temperature eventually approaching at high temperature the value typical of the homopolymer loss peak (approximately 2.7).

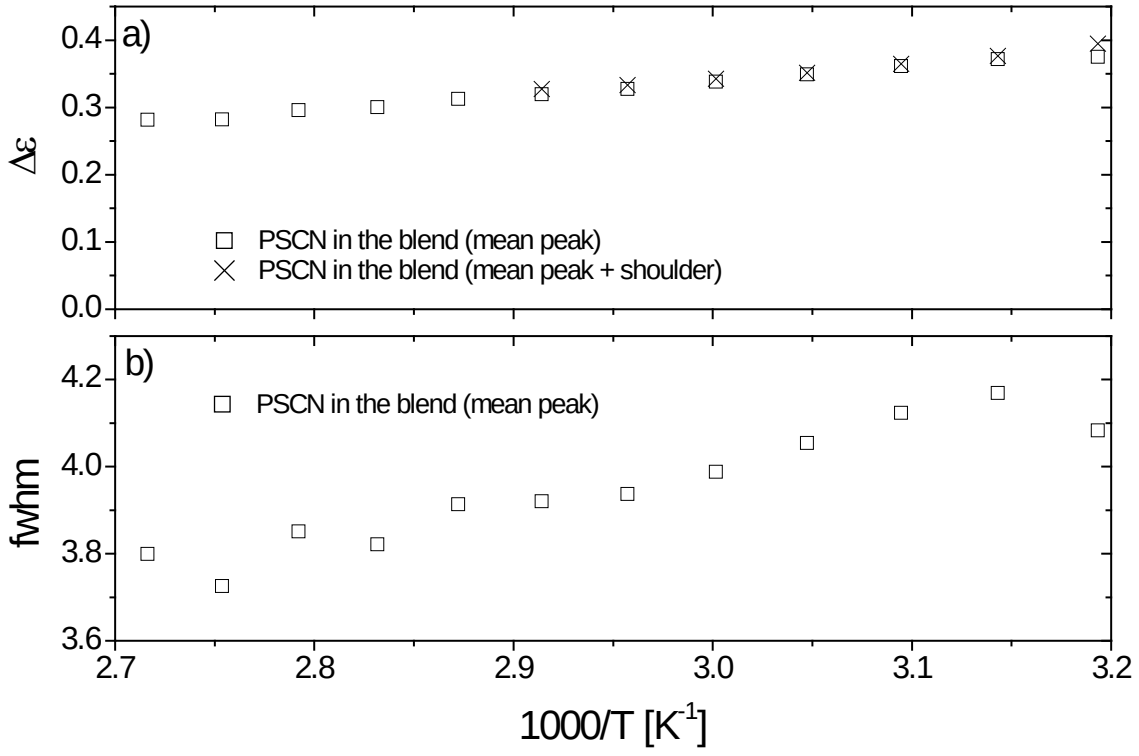

Figure 5.2.1.7. The temperature dependence of the dielectric strength ($\Delta\varepsilon$) and the full-width-half-maximum (*fwhm*) for the PSCN component in the PSCNPS2k / PVME 75/25 blend.

The previous separation procedure also provides the 'fully resolved' contribution of PVME in the same blend. Note that in previous investigations the contributions from PS to the dielectric losses were completely neglected. However, in this type of blends despite that the PS contribution is small, it is very apparent (at this high PS concentration), namely in the low frequency side of the loss peaks from the conventional PS blend (see fig 5.2.1.3).

Now concerning the response of the PVME in the blend (see Figure 5.2.1.8.) we can observed at first sight a main peak appearing at the high frequency regime, which represents the main PVME component dynamics in the blend. However, the low frequency side shoulder is also evident, namely around the average T_g.

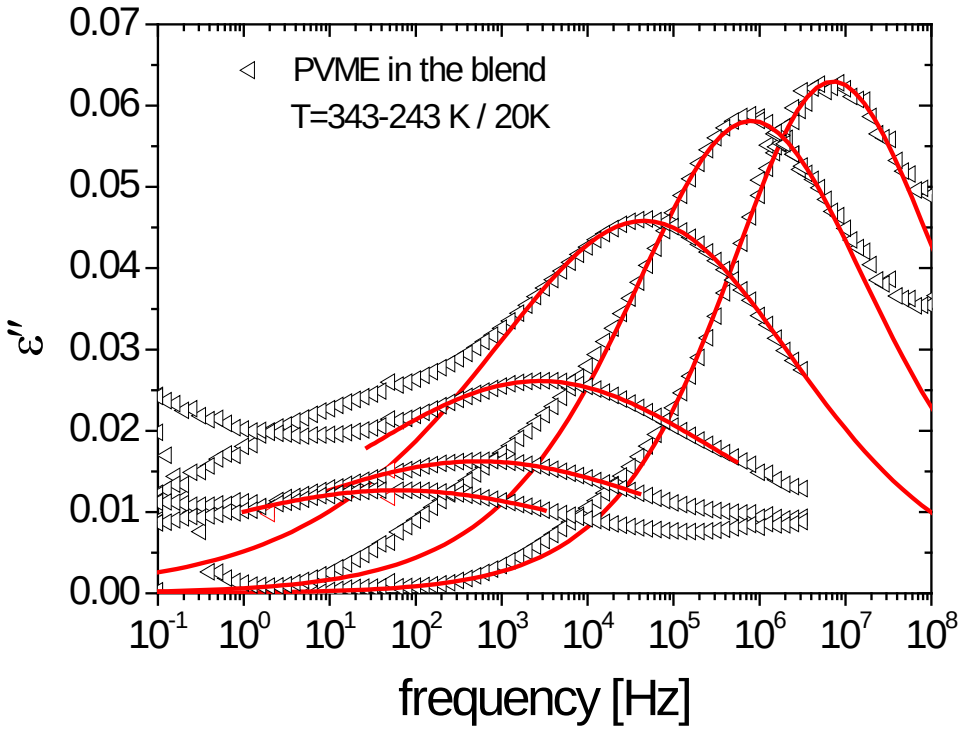

Figure 5.2.1.8. Comparison of the frequency dependence of the dielectric loss (ε") for the PVME contribution in a PS/PVME 75/25 blend where the fitting is focused on the main loss peak.

The main PVME contributions were described using different approaches depending on the temperature range. At very low temperatures due to the symmetry exhibited by the loss peaks a Cole-Cole function was used (γ=1 in the HN equation 2.1.2.13.). However, this symmetry stars disappearing as temperature increases making necessary the use of a conventional Havriliak Negami function. However, at this high temperature regime the high frequency tail goes out of the experimental window, so we decided to fix in the fitting procedure the product β·γ determining the asymptotic behavior at high frequencies to:

$$\beta \cdot \gamma = 0.4 \qquad [5.2.1.4.]$$

that is what is found for the case of the pure PVME [2].

The so obtained parameters are shown in the following table:

T [K]	Δε	τ_{HN} [s]	B	γ	τ* [s]	fwhm DECADES
353.15	0.345	1.43E-8	0.526	0.761	8.75E-9	2.956
343.15	0.363	3.39E-8	0.499	0.801	2.22E-8	3.06
333.15	0.379	7.33E-8	0.452	0.885	5.66E-8	3.275
323.15	0.375	2.30E-7	0.427	0.936	1.98E-7	3.408
313.15	0.374	6.95E-7	0.378	1	8.03E-7	3.727
303.15	0.371	1.68E-6	0.316	1	3.50E-6	4.272
293.15	0.337	1.74E-5	0.294	1	1.74E-5	5.027
283.15	0.268	5.74E-5	0.268	1	5.74E-5	5.563
273.15	0.208	1.22E-4	0.263	1	1.22E-4	5.685
263.15	0.180	2.94E-4	0.249	1	2.93E-4	6.041
253.15	0.163	8.09E-4	0.24	1	8.09E-4	6.279
243.15	0.148	0.003	0.235	1	0.003	6.41
233.15	0.145	0.010	0.220	1	0.010	6.880

Table 5.2.1.3. Havriliak Negami parameters obtained for the α–relaxation characterization of the PVME contribution in the PSCNPS2k / PVME 75/25 blend when only the mean loss peak is considered. In addition, the characteristic relaxation time (τ^*) obtained from the HN parameters as well as the full-width-half-maximum parameter (*fwhm*) are included in the table.

As was the case of the PSCN contribution in the blend, here we also observe that for a complete description of the PVME response we should include the shoulder appearing now at the low frequency regime. Consequently, in a more limited temperature range the response was fitted as a double peak accessing to much more

complete information about the dynamics of the PVME component in the blend. For such a fitting a Cole-Cole function (γ=1 in the HN equation 2.1.2.1.13.) was used to account for the low frequency part of the data and a conventional Havriliak Negami equation [2.1.2.1.13.] with the restriction $\beta \cdot \gamma = 0.4$ [5.2.1.4.] was used describing these high frequency main loss peaks.

The result is shown in Figure 5.2.1.9. and the obtained parameters are summarized in Table 5.2.1.4.

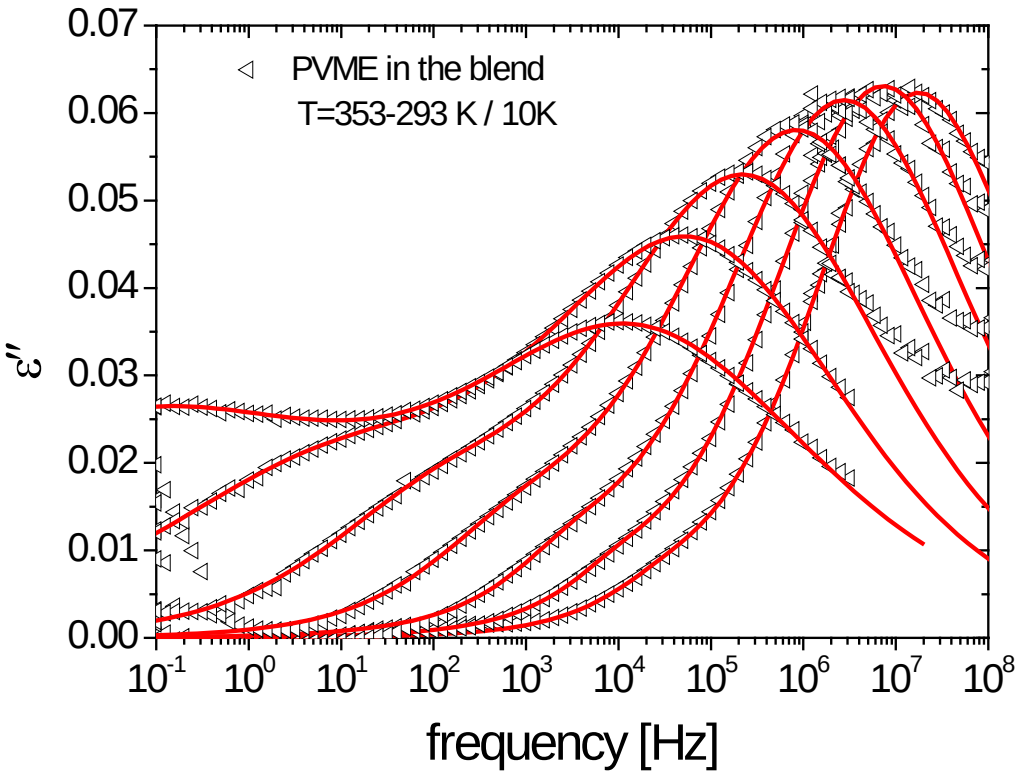

Figure 5.2.1.9. Comparison of the frequency dependence of the dielectric loss (ε") for the PVME contribution in a PS/PVME 75/25 blend where the fitting involves both the mean loss peak and the low frequency tail.

T [K]	$\Delta\varepsilon_1$	τ_{HN1} [s]	β_1	γ_1	τ_1^* [s]	$fwhm_1$ DECADES
353.15	0.005	5.59E-6	0.864	1	5.59E-6	1.399
343.15	0.007	1.68E-5	0.924	1	1.68E-5	1.277
333.15	0.012	5.14E-5	0.806	1	5.14E-5	1.533
323.15	0.031	2.21E-4	0.612	1	2.21E-4	2.172
313.15	0.064	1.64E-3	0.475	1	1.64E-3	2.937
303.15	0.144	2.41E-2	0.326	1	2.41E-2	4.489
293.15	0.263	2.723	0.257	1	2.723	5.836

T [K]	$\Delta\varepsilon_2$	τ_{HN2} [s]	β_2	γ_2	τ_2^* [s]	$fwhm_2$ DECADES	$\Delta\varepsilon_{total}$
353.15	0.340	1.51E-8	0.537	0.745	9.04E-9	2.914	0.346
343.15	0.362	3.33E-8	0.501	0.798	2.17E-8	3.052	0.368
333.15	0.374	7.68E-8	0.461	0.867	5.71E-8	3.23	0.387
323.15	0.368	2.18E-7	0.433	0.924	1.83E-7	3.378	0.399
313.15	0.354	6.48E-7	0.398	1	6.58E-7	3.591	0.418
303.15	0.311	1.79E-6	0.364	1	2.3E-6	3.831	0.455
293.15	0.268	8.88E-6	0.33	1	8.88E-6	4.437	0.531

Table 5.2.1.4. Parameters obtained using a combination of a Havriliak Negami equation and a Cole-Cole function to describe the α–relaxation of the PVME contribution in the PSCNPS2k / PVME 75/25 blend when the total response is considered, being (1) the low frequency tail and (2) the main loss peak. In addition, the characteristic relaxation time (τ*) obtained from the HN parameters as well as the full-width-half-maximum parameter (*fwhm*) and the total dielectric strength ($\Delta\varepsilon_{total}$) are included in the table.

A combination of these two procedures used to describe the α–relaxation processes for the PVME contribution in the blend is shown in Figure 5.2.1.10. where the first methodology applies well at low temperatures, when only a peak is observed, whereas the second one describes the response when the low frequency component is clearly observed in the spectra.

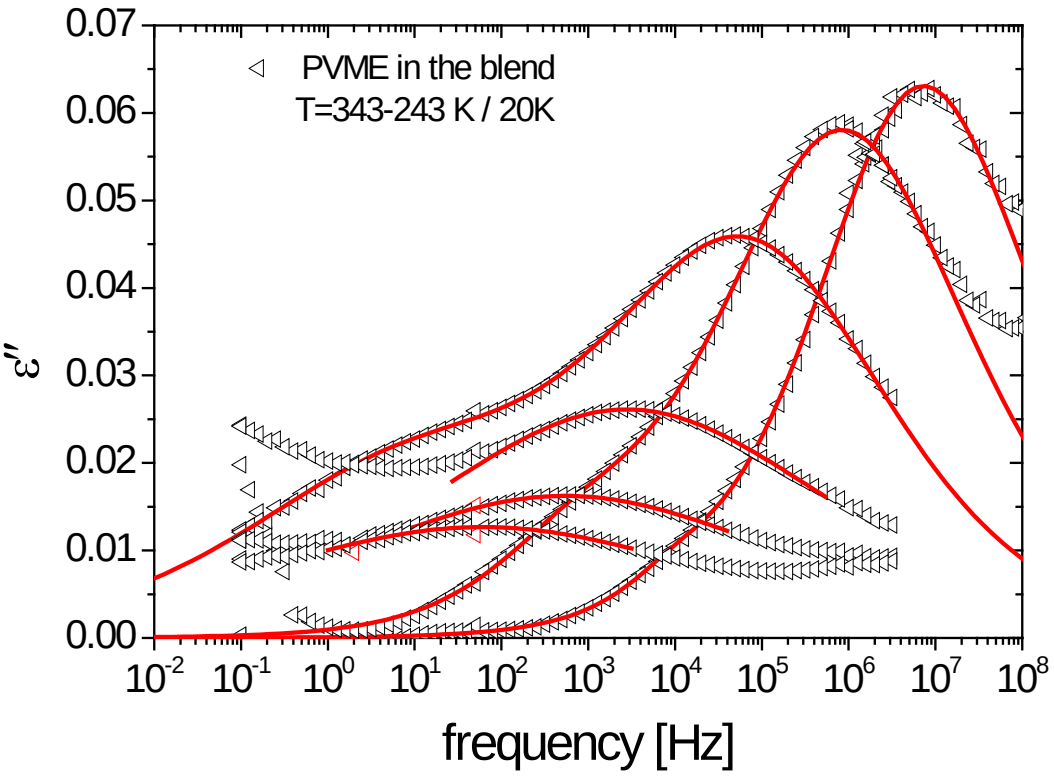

Figure 5.2.1.10. Dielectric segmental relaxation spectra showing the loss permittivity as a function of frequency for the PVME contribution in the -CN functionalized PS blend using a simple HN equation for the highest temperatures and a double HN equation for the rest of the temperature range.

In Figure 5.2.1.11.a) it is represented the temperature dependence of the dielectric strength ($\Delta\varepsilon$) determined directly from the fitting of the main peaks (see Figure 5.2.1.8.) as well as the total dielectric strength value ($\Delta\varepsilon_{total}$) determined as the sum of the two dielectric strengths obtained when the fitting is carried out for a double peak (see Figure 5.2.1.9.), represented in the plot with open squares and X, respectively. On the other hand, Figure 5.2.1.11.b) shows the temperature

dependence of the full-width-half-maximum (*fwhm*) obtained from the β and γ shape parameters of the main loss peaks fittings [2.1.2.1.15.].

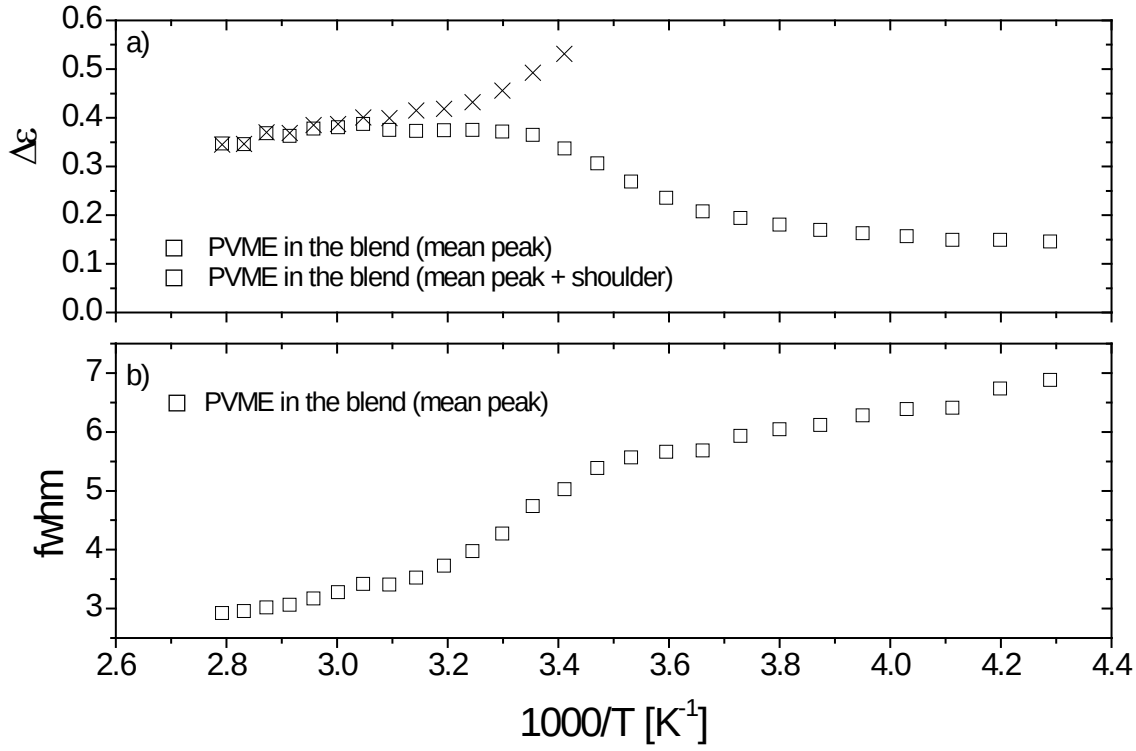

Figure 5.2.1.11. The temperature dependence of the dielectric strength ($\Delta\varepsilon$) and the full-width-half-maximum (*fwhm*) for the PVME component in the PSCNPS2k / PVME 75/25 blend.

Concerning the relaxation strength ($\Delta\varepsilon$), it is clear that the temperature dependence is different from that corresponding to the homopolymer, only the high temperature data (x in the plot) seems to follow the conventional behavior. By decreasing temperature there is a continuous drop of the detected dielectric relaxation, which should be related with dipolar entities that cannot contribute longer most likely due to the presence of a surrounding PS rich environment. This will be discussed in detail below.

On the other hand, the temperature dependence of the *fwhm* is qualitatively closer to that found for the PSCN component but the broadening at low temperature is much more pronounced, likely indicative of an extremely heterogeneous environment.

Finally, Figure 5.2.1.12 summarizes the temperature behavior of the characteristic relaxation times (τ^*) of the blend components as compared with those of the corresponding homopolymers. The relaxation time of the main PVME dielectric relaxation component presents the clear departure of the conventional VFT behavior only achievable at high temperatures. This result is in perfect agreement with what was found before when the PVME dynamics was investigated in blend with conventional PS by dielectric techniques. However, the present approach also allows detecting unambiguously the bimodal-like character of the PVME dynamics in this PS rich blend with a relatively slow and dielectrically weak mode showing the more conventional VFT temperature dependence (see + symbols in Figure). On the other hand, although the PS dynamics have also a bimodal character the dielectric relaxation is largely dominated by the slow mode, both modes presenting a VFT-like temperature behavior.

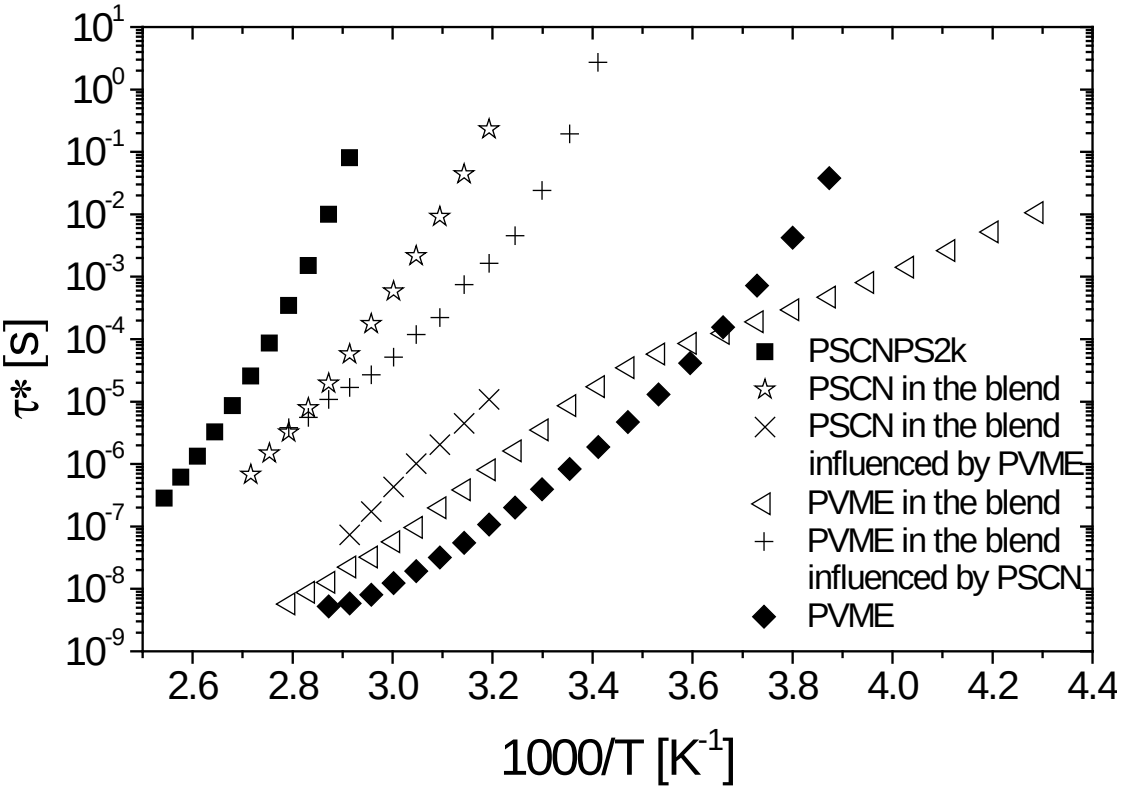

Figure 5.2.1.12. Comparison between the characteristic relaxation times (τ^*) of the pure components of the protonated blend (PSCNPS2k and PVME) and their corresponding PSCN and PVME contributions in the PSCNPS2k / PVME 75/25 blend.

5.2.2. 50/50 PS/PVME Blends

Whereas in the previous section it was studied a PS/PVME system where the PVME was in minority and allowed in this way resolving easily PS component dynamics, this would not be the case for a PS/PVME blend where both components are in the same proportion. In fact, here as the system becomes richer in PVME compared to the previous system studied, the separation of the component dynamics would be more complicated not only because the signal from PSCN decreases but also because that of PVME increases drastically (by a factor of about 2).

In Figure 5.2.2.1. it can be observed how is the behavior of these H/CN functionalized PS/PVME blends with symmetric composition through the

comparison of the frequency dependence of the dielectric loss peaks (ε“) for a given range of temperatures.

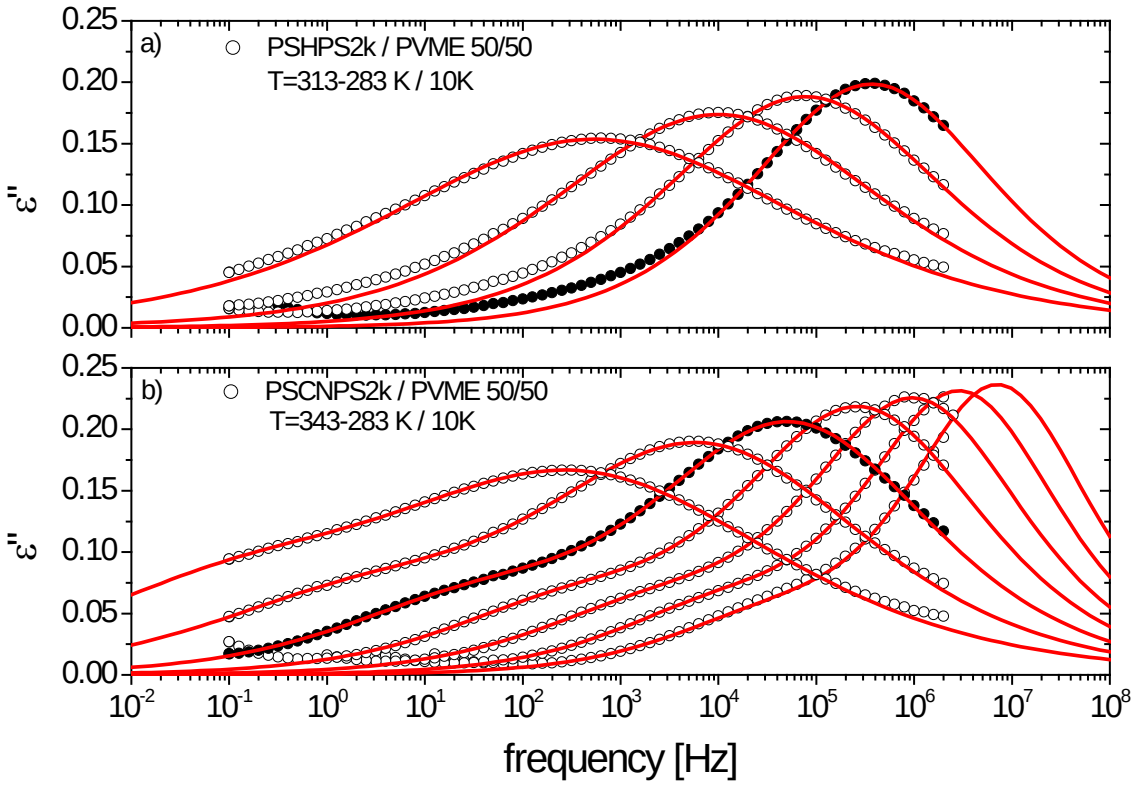

Figure 5.2.2.1. Dielectric segmental relaxation spectra showing the loss permittivity (ε“) as a function of frequency for the –H functionalized PS blend (PS-H-PS2k/PVME) (a) and the –CN functionalized PS blend (PS-CN-PS2k/PVME) (b) at a given range of temperatures.

In this system also the similarity of the glass transitions observed between the -H and the –CN functionalized PS blend by means of DSC allows using both blends together to resolve PS and PVME component dynamics.

As seen previously, for the –CN functionalized PS blend with a composition richer in the PS component (PSCNPS2k / PVME 75/25) (see Figure 5.2.2.2.) an evident double peak response was observed, where PS and PVME components can be

perfectly distinguished due to the low PVME content. However, here as both components forming the blend are in the same proportion the double peak structure becomes less visible decreasing the peak corresponding to the PS component, which appears at the low frequency range and increases that from PVME at high frequencies. Moreover, a small but systematic shift in frequency is generally observed at any temperature for both blends being the H-functionalized PS blend the fastest. These findings make more difficult the detailed separation of the PS and PVME component dynamics since we cannot use the same approach used previously for the 75/25 composition where the PS component dynamics was resolved by subtracting the response of the reference (H-functionalized PS blend) from the response of the CN-functionalized PS blend.

Hence, instead of subtracting both –CN and –H functionalized PS/PVME blends to obtain PS and PVME component responses, here first the –H functionalized PS blend (PSHPS2k / PVME 50/50) dielectric response was analyzed with a Cole-Cole function (γ=1 in the HN equation 2.1.2.1.13.) providing an approximated description of the PVME component dynamics in the blend. The second step of the approach consisted of analyzing the CN-functionalized PS blend (PSCNPS2k / PVME 50/50) as a whole. For the fitting a double Cole-Cole function was required in order to describe both contributions, the main PVME component dynamics in the blend appearing at the high frequency side and the low-frequency shoulder, which would correspond to the PS component in the blend. The parameters obtained for the –H functionalized PS blend (PSHPS2k / PVME 50/50) were used as initial parameters, fixing both β and γ shape parameters, for the fitting of the PVME contribution in the -CN functionalized PS blend (PSCNPS2k / PVME 50/50). Thus, in the fitting of the –CN functionalized PS blend (PSCNPS2k / PVME 50/50) dielectric losses, 5 fitting

parameters were used (3 for the PS component and 2 for the PVME component). Figure 5.2.2.1. shows the fitting obtained for the –H and –CN functionalized PS blends (PSHPS2k / PVME 50/50, PSCNPS2k / PVME 50/50) at different temperatures and the corresponding parameters are summarized in Table 5.2.2.1. and Table 5.2.2.2., respectively.

T [K]	Δε	τ_{HN} [s]	β	γ	τ* [s]	fwhm DECADES
313.15	0.987	4.32E-7	0.487	1	4.32E-7	2.852
303.15	1.073	2.07E-6	0.429	1	2.07E-6	3.295
293.15	1.165	1.6E-5	0.369	1	1.6E-5	3.911
283.15	1.275	2.93E-4	0.301	1	2.93E-4	4.907

Table 5.2.2.1. Cole-Cole parameters obtained for the α–relaxation characterization of the PVME contribution in the PSHPS2k / PVME 50/50 blend. In addition, the characteristic relaxation time (τ^*) obtained from the fitting parameters as well as the full-width-half-maximum parameters (*fwhm*) are included in the table.

T [K]	$\Delta\varepsilon_1$	τ_{HN1} [s]	β_1	γ_1	τ_1^* [s]	$fwhm_1$ DECADES
343.15	0.855	2.14E-8	0.629	1	2.14E-8	2.101
333.15	0.9	5.21E-8	0.59	1	5.21E-8	2.270
323.15	0.96	1.52E-7	0.543	1	1.52E-7	2.508
313.15	1.056	5.52E-7	0.487	1	5.52E-7	2.852
303.15	1.142	2.77E-6	0.43	1	2.77E-6	3.295
293.15	1.224	2.29E-5	0.369	1	2.29E-5	3.911
283.15	1.287	4.09E-4	0.308	1	4.09E-4	4.787

T [K]	$\Delta\varepsilon_2$	τ_{HN2} [s]	β_2	γ_2	τ_2^* [s]	$fwhm_2$ DECADES
343.15	0.173	5.35E-6	0.540	1	5.35E-6	2.523
333.15	0.208	1.79E-5	0.526	1	1.79E-5	2.603
323.15	0.238	8.24E-5	0.480	1	8.24E-5	2.897
313.15	0.251	6.06E-4	0.468	1	6.06E-4	2.987
303.15	0.275	5.95E-3	0.439	1	5.95E-3	3.214
293.15	0.313	9.89E-2	0.394	1	9.89E-2	3.635
283.15	0.344	1.709	0.379	1	1.709	3.796

Table 5.2.2.2. Parameters obtained for the α–relaxation of the PVME (1) and PSCN (2) contributions in the PSCNPS2k / PVME 50/50 blend using a double Cole-Cole equation. In addition, the characteristic relaxation time (τ^*) obtained from the HN parameters as well as the full-width-half-maximum parameter (*fwhm*) are included in the table.

From the obtained parameters it can be seen how the dielectric strength ($\Delta\varepsilon$) and the full-width-half-maximum (*fwhm*) [2.1.2.1.15.] depend on temperature for both PS and PVME contributions as seen in Figure 5.2.2.2. and 5.2.2.3., respectively.

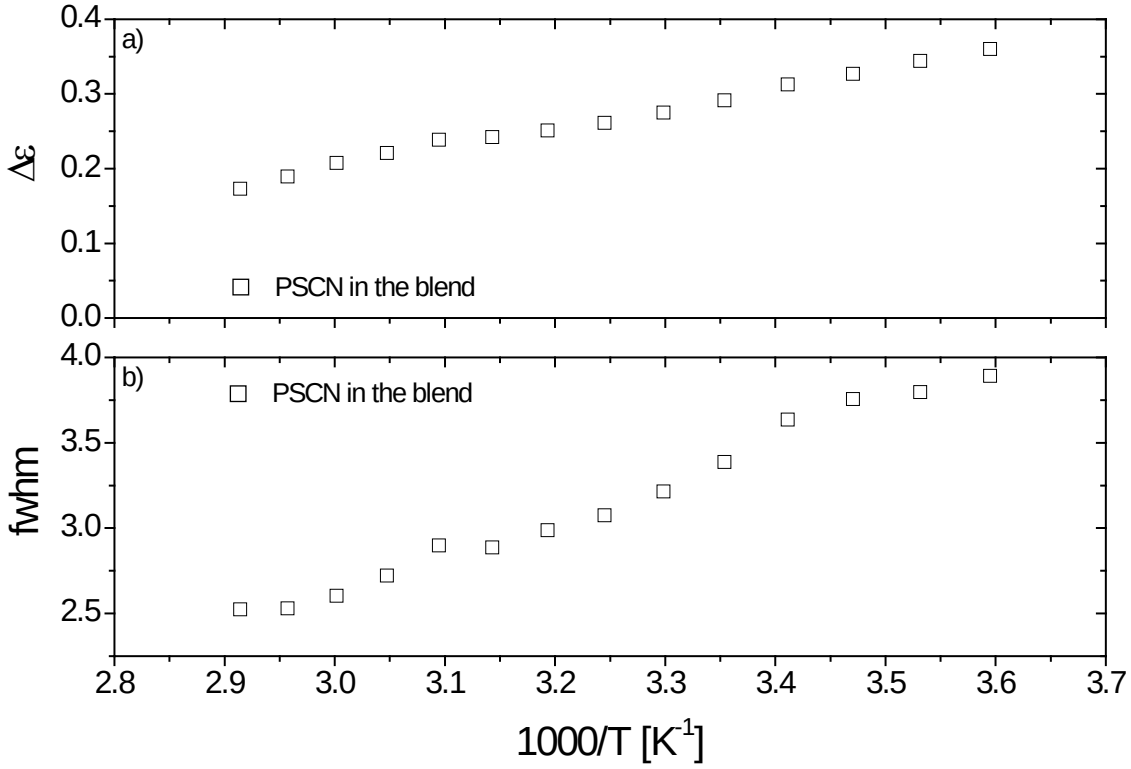

Figure 5.2.2.2. The temperature dependence of the dielectric strength ($\Delta\varepsilon$) and the full-width-half-maximum (*fwhm*) for the PSCN component in the PSCNPS2k / PVME 50/50 blend.

In both cases (PS and PVME contributions) $\Delta\varepsilon$ and *fwhm* follow a rather conventional temperature dependence.

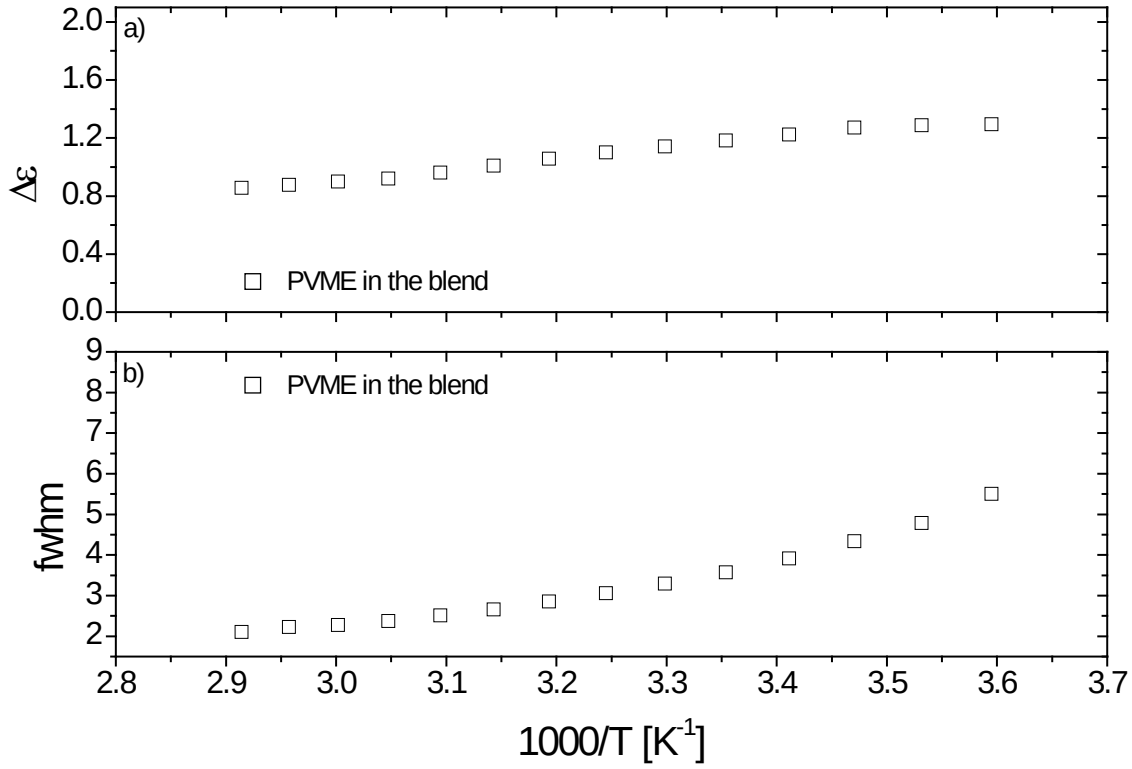

Figure 5.2.2.3. The temperature dependence of the dielectric strength ($\Delta\varepsilon$) and the full-width-half-maximum (*fwhm*) for the PVME component in the PSCNPS2k / PVME 50/50 blend.

From the fitting parameters the characteristic relaxation time for both PS and PVME component in the blend was also determined. The obtained values are shown in Figure 5.2.2.4. where it can be seen a comparison of the relaxation time (τ^*) temperature dependences for the homopolymers and the components in the blend.

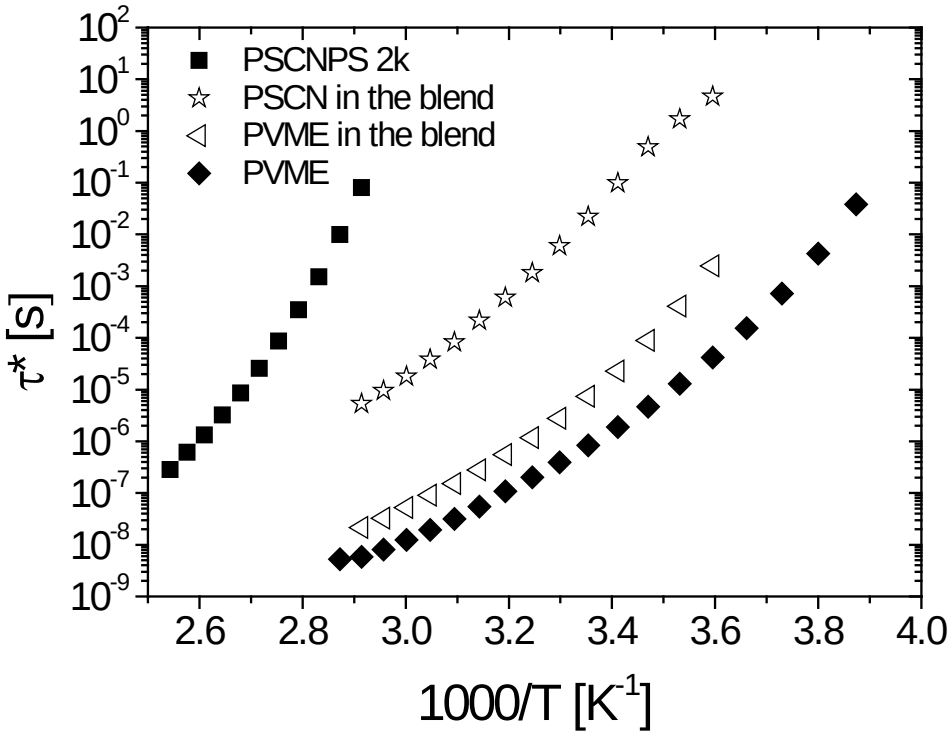

Figure 5.2.2.4. Comparison between the characteristic relaxation times (τ^*) of the pure components of the blend (PSCNPS2k and PVME) and their corresponding PSCN and PVME contributions in the PSCNPS2k / PVME 50/50 blend.

The behavior obtained for this composition is again more conventional and differs from that found for the 75/25 composition and these results will be discussed in detail later.

5.2.3. 25/75 PS/PVME Blends

The study of the PS component dynamics in PS/PVME blends started from the easiest case where PVME was the minority component (PS/PVME 75/25). However, as the blend has become richer in PVME resolving PS dynamics is more difficult. Now, we will present the data of PS/PVME blends with the highest PVME

content where resolving dynamics is expected to be even more complicated than in the previous case (PS/PVME 50/50).

Figure 5.2.3.1. shows the dielectric loss (ε“) frequency dependence for the H/CN-functionalized PS blends at different temperatures.

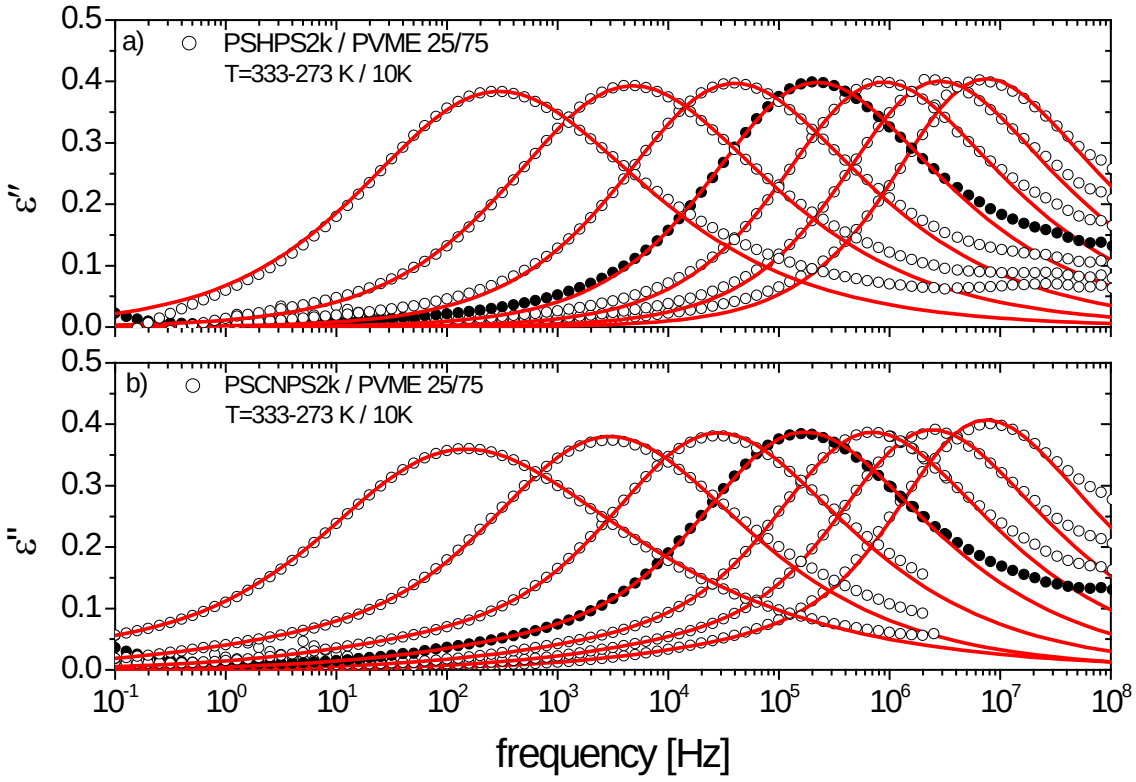

Figure 5.2.3.1. Dielectric segmental relaxation spectra showing the loss permittivity (ε“) as a function of frequency for the –H functionalized PS blend (PS-H-PS2k/PVME) (a) and the –CN functionalized PS blend (PS-CN-PS2k/PVME) (b) at a given range of temperatures.

Here, as in the previous composition (50/50), in spite of both –H and –CN funtionalized PS blends present a very similar T_g it is not possible to resolve PS and PVME component dynamics by subtraction because the involved uncertainties would result in fitting artefacts.

Hence, similar to the approach followed for the 50/50 composition, here first the –H functionalized PS blend (PSHPS2k / PVME 25/75) dielectric response was analyzed with a conventional Havriliak Negami equation [2.1.2.1.13.] where at high

temperature we set $\beta \cdot \gamma = 0.4$ as before [5.2.1.4.] in order to minimize the number of free parameters. In a second step the –CN functionalized PS blend (PSCNPS2k / PVME 25/75) was fitted to determine the dynamical behavior of both PSCN and PVME components in the blend. For that the β and γ shape parameters obtained for the –H functionalized PS blend were imposed for the PVME component, whose response was reflected by the main loss peak, whereas the rest of the obtained parameters were used as initial parameters. On the other hand, the low frequency shoulder was fitted using a Cole-Cole function (γ=1 in the HN equation 2.1.2.1.13.), which results in a total of 5 fitting parameters for the –CN functionalized PS blend (PSCNPS2k / PVME 25/75). Therefore, Figure 5.2.3.1. shows the fitting obtained for the –H and –CN functionalized PS blends (PSHPS2k / PVME 25/75, PSCNPS2k / PVME 25/75) at different temperatures and the corresponding parameters are given in Table 5.2.3.1. and 5.2.3.2., respectively.

T [K]	Δε	τ_{HN} [s]	β	γ	τ* [s]	fwhm DECADES
333.15	1.602	4.44E-8	0.742	0.539	2.12E-8	2.389
323.15	1.638	1.14E-7	0.708	0.565	5.55E-8	2.454
313.15	1.678	3.64E-7	0.681	0.588	1.79E-7	2.512
303.15	1.735	1.41E-6	0.648	0.617	7.16E-7	2.588
293.15	1.790	7.59E-6	0.616	0.649	3.98E-6	2.668
283.15	1.877	5.92E-5	0.568	0.705	3.33E-5	2.810
273.15	1.959	8.56E-4	0.517	0.773	5.35E-4	2.987

Table 5.2.3.1. Parameters obtained for the α–relaxation characterization of the PVME contribution in the PSHPS2k / PVME 25/75 blend. In addition, the characteristic relaxation time (τ*) obtained from the fitting parameters as well as the full-width-half-maximum parameters (*fwhm*) are included in the table.

T [K]	$\Delta\varepsilon_1$	τ_{HN1} [s]	β_1	γ_1	τ_1^* [s]	$fwhm_1$ DECADES
333.15	1.586	4.29E-8	0.742	0.539	2.05E-8	2.389
323.15	1.575	1.31E-7	0.708	0.565	6.34E-8	2.454
313.15	1.599	4..40E-7	0.681	0.588	2.17E-7	2.511
303.15	1.657	1.76E-6	0.648	0.617	8.93E-7	2.589
293.15	1.712	1.03E-5	0.616	0.649	5.39E-6	2.668
283.15	1.783	9.08E-5	0.568	0.705	5.11E-5	2.81
273.15	2.018	2.87E-3	0.525	0.563	1.02E-3	3.471

T [K]	$\Delta\varepsilon_2$	τ_{HN2} [s]	β_2	γ_2	τ_2^* [s]	$fwhm_2$ DECADES
333.15	0.130	3.38E-6	0.508	1	3.38E-6	2.714
323.15	0.132	1.78E-5	0.522	1	1.78E-5	2.630
313.15	0.145	4.88E-5	0.489	1	4.88E-5	2.837
303.15	0.158	2.37E-4	0.474	1	2.37E-4	2.945
293.15	0.166	2.23E-3	0.469	1	2.23E-3	2.979
283.15	0.177	2.81E-2	0.431	1	2.81E-2	3.283
273.15	0.199	1.566	0.333	1	1.566	4.397

Table 5.2.3.2. Parameters obtained for the α–relaxation of the PVME (1) and PSCN (2) contributions in the PSCNPS2k / PVME 25/75 blend. In addition, the characteristic relaxation time (τ^*) obtained from the HN parameters as well as the full-width-half-maximum parameter (*fwhm*) are included in the table.

From the fitting parameters the temperature dependence of the dielectric strength and the full-width-half-maximum (*fwhm*) [2.1.2.1.15.] for the PS and PVME contributions can be obtained as seen in Figure 5.2.3.2. and 5.2.3.3., respectively.

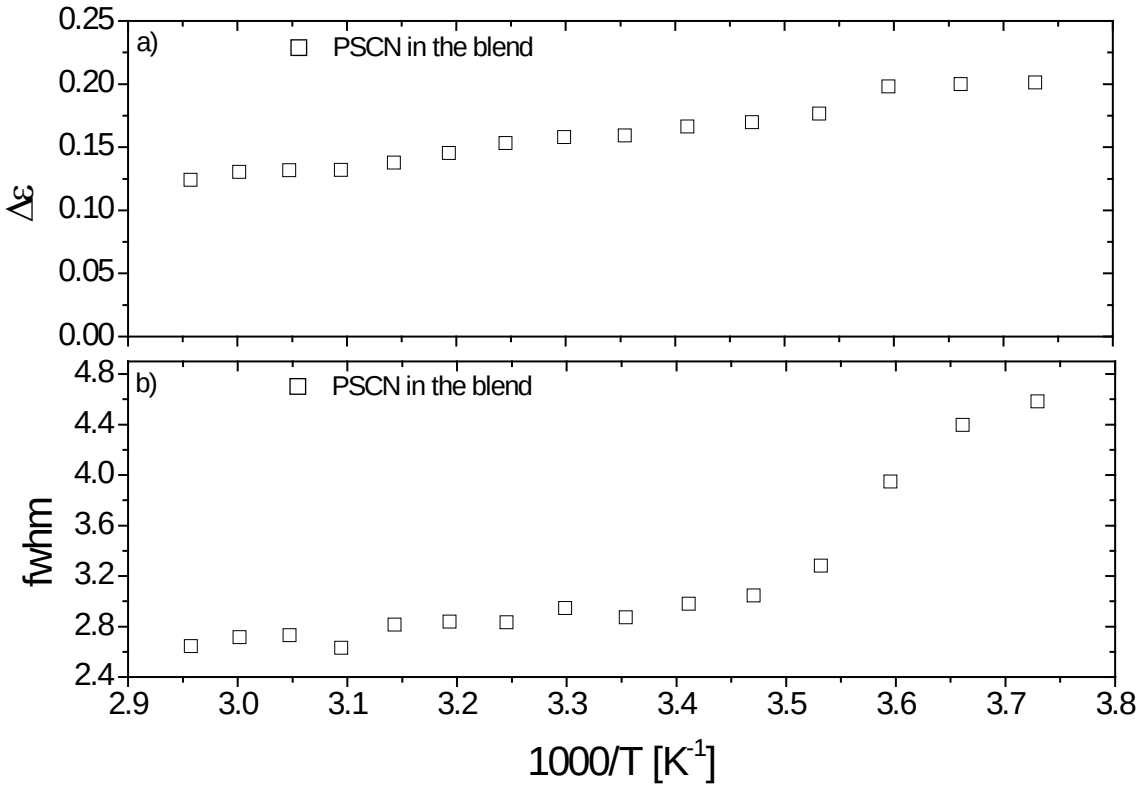

Figure 5.2.3.2. The temperature dependence of the dielectric strength ($\Delta\varepsilon$) and the full-width-half-maximum (*fwhm*) for the PSCN component in the PSCNPS2k / PVME 25/75 blend.

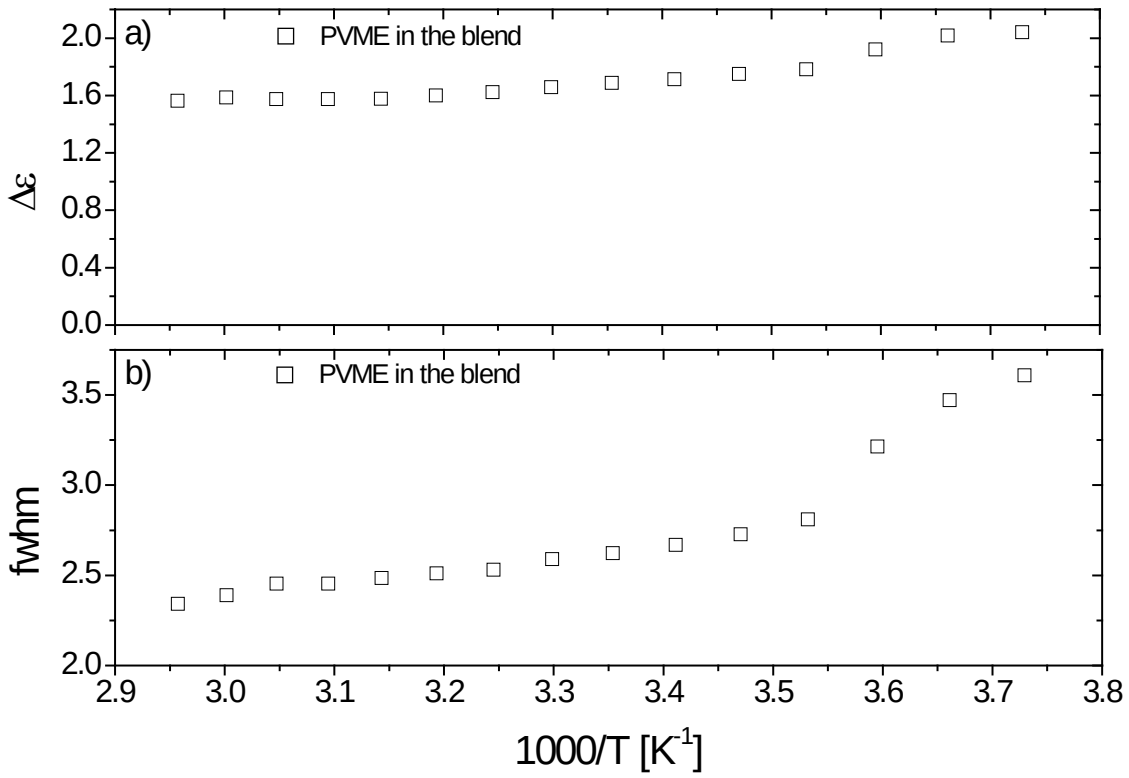

Figure 5.2.3.3. The temperature dependence of the dielectric strength ($\Delta\varepsilon$) and the full-width-half-maximum (*fwhm*) for the PVME component in the PSCNPS2k / PVME 25/75 blend.

Again $\Delta\varepsilon$ and *fwhm* follow a rather conventional temperature dependence although a sharp increasing of *fwhm* is detected for both components at low temperatures as seen in Figures 5.2.3.2. and 5.2.3.3.

On the other hand, the characteristic relaxation times (τ*) of PS and PVME showed also the conventional VFT behavior (see Figure 5.2.3.4.)

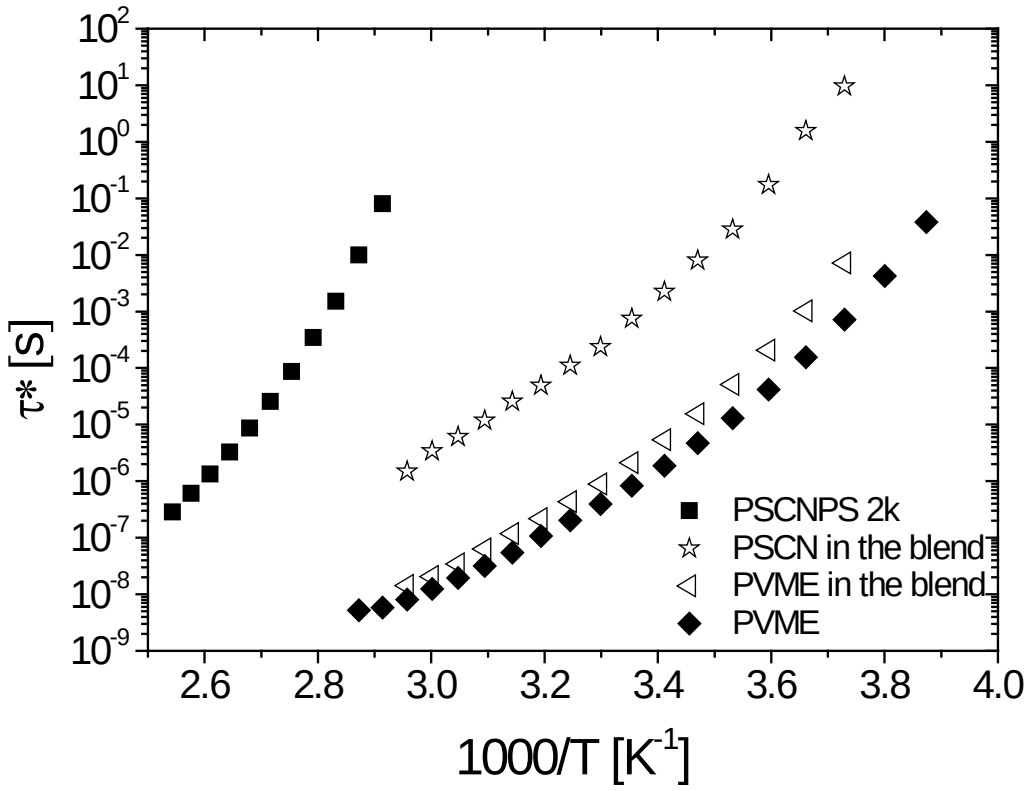

Figure 5.2.3.4. Comparison between the characteristic relaxation times (τ^*) of the pure components of the blend (PSCNPS2k and PVME) and their corresponding PSCN and PVME contributions in the PSCNPS2k / PVME 25/75 blend.

5.3. SANS Results

Small Angle Neutron Scattering (SANS) measurements were employed to study the thermodynamics of the PS/PVME 75/25 blends (see Section 2.2.1.). This type of measurements required using one deuterated component in the blends in order to achieve a sufficient scattering contrast. In our case we chose deuterated polystyrene dPS, since it is the majority component. The measurements were carried out using the D11 instrument at Institut Laue Langevin (ILL), Grenoble, France (see experimental section for the details). Figure 5.3.1. shows the normalized macroscopic differential scattering cross section at different temperatures for –CN deuterated functionalized PS blend (dPSCNPS2k / PVME 75/25).

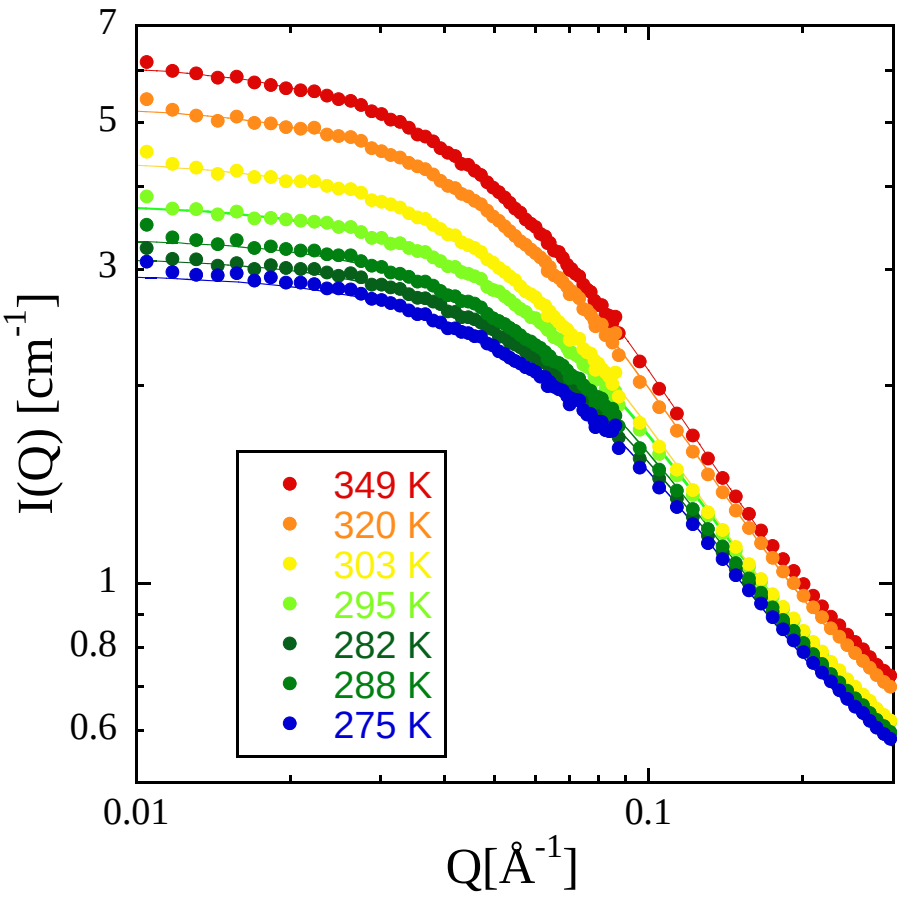

Figure 5.3.1. Normalized macroscopic differential scattering cross section *(dΣ/dΩ)(Q)* at the different temperatures indicated after subtracting the Q^{-4}-increase observed in the low-Q range. Lines are fits with Equation 5.3.3.

The cross sections measured by D11 presented a temperature independent increase at low-Q (Q > 0.012 $Å^{-1}$ approx.) that approximately followed a Q^{-4}-dependence

$$I_{lowQ}(Q) = A \cdot Q^{-4} \qquad [5.3.1.]$$

The origin of this scattering could be attributed to e.g. small bubbles in the sample giving rise to a Porod-like law. In previous studies [3, 4] the increase of the cross-

section in this Q-range has been interpreted in terms of a Debye-Bueche (DB) function [5]

$$I_{DB} \Big/ \left(1 + \left(Q\,\xi_{DB}\right)^2\right)^2 \qquad [5.3.2.]$$

accounting for heterogeneities decaying exponentially on a certain characteristic length scale ξ_{DB}. Then, the observed Q^{-4}-dependent scattering intensity would correspond to the high-Q regime of the DB-law. In our case, we checked that the increase of the intensity follows well a Q^{-4}-dependence down to the lowest Q investigated (Q_{min} = 0.0017Å^{-1} for selected temperatures). Thus, if this scattering could be attributed to a DB-regime, the associated characteristic length scale should be larger than approx. 600Å ($\approx 1/Q_{min}$). At Q-values above 0.01 Å^{-1} the scattering curves present a T-dependent regime, as can be appreciated in Figure 5.3.1. This figure shows the D11 results at different temperatures after subtracting the low-Q scattering accounted by the already mentioned law [5.3.1.]. The data can be perfectly described in terms of a Ornstein-Zernike (OZ) function [5] and a flat background (BG):

$$I\left(Q\right) = \frac{I_{OZ}}{\left(1 + \left(Q\,\xi_{OZ}\right)^2\right)} + BG \qquad [5.3.3.]$$

Both the intensity of the OZ-function I_{OZ} and the characteristic length ξ_{OZ} show a clear temperature dependence, as can be seen in Figure 5.3.2.

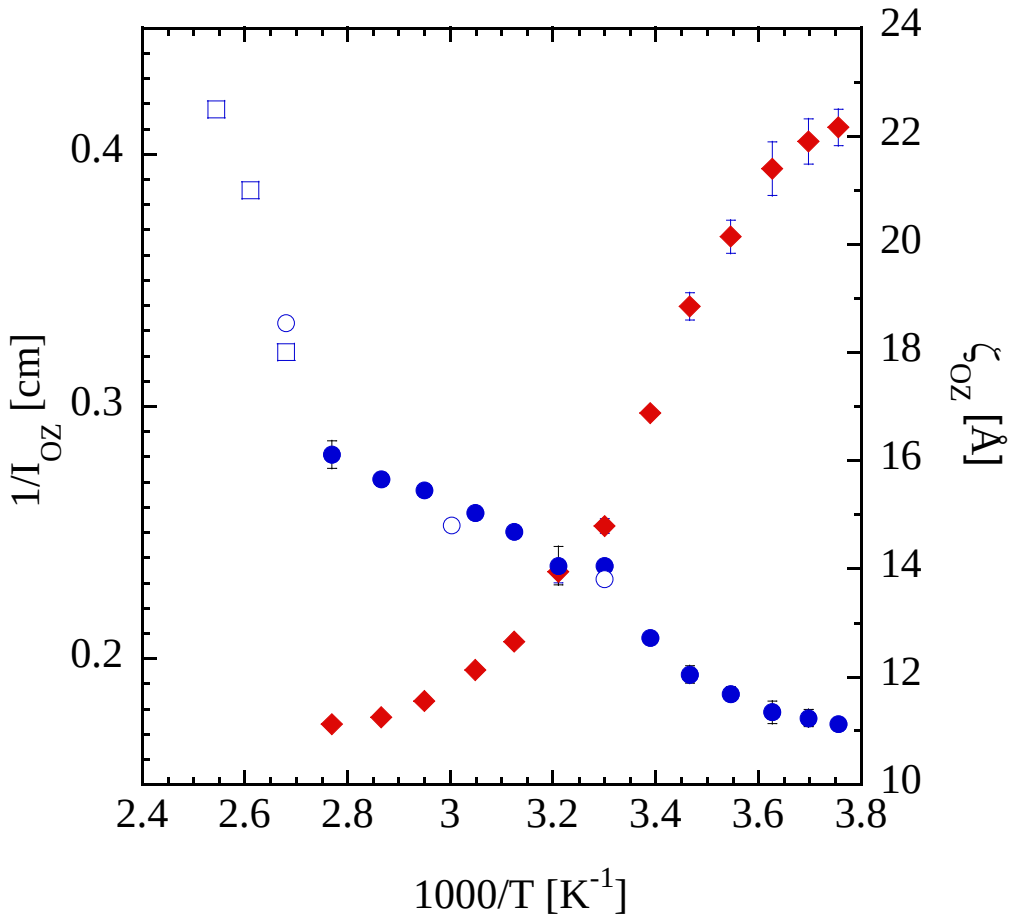

Figure 5.3.2. Temperature dependence for the intensity of the OZ-function (I_{OZ}) (red filled diamonds) and the characteristic length (ξ_{OZ}) (blue filled circles). Values for the characteristic length obtained by Hashimoto et al. [6] (blue open circles) and Han et al. [7] (blue open squares) are also included.

We note that the values of ξ_{OZ} are perfectly compatible with those previously reported by Hashimoto et al [6] on a similar blend, where a conventional (non-functionalized) PS was used. This supports the previous finding that the here used functionalization does not alter miscibility.

The fact that the sample employed for SANS experiments used deuterated functionalized PS lead us to question our self whether this can be directly compared with the previously reported results on the corresponding samples prepared with protonated PS. Thus, DSC and BDS were also used in order to have a complete characterization of these deuterated blends.

By DSC the glass-transition temperatures (T_g) of both deuterated H and CN-functionalized PS blends, called as dPSHPS2k / PVME 75/25 and dPSCNPS2k / PVME 75/25, respectively, have been determined from the peak of the derivative by DSC as seen in Figure 5.3.3.

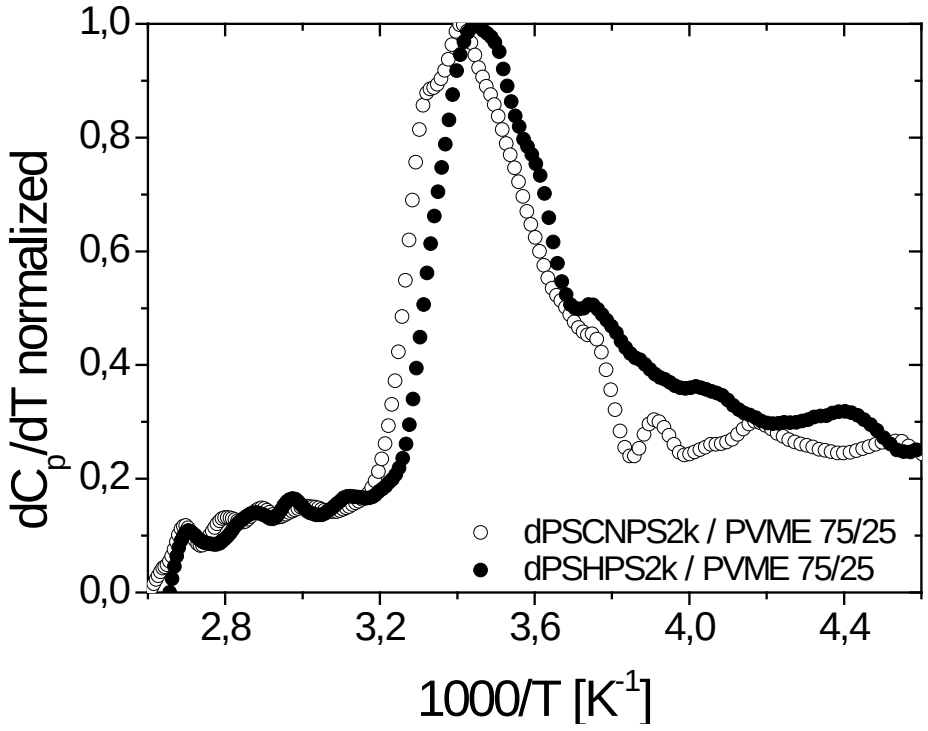

Figure 5.3.3. Comparison of the normalized heat capacity derivative (dC_p/dT_{norm}) as a function of the temperature for the two different deuterated blends having a composition of 75/25.

As seen there is a measurable difference between the T_g values for both deuterated blends. In fact, the difference is of about 5K, which was expected since the preliminary characterization of the deuterated homopolymers, dPSHPS2k and

dPSCNPS2k, showed that they had not exactly the same molecular weight (M_n = 1800 g/mol for dPSHPS2k and M_n = 2200 g/mol for dPSCNPS2k) and as a consequence there was observed a difference in their T_g's being 318K and 326K for the dPSHPS2k and the dPSCNPS2k, respectively. Therefore, this is the explanation for the difference in T_g's of the deuterated PS/PVME blends.

BDS was used as it was done previously for the equivalent blends (PSHPS2k / PVME 75/25, PSCNPS2k / PVME 75/25). Figure 5.3.4. shows the frequency dependence of the loss peak for both deuterated -H and –CN functionalized PS blends.

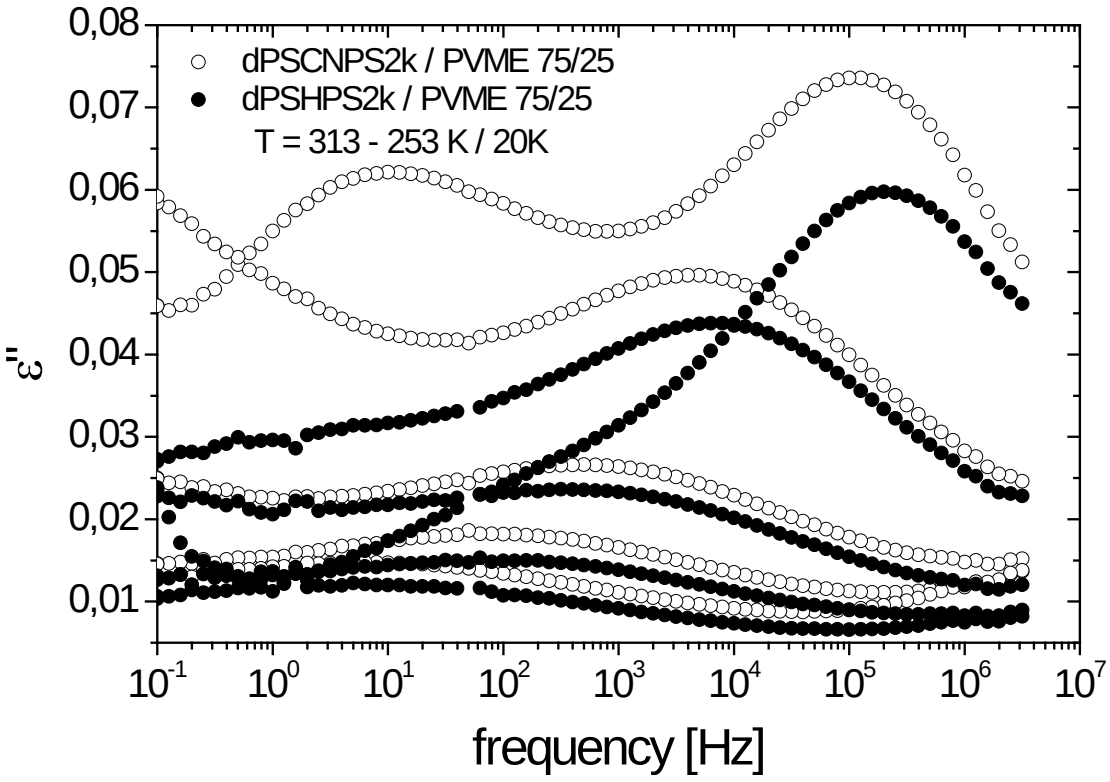

Figure 5.3.4. Dielectric segmental relaxation spectra showing the loss permittivity (ε") as a function of frequency for the deuterated –H functionalized PS blend (dPS-H-PS2k/PVME) and the deuterated –CN functionalized PS blend (dPS-CN-PS2k/PVME) at a given range of temperatures.

As seen in this figure the dynamic behavior of these deuterated H/CN functionalized PS blends is similar to that obtained for protonated H/CN functionalized PS blends and presented in Section 5.2.1. Therefore, an equivalent approach was followed to resolve PS and PVME component dynamics. In Figure 5.3.5. it can be seen the dielectric loss peak as a function of the frequency for both deuterated H/CN functionalized PS blends, being the measured signals, as well as PS and PVME components in the blend at a representative temperature (313K).

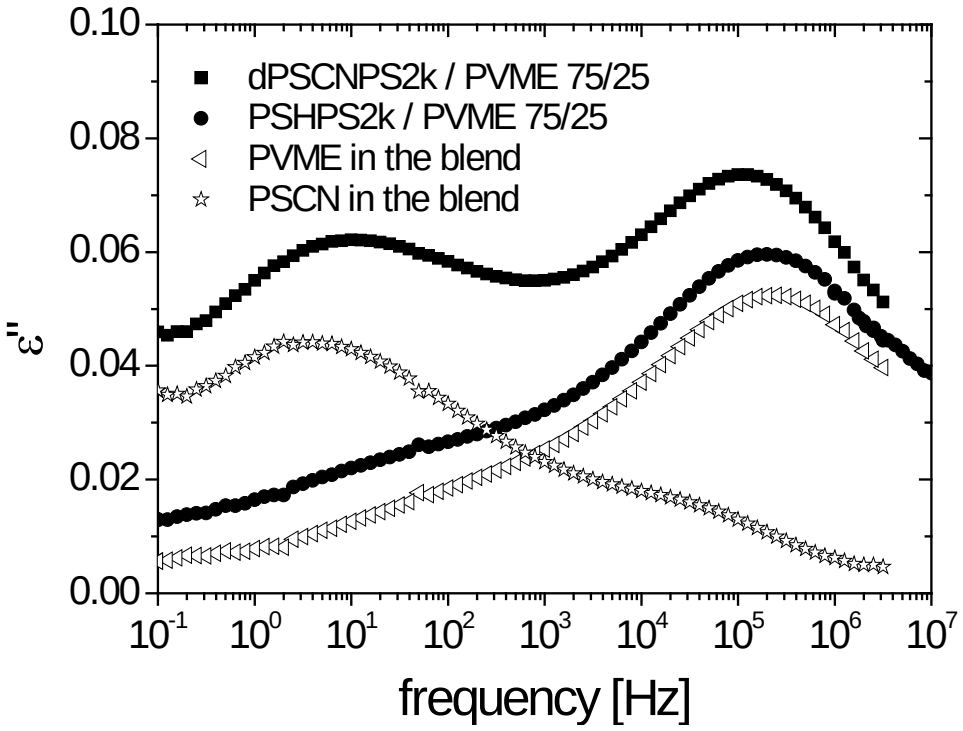

Figure 5.3.5. Dielectric segmental relaxation spectra showing the loss permittivity (ε") as a function of frequency for the H/CN functionalized PS blends, PSHPS2k/PVME 75/25 and dPSCNPS2k/PVME 75/25, respectively, and their PVME and PSCN component dynamics at 313K.

The so-resolved component dynamics at different temperatures are shown in Figures 5.3.6. and 5.3.7. for the PSCN and the PVME contributions, respectively. For the comparative analysis the data representing each component dynamics were fitted by a single main component modeled with a HN function [2.1.2.1.13.]. The results of

such description are summarized in Tables 5.3.1. and 5.3.2. and represented by lines in Figures 5.3.6. and 5.3.7.

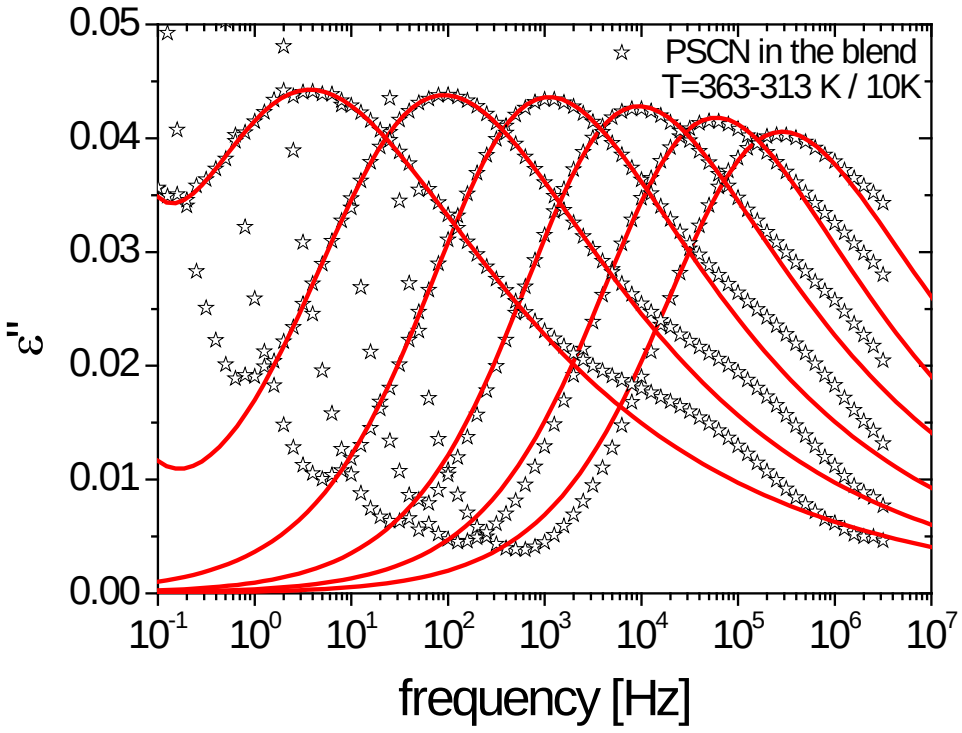

Figure 5.3.6. Dielectric segmental relaxation spectra showing the loss permittivity (ε“) as a function of frequency for the PS contribution in the deuterated -CN functionalized PS blend where the fitting is focused only on the mean loss peak.

T [K]	Δε	τ_{HN} [s]	β	γ	τ* [s]	fwhm DECADES
363.15	0.250	2.43E-6	0.565	0.411	5.56E-7	3.872
353.15	0.255	1.15E-5	0.569	0.414	2.69E-6	3.827
343.15	0.270	8.30E-5	0.584	0.368	1.68E-5	4.019
333.15	0.28	7.16E-4	0.569	0.377	1.43E-4	4.072
323.15	0.301	9.14E-3	0.513	0.409	1.74E-3	4.331
313.15	0.321	0.246	0.506	0.375	0.039	4.648

Table 5.3.1. Havriliak Negami parameters obtained for the α–relaxation characterization of the PSCN contribution in the dPSCNPS2k / PVME 75/25 blend when only the mean loss peak is considered. In addition, the characteristic relaxation time (τ^*) obtained from the HN parameters as well as the full-width-half-maximum parameter (*fwhm*) are included in the table.

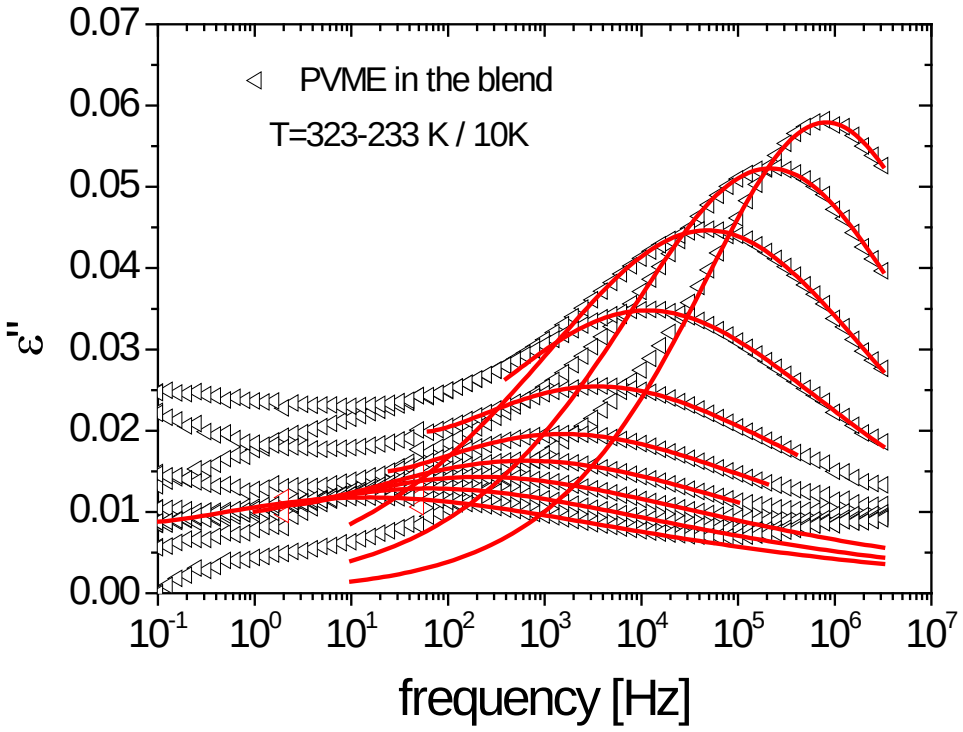

Figure 5.3.7. Dielectric segmental relaxation spectra showing the loss permittivity (ε") as a function of frequency for the PVME contribution in the deuterated -CN functionalized PS blend where the fitting is focused only on the mean loss peak.

T [K]	Δε	τ_{HN} [s]	B	γ	τ* [s]	fwhm DECADES
323.15	0.355	1.96E-7	0.438	1	1.96E-7	3.221
313.15	0.369	7.41E-7	0.384	1	7.41E-7	3.738
303.15	0.361	3.30E-6	0.338	1	3.30E-6	4.314
293.15	0.311	2.94E-5	0.334	0.770	1.37E-5	4.885
283.15	0.251	1.57E-4	0.324	0.653	4.35E-5	5.475
273.15	0.202	6.21E-4	0.337	0.533	9.98E-5	5.839
263.15	0.177	1.06E-3	0.296	0.643	2.45E-4	6.078
253.15	0.162	7.19E-3	0.327	0.463	7.18E-4	6.515
243.15	0.151	2.27E-2	0.309	0.492	2.39E-3	6.693
233.15	0.147	0.107	0.286	0.504	0.010	7.159

Table 5.3.2. Havriliak Negami parameters obtained for the α–relaxation characterization of the PVME contribution in the dPSCNPS2k / PVME 75/25 blend when only the mean loss peak is considered. In addition, the characteristic relaxation time (τ*) obtained from the HN parameters as well as the full-width-half-maximum parameter (*fwhm*) are included in the table.

Figures 5.3.8. and 5.3.9. present the temperature dependence of the main relaxation parameters.

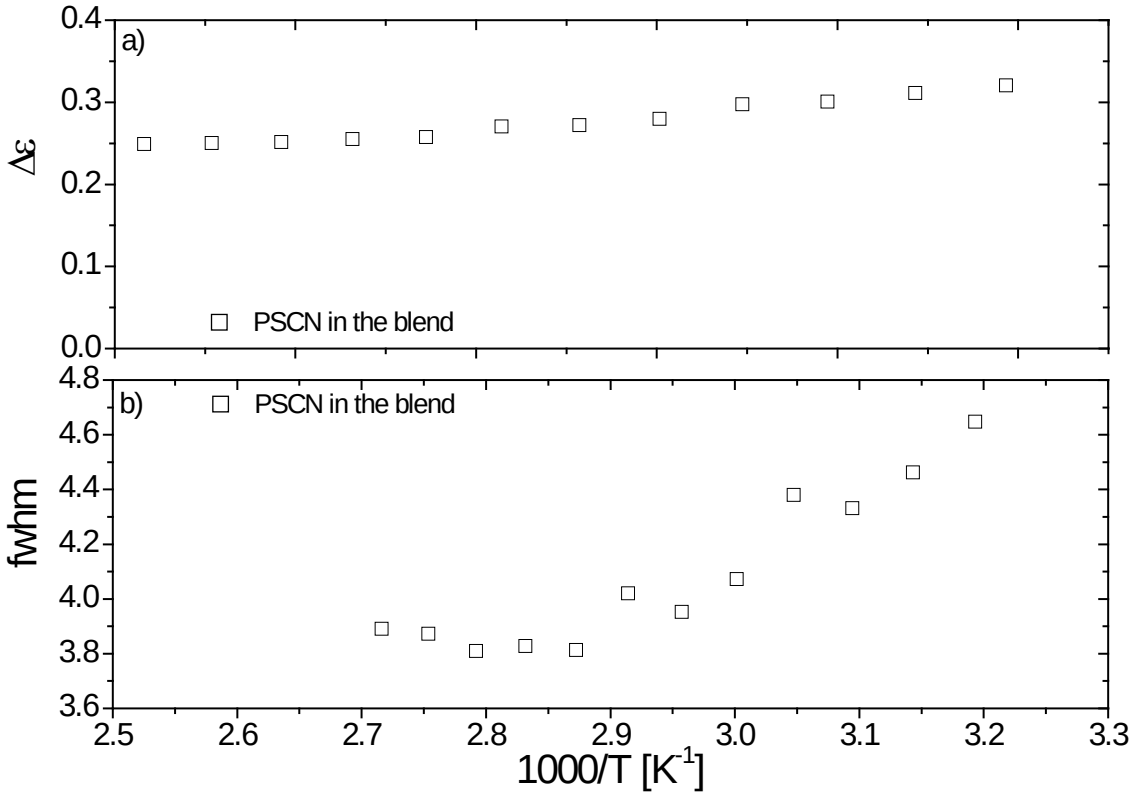

Figure 5.3.8. The temperature dependence of the dielectric strength ($\Delta\varepsilon$) and the full-width-half-maximum (*fwhm*) for the PSCN component in the dPSCNPS2k / PVME 75/25 blend.

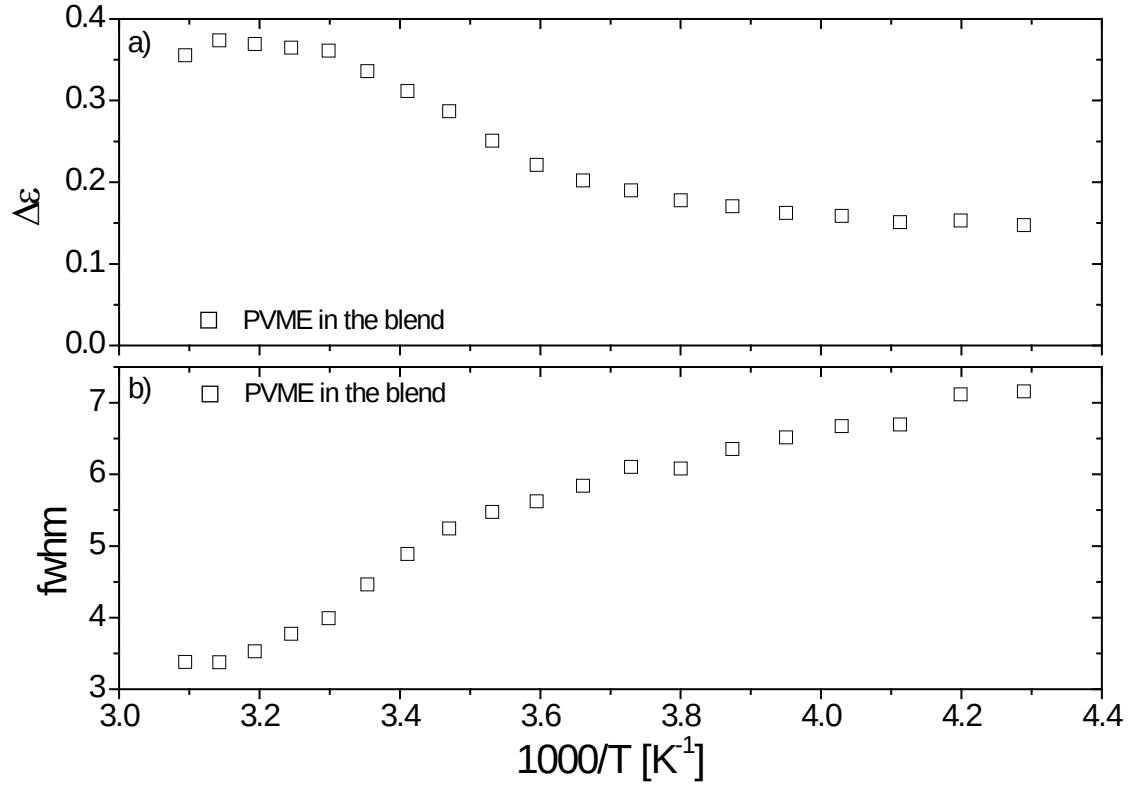

Figure 5.3.9. The temperature dependence of the dielectric strength ($\Delta\varepsilon$) and the full-width-half-maximum (*fwhm*) for the PVME component in the dPSCNPS2k / PVME 75/25 blend.

The overall behavior observed using deuterated PS is similar to that found before from the non-deuterated blends. To stress the similarities and put in evidence minor differences, in Figure 5.3.10. we have included the characteristic time scales (τ^*) of the components main relaxation obtained using all the samples in a single plot.

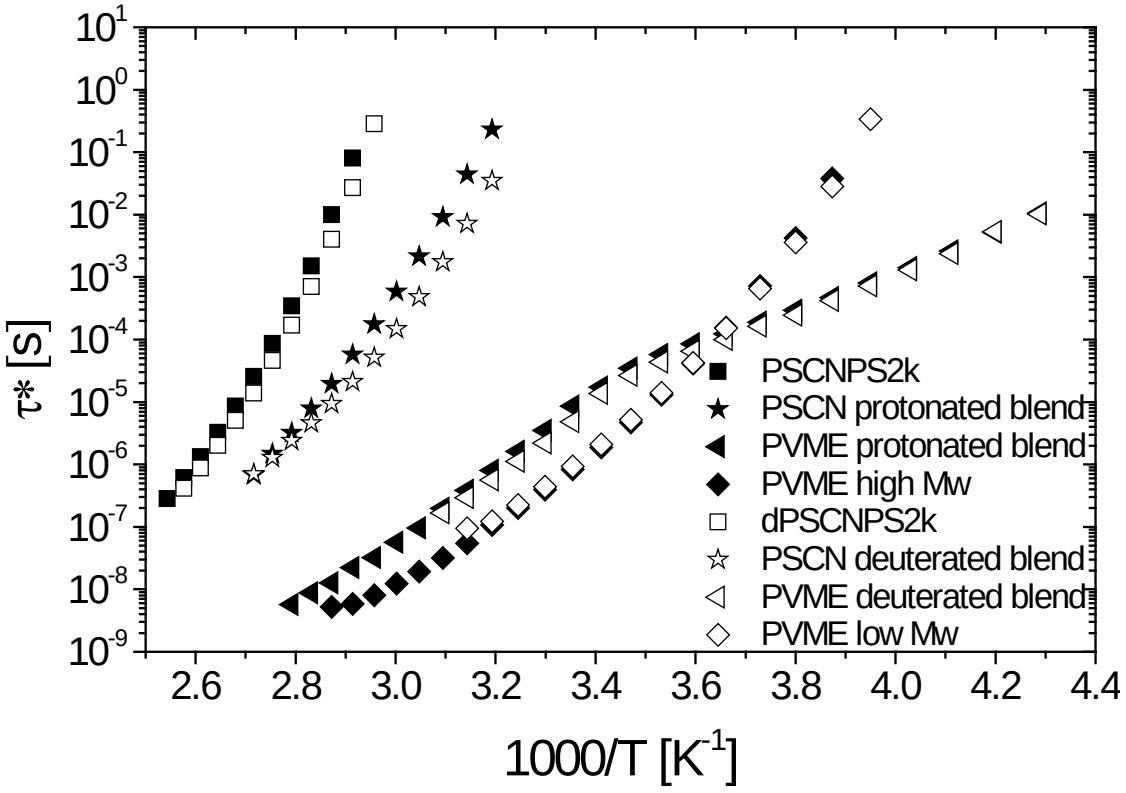

Figure 5.3.10. Comparison between the characteristic relaxation times (τ^*) of the pure components of the deuterated blend (dPSCNPS2k and PVME) and their corresponding PSCN and PVME contributions in the dPSCNPS2k / PVME 75/25 blend.

It is evident that PVME times obtained form non-deuterated and deuterated blends nearly superimpose. Concerning the PS contribution, it is clear that both the deuterated and non-deuterated PSCN homopolymers are slightly different, this difference is also apparent for the main PS component in the blends. Both results are naturally explained by the small differences found in the glass transition temperature associated to minor differences in molecular weight.

The result of this detailed comparison clearly demonstrates that the information obtained by SANS experiments on the blends with deuterated PSCN can be considered also valid for non-deuterated blends as far as the temperature variation observed in the parameters describing SANS experiments is rather smooth.

1 . S. Plaza-García, R. Lund, A. Alegría, J. Colmenero, J. Janoski and R. P. Quirk, Macromolecules, 44, 7810 (2011)

2 . A. Arbe, A. Alegría, F. Alvarez, J. Colmenero and B. Frick, Progr. Colloid Polym. Sci., 91, 24 (1993)

3 . S. Schramm,T. Blochowicz, E. Gouirand, R. Wipf, B. Stühn, Y. Chushkin, The Journal of Chemical Physics, 132, 224505 (2010)

4 . S. Koizumi, Soft Matter, 7, 3984, 2011

5 . J. S. Higgins and H. C. Benoit, “Polymers and Neutron Scattering”, Clarendon Press, Oxford (1994)

6 . H. Takeno, S. Koizumi, H. Hasegawa and T. Hashimoto, Macromolecules, 29, 2440 (1996)

7 . C. C. Han, B. J. Bauer, J. C. Clark, Y. Muroga, Y. Matsushita, M. Okada, Q. Tran-cong and T. Chang, Polymer, 29, 2002 (1988)

6. Polystyrene/Poly (vinyl methyl ether) (PS/PVME) Blends Discussion

In the previous chapter we have presented the results obtained from calorimetric and dielectric measurements on blends of PVME with –CN and –H functionalized PS, which allowed us to resolve the segmental dynamics of both components. As it was already commented the PS/PVME blend has been long investigated in the past but not specific information on the PS component was extracted. On the other hand, the dynamics of the PVME in the blends as detected in these systems conforms perfectly what was reported before with the single exception of the blends richer in PS where we were able to probe that in this particular blend the PVME dynamics has a bimodal character. As consequence, the following discussion will be mainly focused on the PS component dynamics in the different blends although the data concerning the PVME dynamics in the blends investigated here will be also considered. At the end, we will discuss how the PS dynamics plays a crucial role on that of PVME in the PS/PVME 75/25 where the slow PS acts as a frozen matrix at low temperatures influencing the PVME behavior.

To start, we will focus first on the results obtained by DSC, which is a technique sensitive to the overall dynamical properties. As expected for miscible and homogeneous polymer blends, a single glass transition is observed for all cases (see Figure 5.1.1.), which implies that no phase separation takes place during the blend preparation or the subsequent measurements. Subsequently, before going into detail about our H/CN functionalized PS/PVME blends it was required to check that there was not a significant difference between using PS/PVME blends made of

functionalized PS and the corresponding blends made of conventional PS. For that calorimetric results show, in fact, that functionalization does not change very much the overall dynamical properties since the –H functionalized PS blends (PSHPS2k/PVME) and the conventional PS blends (PS2300/PVME) exhibit a very similar T_g as it is shown in Table 5.1.1. and in Figure 5.1.1. Moreover, as shown above, blends of PVME with -H and –CN functionalized PS present a close DSC behavior.

Because the source for resolving the PS component dynamics in the PS/PVME blends is the system with -CN functionalized PS, in the following discussion we will use the DSC data from this system. Figure 6.1. shows that the composition dependence of the average glass-transition temperature $<T_g>$ (taking it as the middle point of the C_p step in DSC measurements) can be well described by means of the Brekner equation [1]:

$$T_g(\phi_{PS}) = T_{gPVME} + (T_{gPS} - T_{gPVME})\left[(1 + K_1)\,\phi_{PS} - (K_1 + K_2)\,\phi_{PS}^2 + K_2\,\phi_{PS}^3\right] \qquad [6.1.]$$

where ϕ_{PS} is the bulk concentration in the higher T_g component (PS), T_{gPS} and T_{gPVME} are the respective glass transition temperatures of the pure PS and PVME components forming the blend, and K_1 and K_2 are fitting parameters, which would account of weak interactions between components. When the values of K_1 and K_2 previously reported for a conventional PS/PVME blend with a PS having a considerably higher molecular weight (M_n=64 Kg/mol) [1] (being K_1 =-0.707 and K_2 = 0.462) are used, the resulting description of the data is very satisfactory (see solid line in Figure 6.1).

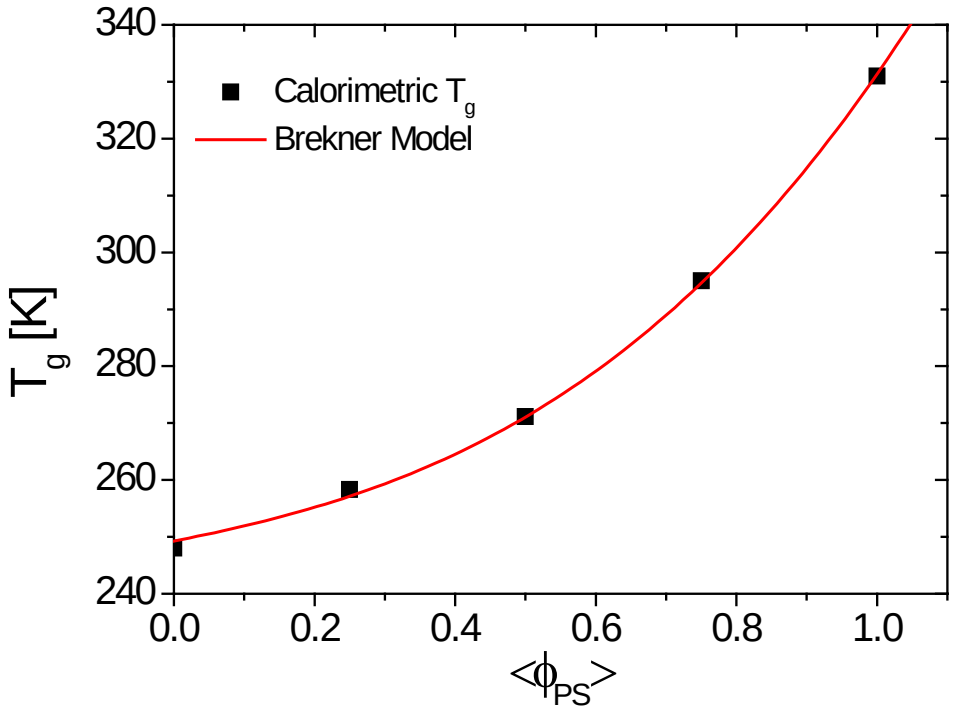

Figure 6.1. Calorimetric glass transition of the PSCNPS 2k and PVME homopolymers and their corresponding blends as a function of the PS composition fitted with the Brekner model.

PS dynamics in the blend:

Let now consider the dynamics of the PS component in the blend. The characteristic relaxation time (τ^*) temperature dependence of the PSCN component in the three different blend compositions is shown in Figure 6.2. These data were fitted using the Vogel-Fulcher-Tamman (VFT) equation [2.1.2.1.20.]. The parameters resulting from such a fitting are given in Table 6.1. and the corresponding curves are shown in Figure 6.2. It should be noted that for the fitting the VFT characteristic relaxation time (τ_{VFT}) was fixed using the value obtained for the PSCNPS 2k homopolymer. From such a fitting we can characterize the PS dynamics in each blend by an "effective" glass transition (T_{geff}). The value of the "effective" glass transition

temperature for each composition is calculated as the temperature at which the main relaxation time (τ*) of the PS component takes a value of 10 s (see Figure 6.2.). The resulting values are also included in the Table 6.1.

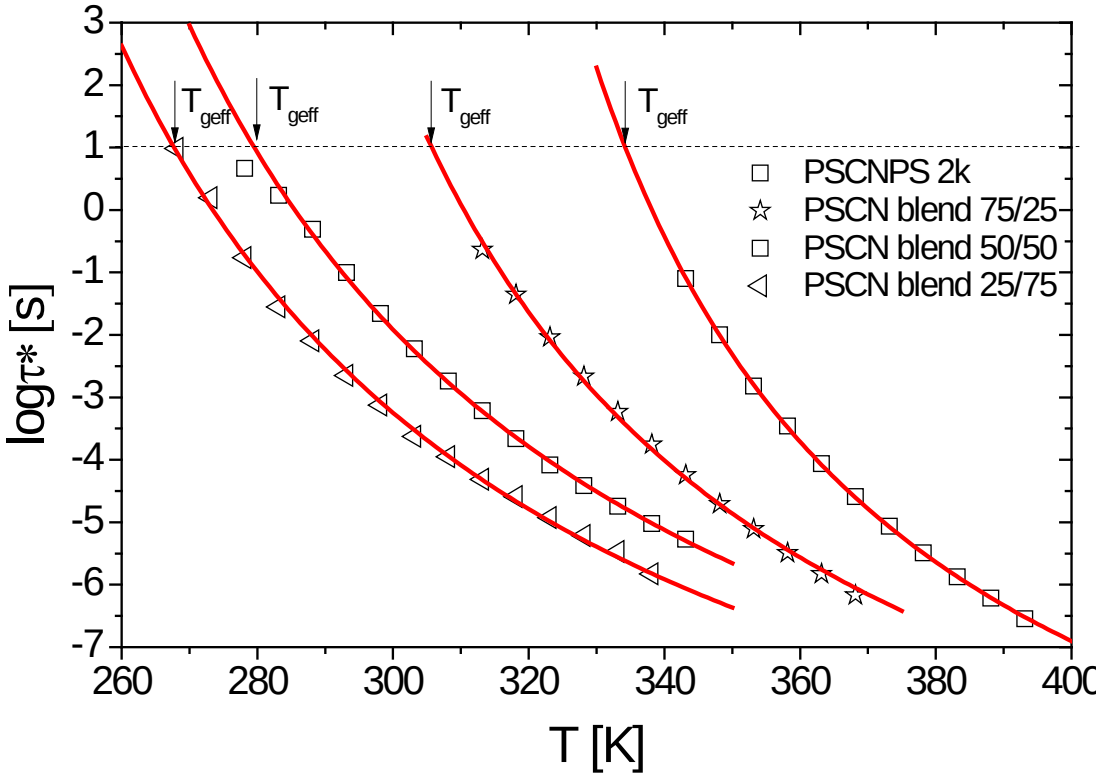

Figure 6.2. Comparison of the temperature dependence of the characteristic relaxation time (τ*) for the homopolymer of higher T_g forming the blend (PSCNPS 2k) and the various PSCN component dynamics of the different blend compositions (25/75, 50/50 and 75/25).

Code	τ_{VFT} [s]	B	T_0	T_{geff} [K]	m
PSCNPS 2k	9.78E-14	1653	282.9	333.9	212
PSCN blend 75/25	9.78E-14	1987	244.1	305.7	160
PSCN blend 50/50	9.78E-14	2512	201.7	279.5	116
PSCN blend 25/75	9.78E-14	2394	193.5	267.7	116

Table 6.1. Parameters obtained from the Vogel-Fulcher-Tamman fits of the main α–relaxation time of the above PS component dynamics. It should be noted that for the fitting the VFT characteristic relaxation time (τ_{VFT}) was fixed using the value obtained for the PSCNPS 2k homopolymer. The calculated "effective" T_g's and the "*m*" fragility indexes are also included.

As seen in Figure 6.3 the dynamics of the PSCN component in the blend becomes faster and the "effective" T_g progressively decreases as the PVME content in the blend increases as expected but the evolution is different than that of the average T_g. As it was already mentioned a way to account for this fact is to consider that due to chain connectivity the 'local concentration' experienced by a given segment of a component is always richer than average in this component. In this context the effective PS concentration (ϕ_{PSeff}) can be defined in terms of the PS self concentration (ϕ_s^{PS}) as (see Equation 2.2.2.1.)

$$\phi_{PSeff} = \phi_s^{PS} + \left(1 - \phi_s^{PS}\right)\phi_{PS} \qquad [6.2.]$$

where ϕ_s^{PS} would account for the volume fraction around the reference PS segment occupied by segments (of the same component) belonging to the same chain, which obviously depends on the size of the relevant volume. In the limit of large volume $\phi_s^{PS} \to 0$ and $\phi_{PSeff} = \phi_{PS}$. In the other extreme case of very small relevant volume $\phi_s^{PS} \to 1$ and $\phi_{PSeff} = \phi_s^{PS}$. The experimental results in polymer blends evidence in general an intermediate situation.

In the Lodge and Mc-Leish approach [2] the "effective" T_g of each of the blend components as a function of the concentration (ϕ) can be calculated from the calorimetric T_g ($T_g(\phi)$) using the following equation $T_{geff}(\phi) = T_g\left(\phi_{eff}\right)$. In this framework, Equation 6.1. can be rewritten in terms of the component glass transition T_{geffPS} and effective concentration as:

$$T_{geffPS}(\phi_{PS}) = T_{gPVME} + (T_{gPS} - T_{gPVME})\left[(1+K_1)\,\phi_{PSeff} - (K_1+K_2)\,\phi_{PSeff}^2 + K_2\,\phi_{PSeff}^3\right]$$

[6.3.]

In this way, by considering equation [6.2.], equation [6.3.] can be finally rewritten as

$$T_{gPS}(\phi_{PSeff}) = T_{gPVME} + (T_{gPS} - T_{gPVME})\left\{(1+K_1)\left[\phi_S^{PS} + (1-\phi_S^{PS})\,\phi_{PS}\right] - (K_1+K_2)\left[\phi_S^{PS} + (1-\phi_S^{PS})\,\phi_{PS}\right]^2 + K_2\left[\phi_S^{PS} + (1-\phi_S^{PS})\,\phi_{PS}\right]^3\right\},$$

[6.4.]

which allows determining the "self-concentration" value, which is the only unknown parameter. As can be seen in Figure 6.3. this approach allows a good description of the concentration dependence of the effective T_g of PS in the blends with a "self-concentration" of this PS component in the blend of $\phi_s^{PS} = 0.24$. This value is very close to that obtained theoretically by Lodge and McLeish [2] being $\phi_S^{PS} = 0.27$. They considered the Kuhn length (l_k) to determine the self-concentrations, which were calculated as the volume fraction occupied by a Kuhn length's segment inside a cube of size l_k. Therefore, our result shows that the volume relevant for the glass-transition of PS is close to that assumed in the Lodge and McLeish approach [2]. However, Ediger et al. [3] by means of Nuclear Magnetic Resonance (NMR) obtained a much larger value (of approximately) $\phi_S^{PS} = 0.5$ for the self-concentration of the PS in the same system. This difference could be associated to the experimental method used, since with NMR they probed the PS dynamics at high temperatures far from T_g. If one considers that the size of the relevant volume decreases with temperature values for the self-concentrations higher than at T_g should be expected. Now, comparing with other similar polymers, this value of $\phi_s^{PS} = 0.24$ obtained by us is very close to that found for the PoClS

(polyorthochlorostyrene) in blends of PoClS/PVME whose components present very different T_g's PoClS having the larger T_g and being structurally comparable with PS. In that case Zacharius et al. obtained a value of $\phi_s^{PoClS} = 0.22$ [4].

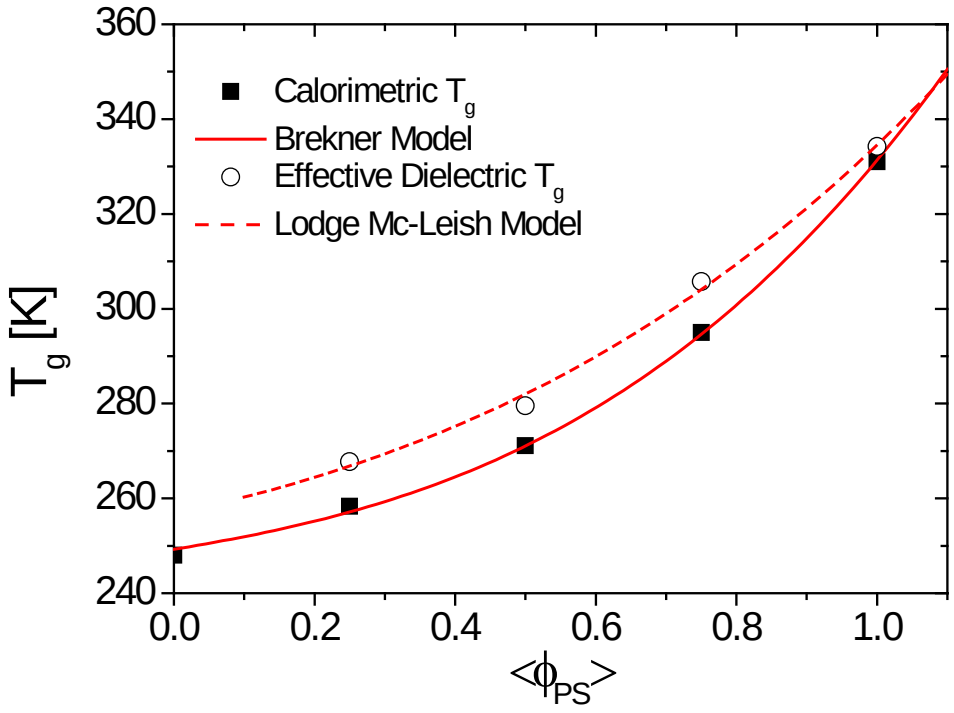

Figure 6.3. Calorimetric glass transition of the PSCNPS 2k and PVME homopolymers and their corresponding blends as a function of the PS composition fitted with the Brekner model. Effective glass transition of the PS component as a function of the PS composition fitted with the Lodge and Mc-Leish model.

The effective T_g does not characterize completely the component dynamics in the blends. From simple inspection of Figure 6.3., it is evident that the curvature determining the temperature dependence varies significantly from the homopolymer case (PSCNPS 2k) to the three different blends with decreasing the content of PS in the blend. A common way to characterize this feature is by means of the so-called fragility index (m) introduced in Section 2.1.2. The fragility index (m) can be determined from the VFT parameters used to describe the experimental data as:

$$m = \frac{B \cdot T_g}{\left(T_g - T_0\right)^2} \qquad [6.5.]$$

The obtained fragility indexes are given in Table 6.1.

It can be clearly observed a strong variation of the fragility index (*m*) decreasing dramatically from the homopolymer case (PSCNPS 2k) to the blend having the same proportion of PS and PVME. However, from this later to the blend richer in the fast component (PVME) it seems that the fragility index (*m*) does not change significantly and subsequently there is as kind of compensation in the variation of *B* and T_0. As the fragility index refers to the temperature dependence of glass-forming systems near T_g, the differences in fragility become evident by plotting the characteristic relaxation time (τ*) as a function of T_g/T (see Figure 6.4.). Here, it is clear that the major differences in the temperature dependence respect to the homopolymer occur near T_g but all the set of data show a more similar slope in the high temperature range.

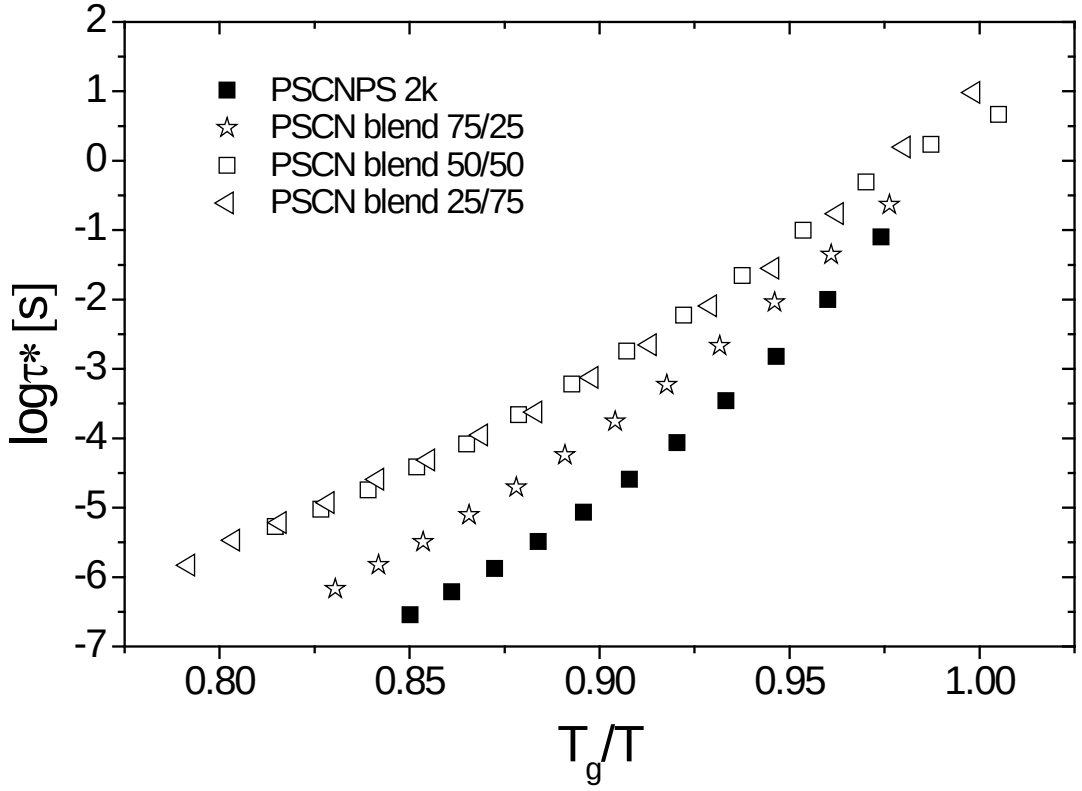

Figure 6.4. Segmental relaxation times (τ*) of the PSCNPS 2k homopolymer and the PSCN component dynamics in the corresponding blends as a function of T_g/T as a well-description of the fragility.

PVME dynamics in the blend:

Now focusing on the dynamics of the PVME component in the blend, a similar procedure to that followed for the PSCN component was used. Figure 6.5. shows the temperature dependence of the PVME characteristic relaxation times (τ*) fitted with a Vogel-Fulcher-Tamman equation [2.1.2.1.20.]. This will allow to determine the "effective" T_g's of the PVME in the corresponding blends and the fragility index. However, it should be stress that for the particular case of the PVME component of the blend having a 75/25 composition richer in PS, the bimodal character of the dielectric relaxation process (which will be discussed below) prevents using any of

the two resolved peak positions to characterize properly the average PVME time scale. Instead in Figure 6.5. we have included the relaxation time data obtained from the frequency for which the whole loss peak is divided in two equal areas. This would correspond to the middle point in the $\varepsilon'(\omega)$ step, i.e. that would also be obtained form the loss peak position in the case of a single and symmetric dielectric relaxation process, as it is for example the case for the 50/50 blend sample.

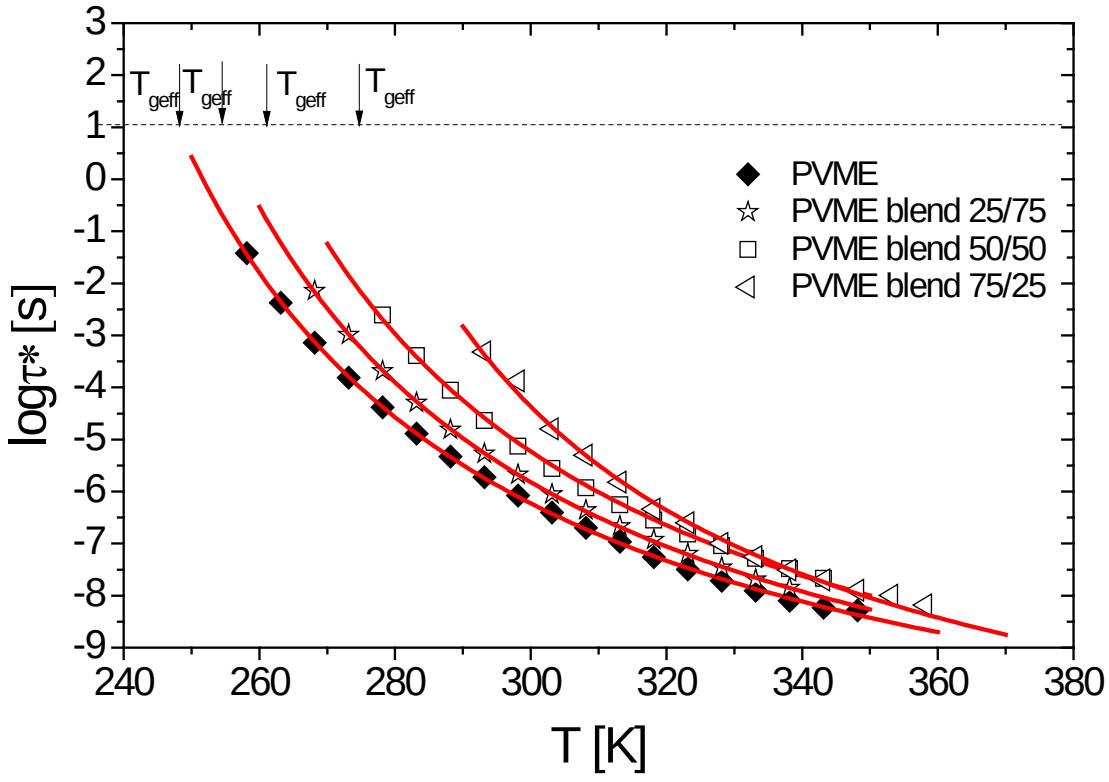

Figure 6.5. Comparison of the temperature dependence of the characteristic relaxation time (τ^*) for the homopolymer of lower T_g forming the blend (PVME) and the various PVME component dynamics of the different blend compositions (25/75, 50/50 and 75/25).

The parameters corresponding to the VFT fits together with the effective T_g values and fragility indexes (m) are shown in Table 6.2. Again, in the fitting procedure for the blends data, the pre-exponential factor τ_{VFT} was fixed to that obtained from pure PVME.

Code	τ_{VFT} [s]	B	T_0	T_{geff} [K]	m
PVME	1.58E-13	1504	200.6	248	166
PVME blend 25/75	1.58E-13	1492	207.2	254.1	172
PVME blend 50/50	1.58E-13	1514	213.1	260.8	174
PVME blend 75/25	1.58E-13	1257	235.3	274.8	220.73

Table 6.2. Parameters obtained from the Vogel-Fulcher-Tamman fits of the main α–relaxation time of the above PVME component dynamics. It should be noted that for the fitting the VFT characteristic relaxation time (τ_{VFT}) was fixed using the value obtained for the PVME homopolymer. The calculated "effective" T_g's and the "*m*" fragility indexes are also included.

By following the same approach as for PS component the "self-concentration" of the PVME component in the blend has been calculated. Then, by considering now the effective concentration of PVME, $\phi_{PVMEeff} = \phi_s^{PVME} + \left(1 - \phi_s^{PVME}\right)\left(1 - \phi_{PS}\right)$, the effective PS concentration around a PVME segment is $1 - \phi_{PVMEeff} = \left(1 - \phi_s^{PVME}\right)\phi_{PS}$, and therefore, the equation describing the data now is:

$$T_{gPVMEeff}\left(\phi_{PS}\right) = T_{gPVME} + \left(T_{gPS} - T_{gPVME}\right)\left\{\left(1 + K_1\right)\left[\phi_{PS}\left(1 - \phi_s^{PVME}\right)\right] - \left(K_1 + K_2\right)\left[\phi_{PS}\left(1 - \phi_s^{PVME}\right)\right]^2 + K_2\left[\phi_{PS}\left(1 - \phi_s^{PVME}\right)\right]^3\right\}$$

[6.6.]

where ϕ_S^{PVME} is the "self-concentration" of the PVME component in the blend.

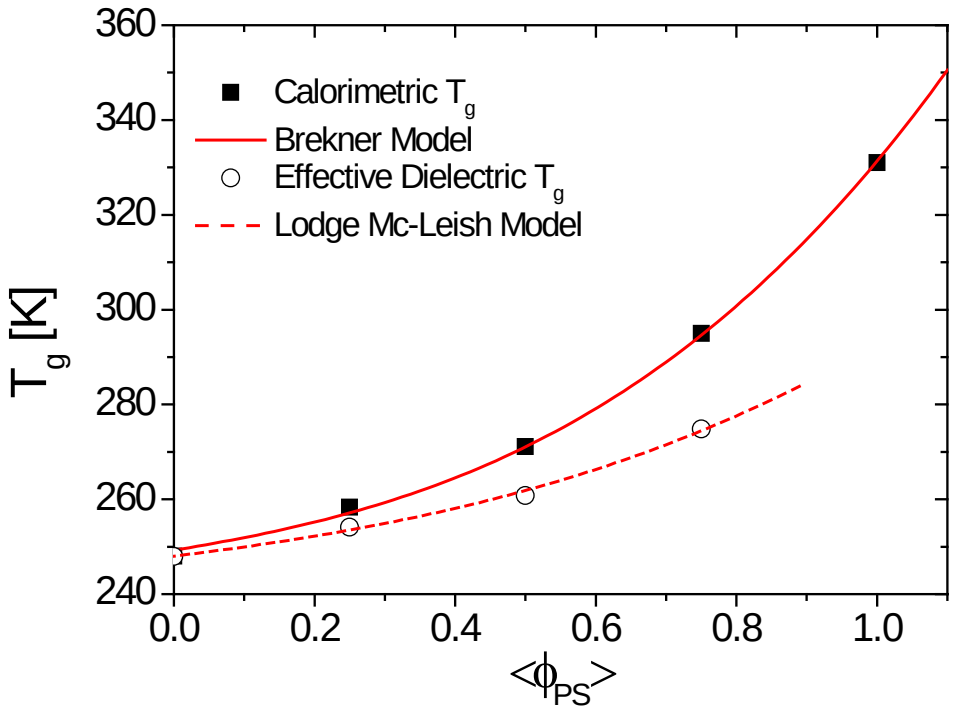

Figure 6.6. Calorimetric glass transition of the PSCNPS 2k and PVME homopolymers and their corresponding blends as a function of the PS composition fitted with the Brekner model. Effective glass transition of the PVME component as a function of the PS composition fitted with the Lodge and Mc-Leish model.

From the fitting of the "effective" T_g ($T_{geffPVME}$) as a function of the content of PS (ϕ_{PS}) in the blend it was found that the "self-concentration" of the PVME component in the blend was $\phi_S^{PVME} = 0.27$, comparable but higher than that obtained in previous investigations [1] on a blend with conventional PS of higher molecular weight where $\phi_S^{PVME} = 0.25$ was found. Comparing the value obtained by us for the self-concentration of PVME with that obtained theoretically by Lodge and McLeish [2], where a value of $\phi_S^{PVME} = 0.25$ is given, we can see that both values are close although this latter is slightly smaller. It is worthy of remark that in the previous investigations the effective T_g values of PVME were obtained by a different dielectric technique, namely Thermally Stimulated Depolarization Current. This

technique works on a continuous heating (as DSC) and detects when a frozen oriented dipoles system is able to recover the random orientation characteristic of the equilibrium situation, which defines T_g. Therefore, in this latter case the relevant volume is that at T_g whereas for the PVME results obtained in the present work we extrapolated higher temperature data to obtain the effective T_g, and in this way the relevant volume would be slightly smaller.

Concerning fragility, the fragility index "*m*" was determined as for the case of the PSCN component in the blend by means of equation [6.5.], the resulting values being included in Table 6.2. The values obtained are all close, which would be indicative of similar temperature dependence irrespective of the concentration except for the PVME in the blend having the lowest concentration of PVME (PVME blend 75/25). This is further evident by representing the characteristic relaxation time (τ*) as a function of T_g/T:

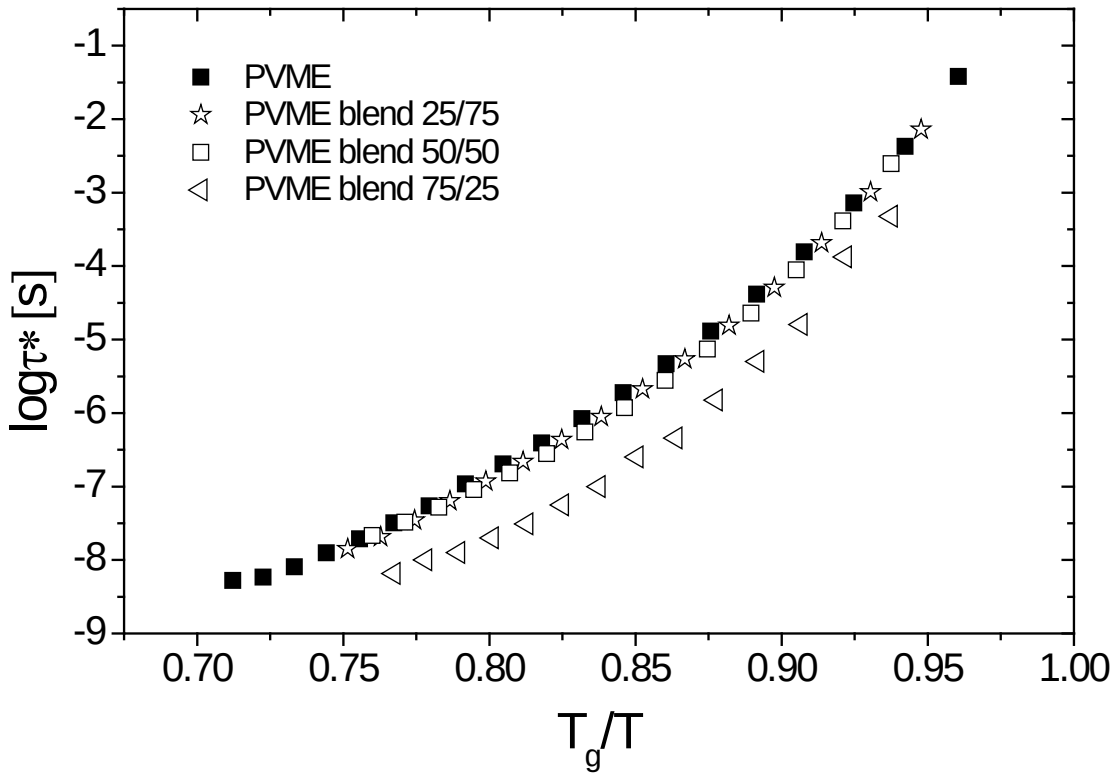

Figure 6.7. Segmental relaxation times (τ^*) of the PVME homopolymer and the PVME component dynamics in the corresponding blends as a function of T_g/T as a well-description of the fragility.

This result is in good agreement with the earlier observation made for blends with content of PS lower than 50% weight [5] where it was found that the characteristic time of PVME in the blends can be described by the same VFT parameters as pure PVME except the T_0 value, a result that has been also reported for other systems investigated by NMR [6, 7 , 8].

Effect of the PS dynamics on the PVME behavior:

The dielectric experiments on PVME/PS blends rich on PS evidenced (here and in previous results [9, 10, 11, 12, 13]) a non-conventional behavior, where the main dielectric relaxation peak frequency changes with temperature in such a way that

whereas at high temperatures follows an usual VFT-like dependence, it crosses over to an Arrhenius-like behavior on cooling. Similar experimental facts have afterwards been observed by different techniques for the low T_g component of blends richer in the other component with a much higher T_g.

Moreover, the combination of BDS and the well-defined PS functionalization, which allow detecting PS response in PS/PVME blends as it has been previously commented, as well as the 75/25 asymmetric composition richer in PS enable us to detect the bimodal character of the PVME dielectric relaxation process in this particular blend and characterize this slow PVME mode.

On the other hand, SANS measurements were performed in order to check that miscibility was not affected when functionalized PS were used to investigate the dynamics of PS/PVME blends instead of using a conventional PS. In fact, looking at the dielectric results it can be observed that both protonated and deuterated PS/PVME blends perfectly compare. However, the SANS measurements were extended towards the low temperature regime where the BDS results evidence a crossover to the Arrhenius-type temperature dependence.

Figure 6.8. summarizes the main results obtained from DSC, BDS and SANS for this 75/25 particular composition.

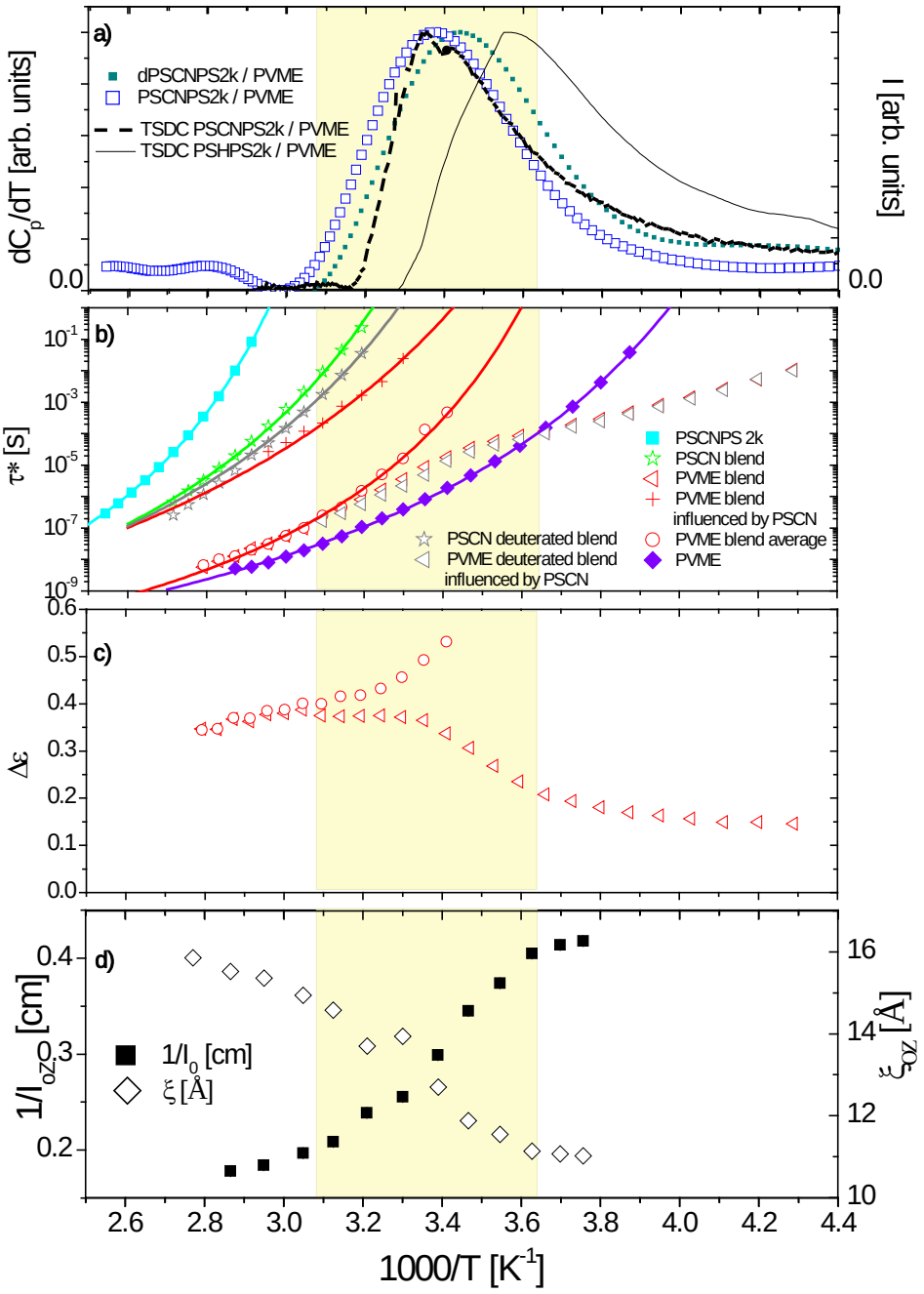

Figure 6.8. (a) Heat capacity derivative (*dCp/dTnorm*) as a function of the temperature for both the protonated and the deuterated –CN functionalized PS/PVME blends, PSCNPS2k / PVME 75/25 and dPSCNPS2k / PVME 75/25, respectively. TSDC spectra obtained for both the –H and the –CN functionalized PS/PVME blends, PSHPS2k / PVME 75/25 and PSCNPS2k / PVME 75/25, respectively. (b) Comparison between the characteristic relaxation times (τ^*) of the pure components forming the protonated and the deuterated blend (PSCNPS2k , dPSCNPS2k and PVME) and their corresponding PSCN and PVME contributions in the blend. (c) The temperature dependence of the dielectric strength ($\Delta\varepsilon$) for the PVME component in the protonated blend. (d) Temperature dependence of the intensity of the Ornstein-Zernike (OZ) function (I_{OZ}) and the characteristic screening length or mesh size (ξ_{OZ}).

As seen, in Figure 6.8.a) we have included the results obtained by Thermally Stimulated Depolarization Current (TSDC) for the –H and the –CN functionalized PS/PVME blends. This technique, which can be considered as a dielectric sensitive equivalent of DSC, has the advantage of directly determining the T_g sensed by the dielectrically active segments present in the blend, i. e. the dipoles that become mobile enough to randomize, represented as a peak that indicates the effective T_g (T_{geff}) as seen in Figure 6.8.a). In particular, the two TSDC curves evidenced how the dipoles of the –H and the –CN functionalized PS/PVME blends reach the equilibrium.

Before entering into details in Figure 6.8. it should be emphasized that the blends employed for this study were dynamically asymmetric, i.e. there is a difference in mobility, very different T_g's, between the two components forming the blends, a slow component (PS) and a fast component (PVME). The dynamic asymmetry can be defined as $\Delta = \tau^{A}_{AB} \big/ \tau^{B}_{AB}$, where A and B in this case would refer to PS and PVME, respectively. It should be noted also that it dramatically changes with temperature being high at low temperatures.

Looking at Figure 6.8. it is evident that we can distinguish three temperature regimes. The high temperature regime is characterized by exhibiting a conventional behavior. This is reflected in SANS results where the intensity of the Ornstein-Zernike (OZ) function (I_{OZ}) and the characteristic length (ξ_{OZ}) slightly vary with temperature as expected (see Figure 6.8.d)). From BDS (see Figure 6.8. b) and c)) it can be observed a different dynamical behavior between PS and PVME components in the blend reflecting very different segmental mobilities due to their very different effective T_g's. In this high temperature regime, where the dynamic asymmetry is

very small and in particular above the T_g of the slowest component in the blend (PS), both components are in the super-cooled liquid state. In this region the fast PVME segments do not restrict the PS motions, and the PS component in the blend is in a situation close to that of the metastable equilibrium of the super-cooled liquid.

Nevertheless, as temperature decreases the dynamic asymmetry drastically increases. Concerning the PS component in the blend it can be observed that it is getting more and more frozen with decreasing temperature until it approaches the glass transition where the effective T_g for the PS component in the blend (T_{geffPS}) can be defined, which corresponds well with the calorimetric peak and the maximum of the TSDC curve from the –CN functionalized PS/PVME blend (PSCNPS2k / PVME 75/25). On the contrary, the dynamic behavior found for the PVME component in the blend is really different from that of the PS component. In fact, for the PVME component it is shown that whereas at the high temperature regime the dynamics can be well described by a VFT law and there is a single dominant dielectric mode, as temperature decreases there is an evident change in the behavior and the main dynamics tends to obey an Arrhenius-type behavior, which was first noticed by Sy and Mijovic in poly(vinylidene fluoride)/ poly(methyl methacrylate) blends [14]. This behavior was also found on poly(ethylene oxide)/ poly(methyl methacrylate) (PEO/PMMA) blends by means of Quasielastic Neutron Scattering experiments and molecular-dynamics simulations [15]. Such change of the dynamics found over the temperature range investigated implies a clear crossover than can be detected at a temperature of the order of 280K and at the same time coincides with the temperature range over which the broad calorimetric T_g extends as it is clearly indicated by the yellow region. It should be noted that along

this temperature range where the crossover takes place, the inverse of the intensity of the Ornstein-Zernike (OZ) function (I_{OZ}) starts getting constant, which can be interpreted as the formation of some kind of gel-like structure due to the freezing of the concentration fluctuations in the blend. Taking into account this assumption, it can be understood why the temperature where the freezing of concentration fluctuations occurs is lower than the calorimetric T_g of the blend. It can be interpreted in the sense that the PVME chains still move even below this calorimetric T_g, which would be based on the dynamical decoupling. Therefore, it would explain why both the concentration fluctuations and the scattering intensity change even below the calorimetric T_g. Hence, it can be said that at low temperatures, below the effective T_g of the PVME ($T_{geffPVME}$), the PVME segments (most of them in the case of blends with a high PS concentration) move within some kind of frozen network imposed by the PS component. This movement of the PVME can take place because despite PVME molecules are trapped by the frozen PS surrounding, the PVME dipoles can still move locally in the regions richer in PVME although their movements are not able to maintain the equilibrium. Moreover, the crossover is detected also in the decrease found for the dielectric strength ($\Delta\varepsilon$) of the main PVME contribution in the blend where the inflection point occurs around the effective T_g of the PVME in the blend (see Figure 6.8.c)). It fits well with the peak detected by TSDC on the –H functionalized PS/PVME blend (PSHPS2k / PVME 75/25) for the PVME component in this blend ($T_{geffPVME}$) (see Figure 6.8.a)) and also with the extrapolation used before to define the effective T_g for this composition. In the low temperature limit, the dielectric strength ($\Delta\varepsilon$) takes a value that represents 30% of the total value reached at the high temperature regime. This 30% indicates that this anomalous dynamical behavior is not an usual

secondary relaxation as it could be interpreted by the Arrhenius trend found for the PVME component in the blend at very low temperatures, but a relevant relaxation process involving important molecular reorientations. In fact, in this temperature region the dynamics of the PVME is found to be confined and thus consists of localized motions with low degree of cooperativity. Furthermore, in this low temperature regime when comparing the dynamics of the pure PVME and the PVME component in the blend it can be clearly seen that the PVME local motions in the blend can be ever faster than in the pure PVME. This phenomenon, which was attributed in the past to the lack of packing in the blend involving regions with a higher free-volume than in the pure PVME [5], can be explained by the above mentioned nonequilibrium effects [8, 11].

1 . E. Leroy, A. Alegría and J.Colmenero, Macromolecules, 35, 5587 (2002)

2 . T. P. Lodge, T. C. B. McLeish, Macromolecules, 33, 5278 (2000)

3 . L. Zhang, T. R. Lutz, J. Zhao and M. D. Ediger, Wiley InterScience, 2253 (2007)

4 . S. L. Zacharius, G. T. Brinke, W. J. MacKnight and F. E. Karasz, Macromolecules, 16, 381 (1983)

5 . I. Cendoya, A. Alegría, J. M. Alberdi and J. Colmenero, Macromolecules, 32, 4065 (1999)

6 . Y. He, T. R. Lutz and M. D. Ediger, Macromolecules, 37, 9889 (2004)

7 . T. R. Lutz, Y. He and M. D. Ediger, Macromolecules, 38, 9826 (2005)

8 . T. R. Lutz, Y. He and M. D. Ediger, Macromolecules, 36, 1724 (2003)

9 . O. Urakawa, T. Sugihara and K. Adachi, Polym. Appl. (Jpn.), 51, 10 (2002)

10 . C. Lorthioir, A. Alegría and J. Colmenero, Eur. Phys. J. E, 12, S01, 029 (2003)

11 . C. Lorthioir, A. Alegría and J. Colmenero, Phys. Rev. E., 68, 031805 (2003)

12 . S. Koizumi, J. Polym. Sci. Part B: Polym. Phys., 42, 3148 (2004)

13 . G. A. Schwartz, J. Colmenero and A. Alegría, Macromolecules, 40, 3246 (2007)

14 . J. W. Sy and J. Mijovic, Macromolecules, 33, 933 (2000)

15 . A. C. Genix, A. Arbe, F. Alvarez, J. Colmenero, L. Willner and D. Richter, Phys. Rev. E., 72, 031808 (2005)

7. Conclusions

This work has shown that a well-defined polystyrene functionalization where a functional group (X: H, CN) is placed either at the end or in the middle of the chain in a controlled way offers the possibility of studying molecular dynamics selectively. In this way, we have evidenced the dependence on the chain site of the segmental polymer dynamics. In addition, it has allowed us using the dielectric spectroscopy technique to resolve in detail the dynamics of the two components in a miscible polymer blend.

The above experimental results clearly show that the functionalization of polystyrene with -H and –CN groups, the latter having a strong dipole moment, does not affect the overall behavior reflecting thermal and mechanical responses similar to those observed for conventional polystyrene. In particular, it was observed that the polymers exhibit a nearly identical T_g and viscosity for each pair of –H/-CN functionalized polystyrenes. Moreover, this fact was confirmed for two different molecular weights (2k and 4k) and functionalization sites (chain-end and in-chain). Contrary, dielectric relaxation experiments gives rise to distinct results due to the strong dipole moment of the –CN group. Thus, when using this technique, the signal from the –CN functionalized polymer highlights the motions in the surrounding of this molecular group, the –H functionalized polystyrene being the reference as it would reflect the overall properties.

Concerning the local dynamical processes present in these functionalized polystyrenes, it was found that both molecular weight and functionalization-site played an important role in the local molecular motions of the functional group. The local dynamics is faster for the polymers with higher molecular weights (4k) and also for end-functionalized PS the motions of the –CN group are faster than for middle-chain counterpart.

On the other hand, the segmental dynamics, which was analyzed in much more detail than the secondary relaxation dynamics, presented some contributions sensitive to functionalization site (site-dependent segmental dynamics). In the case of the chain-end functionalized polymers, at the high temperature regime it was observed an evident faster than average dynamics of the end segments, while approaching T_g the chain-end fluctuations started reflecting more the overall dynamics. Nevertheless, the situation differed for the case of the in-chain functionalized polymers, since at high temperatures the dynamics of the middle-chain fluctuations appeared to be very similar to that of the overall dynamics although at the lowest temperatures, close to T_g, the middle-chain segments seemed to reflect an appreciable slower than average dynamics. The fact that the chain-end segments reflect the overall dynamics close to T_g has been associated with growing regions where cooperative motions involves many types of segments including the chain-end segments. This can also explain the slower than average dynamical behavior obtained for the in-chain segments due to the lower probability of finding chain-ends around, even at T_g.

The fact that the dynamics of polystyrene seem to be not modified by the introduction of a –CN group in the middle of the chain make these in-chain functionalized PS in combination with dielectric spectroscopy an ideal tool to investigate PS/PVME blends dynamics and resolve not only PVME dynamics, which has already been extensively studied, but also PS dynamics. The PS dynamics is detected in the dielectric spectroscopy experiments due to the strong dipole moment introduced by the –CN group. Furthermore, the corresponding blend with the –H functionalized PS highlights the PVME dynamical features. From this comparison the individual contributions have been extracted. Moreover, as it was checked that the functionalization of the PS did not affect significantly the miscibility of the PS/PVME system, note that only a functional group per chain is added, the obtained results are also attributed to conventional PVME/PS blends.

As the used approach consist in the addition of a unique functional group per PS chain the analysis of the blends richer in PS are more detailed. At lower PS concentrations the uncertainties clearly increase. The calorimetric T_g's and the effective T_g's, determined by DSC and BDS, respectively, allowed obtaining the self-concentration for each of the components in the blend. By the Lodge-McLeish model the self-concentration for the PS and PVME were found to be ϕ_S^{PS}=0.24 and $\phi_s^{PVME} = 0.27$. For the blends having a lower concentration of PS (PS/PVME 25/75 and 50/50) a rather conventional behavior was detected for the component dynamics where the relaxation time of both components in the blend follow a Vogel-Fulcher-Tamman (VFT) law behavior. On the other hand, for the blend richer in PS (PS/PVME 75/25) functionalization enables performing the detailed analysis of both PS and PVME components of the blend, and in this way it was possible to probe in a non-ambiguous way the bimodal character of the PVME dynamics. It should be

remarked that this bimodal character changes with temperature and two different dynamical behaviors can be distinguished. On one hand, at the high temperature regime a unimodal and conventional character of the PVME dynamics is observed, which reflects in a VFT trend for the characteristic relaxation time (τ^*) and a dielectric strength ($\Delta\varepsilon$) that increases with temperature. However, as the characteristic time (τ^*) of the PS component dynamics approaches 10 s, the PVME dynamics starts exhibiting the bimodal character. In this regime, we resolved a distinct slow and dielectrically weak mode that follows the conventional VFT behavior and grows in intensity, being always minority, as temperature decreases. In addition, by decreasing temperature the time scale (τ^*) of the fast main mode depict a crossover from the conventional VFT behavior towards a non-conventional Arrhenius behavior that takes place once the relaxation time (τ^*) of the slow mode approaches 10 s. Furthermore, in the temperature range where such crossover takes place, a step decreasing of the dielectric strength ($\Delta\varepsilon$) is detected to a low temperature limiting value representing 30% of the total value found for the dielectric strength ($\Delta\varepsilon$) at the high temperature regime. These anomalies observed for the dynamics of the PVME component in the blend can be associated with the confinement of the PVME segments within a majority frozen PS network. SANS measurements were performed to confirm that a freezing of the concentration fluctuations at this low temperature range occurs as would be expected under this interpretation.

Publications

The present thesis work has given rise to the following publications:

"Polymer Dynamics of Well-defined, Chain-end Functionalized Polystyrenes by Dielectric Spectroscopy" R. Lund, S. Plaza-García, A. Alegría, J. Colmenero, J. Janoski, S. Roy Chowdhury and R. P. Quirk, Macromolecules, 42, 8875 (2009).

"Dielectric relaxation of various end-functionalized polystyrenes: Plastification effects versus specific dynamics" R. Lund, S. Plaza-García, A. Alegría, J. Colmenero, J. Janoski, S. Roy Chowdhury and R. P. Quirk, Journal of Non-Crystalline Solids, 356, 676 (2010).

"Site-Dependent Segmental Dynamics Revealed using Broadband Dielectric Spectroscopy on Well-defined Functionalized Polystyrenes" S. Plaza-García, R. Lund, A. Alegría, J. Colmenero, J. Janoski and R. P. Quirk, Macromolecules, 44, 7810 (2011).

"PS Functionalization as a Tool to Selectively Study the two Component Dynamics in PS/PVME Miscible Blends by Dielectric Spectroscopy" S. Plaza-García, R. Lund, A. Arbe, A. Alegría, R. P. Quirk and J. Colmenero (In preparation).

"Detailed Investigation of the PVME Dynamics in Asymmetric Blends with Functionalized PS" S. Plaza-García, R. Lund, A. Arbe, A. Alegría, R. P. Quirk and J. Colmenero (In preparation).

SUMMARY

The combination of well-defined functionalized polymers and BDS has allowed us studying the behavior of a polymer when a functional group (H, CN) is added at the end or in the middle of the chain. The results evidence clear differences in the dynamics depending on the position of the functional group, being faster and more heterogeneous when the functional group is located at the chain-end (PS-CN), and very similar to the reference (-H) when the functional group is placed in the middle of the chain (PS-CN-PS). This latter result has enabled us resolving the two component dynamics in the PS/PVME miscible blends by dielectric relaxation techniques. This required a combined analysis of the dielectric spectra of PS-CN-PS/PVME and PS-H-PS/PVME blends. In this way we also analyzed for the first time the concentration dependence of the effective T_g of both components. The results obtained agree well with those expected on the basis of the Self-Concentration as calculated from the Kuhn length of the components. Furthermore, the present results allowed us to demonstrate unambiguously the bimodal character of the PVME component in PS rich blends. A detailed analysis evidences that both modes are relevant in determining the effective glass transition of the PVME component.